Zircon U-Pb Age Constraints on the Exhumation of the Lesser Himalayas from the Laxmi Basin, Arabian Sea

Peng Zhou[1], Daniel Fritz Stockli[2], Thomas Ireland[3], Richard W. Murray[3], and Peter Clift[4]

[1]Unknown
[2]University of Texas at Austin
[3]Boston University
[4]Louisiana State University

November 22, 2022

Abstract

The Indus Fan, located in the Arabian Sea, contains the bulk of the sediment eroded from the Western Himalaya and Karakoram. Scientific drilling in the Laxmi Basin by the International Ocean Discovery Program (IODP) provides an erosional record from the Indus River drainage dating back to 10.8 Ma, and with a single sample from 15.5 Ma. We dated detrital zircon grains by U-Pb geochronology to reconstruct how erosion patterns changed through time. Long-term increases in detrital zircon U-Pb components of 750–1200 Ma and 1500–2300 Ma show increasing preferential erosion of the Himalaya relative to the Karakoram at 7.99–7.78 Ma and more consistently starting by 5.87 Ma. An increase in the contribution of 1500–2300 Ma zircons starting by 1.56 Ma indicates significant unroofing of the Inner Lesser Himalaya (ILH) by that time. The trend in zircon U-Pb age populations is consistent with bulk sediment Nd isotope data implies greater zircon fertility in Himalayan bedrock compared to the Karakoram and Transhimalaya. The initial change in spatial erosion patterns at 7.0–5.87 Ma occurred during a time of drying climate in the Indus foreland. The increase in ILH erosion postdates the onset of dry-wet glacial-interglacial cycles suggesting some role for climate control. However, erosion driven by rising topography in response to formation of the Lesser Himalayan thrust duplex, especially during the Pliocene may also be important. The influence of the Nanga Parbat Massif to the bulk sediment flux is modest, in contrast to the situation in the eastern Himalaya syntaxis.

Peng Zhou[1,2], Daniel F. Stockli[3], Thomas Ireland[4], Richard W. Murray[5], Peter D. Clift[1]

[1] Department of Geology and Geophysics, Louisiana State University, Baton Rouge, LA 70803, USA

[2]Department of Physics, Geology, and Engineering Technology, Northern Kentucky University, Highland Heights, KY 41099, USA

[3] Department of Geological Sciences, Jackson School of Geosciences, University of Texas, Austin, TX 78712-1722, USA

[4] Department of Earth and Environment, Boston University, Boston, MA 02215, USA

[5] Woods Hole Oceanographic Institution, Woods Hole, MA 02543, USA

Corresponding author: Peter Clift (pclift@lsu.edu)

Key Points:

- First basin-wide study of how regional erosion patterns have changed through time since 15.5 Ma in the Western Himalaya and Karakoram.

1

- Geochemical and geochronological analyses show increased relative erosion from the Himalaya compared to the Karakoram at 7.99–7.78 Ma.
- Changing patterns of erosion correlate with climatic drying at ˜7.7–6.3 Ma, and relate to solid Earth tectonic forces building topography.

Abstract

The Indus Fan, located in the Arabian Sea, contains the bulk of the sediment eroded from the Western Himalaya and Karakoram. Scientific drilling in the Laxmi Basin by the International Ocean Discovery Program (IODP) provides an erosional record from the Indus River drainage dating back to 10.8 Ma, and with a single sample from 15.5 Ma. We dated detrital zircon grains by U-Pb geochronology to reconstruct how erosion patterns changed through time. Long-term increases in detrital zircon U-Pb components of 750–1200 Ma and 1500–2300 Ma show increasing preferential erosion of the Himalaya relative to the Karakoram at 7.99–7.78 Ma and more consistently starting by 5.87 Ma. An increase in the contribution of 1500–2300 Ma zircons starting by 1.56 Ma indicates significant unroofing of the Inner Lesser Himalaya (ILH) by that time. The trend in zircon U-Pb age populations is consistent with bulk sediment Nd isotope data implies greater zircon fertility in Himalayan bedrock compared to the Karakoram and Transhimalaya. The initial change in spatial erosion patterns at 7.0–5.87 Ma occurred during a time of drying climate in the Indus foreland. The increase in ILH erosion postdates the onset of dry-wet glacial-interglacial cycles suggesting some role for climate control. However, erosion driven by rising topography in response to formation of the Lesser Himalayan thrust duplex, especially during the Pliocene may also be important. The influence of the Nanga Parbat Massif to the bulk sediment flux is modest, in contrast to the situation in the eastern Himalaya syntaxis.

Keywords: Erosion, zircon, monsoon, Himalaya.

1 Introduction

Collision between India and Eurasia, starting about 50–60 Ma [*Garzanti et al.*, 1987; *Jaeger et al.*, 1989; *Klootwijk et al.*, 1992; *Najman et al.*, 2010], has resulted in the formation the largest mountain ranges on Earth. The timing of collision remains controversial but is best addressed by consideration of the stratigraphic record that shows the onset of mixed Indian-Eurasian sediments. Sedimentary rocks in the central and eastern Himalaya imply initial collision at 59 ± 1 Ma [*Hu et al.*, 2016]. Recent work combining Hf isotopes with U-Pb ages in zircon grains from the Tethyan Himalaya now show that sediment eroded from Eurasia, rather than oceanic island arcs, was reaching NW India by 54 Ma, requiring India-Eurasia collision before than time [*Najman et al.*, 2017]. The Himalaya have continued to evolve both in topography and structure as a result of ongoing tectonic deformation coupled with erosion, largely modulated by the strength of summer monsoon rains [*Bookhagen et al.*, 2005; *Clift et al.*, 2008b; *Wobus et al.*, 2003]. Sediments eroded from the Western Himalaya has been deposited in the Arabian Sea where they form the second largest sediment body on Earth, the Indus submarine fan [*Clift et al.*, 2001; *Kolla and Coumes*, 1987].

The sedimentary deposits of the Indus submarine fan represent an archive of the erosion and weathering processes in the Western Himalaya since the onset of continental collision, at least since ˜45 Ma [*Clift et al.*, 2001]. While bedrocks exposed at the surface in the mountains can be used to reconstruct the uplift and exhumation of those particular rock formations, the submarine fan sedimentary record captures spatial and temporal variations of the long-term history of denudation, albeit one buffered by sediment transport processes. Because older portions of bedrocks have been completely removed by erosion and their exhumation history no longer accessible, the sedimentary record becomes the only record of the earlier erosion and exhumation history. Although this record is partially available in the Himalayan foreland basin, these proximal, continental syn-tectonic deposits are more difficult to date at high resolution, and the sequence is truncated by significant unconformities, and deformed by progressive incorporation into the sub-Himalayan fold and thrust belt [*Najman*, 2006]. Moreover, any given section in the accreted foreland basin can only represent the sediment deposited from paleo-rivers that once flowed in front of the mountains in that region.

2

As such a given section would preserve a history of erosion in a limited catchment of a particular part of the mountains, but does not provide a more integrated orogen-scale overview.

Sediments from the western Himalaya are delivered to the Arabian Sea by the Indus River and its eastern tributaries in the Punjab (Fig. 1A). The Indus is particularly sensitive to variations in the strength of the Asian monsoon because it lies on the western edge of the zone affected by this climatic phenomenon. As a result, variations in monsoon strength can have a major impact on both patterns and rates of erosion in the various ranges that comprise the western end of the Himalayan mountain chain (Fig. 1B). A number of studies have suggested that changes in monsoon intensity have significantly impacted the erosion history of the western Himalaya [*Bookhagen et al.*, 2005; *Clift et al.*, 2008a; *Clift et al.*, 2008b].

Debate continues regarding what controls the erosion of the Himalaya, with some workers favoring tectonic processes that drive rock uplift [*Burbank et al.*, 2003], as being the critical control, while others have argued for a dominance by monsoon rainfall and/or glaciation [*Whipple*, 2009; *Wobus et al.*, 2003]. These focus the sediment producing regions across a relatively narrow band of the range front and in turn drive exhumation of deep buried rocks [*Thiede et al.*, 2004]. It is however known that the erosion of the Himalaya is sensitive to climate change because sediment supply during and shortly after the Last Glacial Maximum (LGM) was preferentially focused in the Karakoram, while the strongest erosion has shifted into the Lesser Himalaya since the onset of the Holocene [*Clift et al.*, 2008a].

In this study we focus on the Late Miocene-Recent history and examine evidence for coupling between the tectonic evolution and the changing strength of summer monsoon rains. We take advantage of recently recovered sediments collected by the International Ocean Discovery Program (IODP) in 2015 from the Eastern Arabian Sea, which provide a record of erosion extending back to ˜10.8 Ma, with one sample dated at ˜15.5 Ma [*Pandey et al.*, 2016d]. An earlier lower-resolution study using detrital zircon grains and numerous bulk sediment Nd and Sr isotopes argued that changes in erosion across the Indus Basin were unconnected to climate change and largely manifest as increasing erosion of the Lesser Himalaya, especially starting at 1.9 Ma [*Clift et al.*, 2019b]. We test this model using an expanded set of new U-Pb ages from detrital zircon sand grains (1882 new ages from 15 additional samples, compared to 1335 ages from ten samples in the earlier work) coupled with a more sophisticated statistical treatment of the total data set in order to reconstruct the evolving patterns of erosion.

2 Geologic Setting

The sediments analyzed in this study were retrieved from the Laxmi Basin in the Eastern Arabian Sea (Fig. 1A and 1B). This basin is separated from the rest of the Arabian Sea by a continental block known as Laxmi Ridge [*Pandey et al.*, 1995]. Rifting in Laxmi Basin preceded the breakup of the main Arabian basin, west of Laxmi Ridge, and likely occurred in the latest Cretaceous [*Bhattacharya et al.*, 1994]. Since that time 2–3 km of sediment have accumulated in the Laxmi Basin. Initial provenance investigation of these sediments using Nd isotopes and limited zircon U-Pb dating indicates that while some fine-grained material might be derived in from peninsular India, immediately to the east of the Laxmi Basin, most of the sediment was sourced from the Indus Delta, located around 800 km towards the north [*Clift et al.*, 2019b]. Continuous sedimentation in Laxmi Basin was interrupted by the emplacement of a large mass transport complex (MTC) just before 10.8 Ma, which eroded most of the Middle Miocene at Site U1456 [*Calvès et al.*, 2015; *Dailey et al.*, 2019]. At Site U1457 the MTC removed almost the entire sediment fill from the edge of Laxmi Ridge leaving only a thin deposit of red Paleocene mudstones [*Pandey et al.*, 2016b].

We also compare our sediments with those recovered as drill cuttings from the industrial borehole Indus Marine A-1 located on the Indus shelf (Fig. 1A). Because Indus Marine A-1 is located close to the Indus River mouth the source of sediment is more straight forward, and cannot have involved influence from the Indian Peninsula, as might be the case in the Laxmi Basin. This site penetrated into the Middle Miocene [*Shuaib*, 1982] and drill cuttings have been used to look at the evolving provenance using Nd isotope methods, going back further in time than possible at the IODP sites [*Clift and Blusztajn*, 2005; *Clift et al.*, 2019b]. The Indus Marine A-1 drill site is located on the relatively flat continental shelf and is only

affected by growth faulting, but has otherwise escaped major tectonic deformation since the breakup of the Arabian Sea, except along its western edge adjacent to the Murray Ridge [*Clift et al.*, 2002a;*Gaedicke et al.*, 2002]. Unfortunately, the recovered sediments from Indus Marine A-1 are fine-grained and are not conducive to detrital zircon U-Pb dating in this proximal area. We examined the major element chemistry of the sediments at Indus Marine A-1 for comparison with the more distal drill sites sampled by IODP in order to demonstrate their Indus provenance. Neodymium isotope data indicate that Indus Marine A-1 sediments were derived from the Indus River, consistent with their proximal location, providing a useful comparison with the deep-water materials [*Clift and Blusztajn*, 2005].

Determining the provenance of the sediment delivered to the Arabian Sea is facilitated by the leverage of the significant spatial diversity of bedrock ages and lithologies within the Indus drainage basin [*Hodges*, 2000; *Searle*, 1996]. Geochemical and isotopic differences between bedrock sources are transferred to the eroded sediment and although grains may be altered during the transport process, many of these differences are preserved in the final deposited sediment, allowing us to deconvolve the sources and variations using appropriate proxies. Figure 1C shows the various mountain ranges that comprise the main distinct source regions to the modern Indus River, including the Greater and Lesser Himalaya, the Tethyan Himalaya that lie further north, and that represent the telescoped, passive continental margin of Greater India [*Garzanti et al.*, 1987]. This unit is separated by the Indus Suture Zone from magmatic arc rocks of the Transhimalaya and Kohistan (Fig. 1C) that were largely emplaced in the Cretaceous and Paleogene [*Khan et al.*, 1997; *Rolland et al.*, 2002]. Further north, across the Shyok Suture Zone, lie the Karakoram, the old active margin of continental Eurasia, which also comprises Mesozoic arc rocks, and experienced magmatism after India-Euasia collision, most notably in the form of the Early Miocene Karakoram Batholith [*Ravikant et al.*, 2009; *Searle et al.*, 1989]. The Karakoram region was uplifted in response to both compressional tectonics and strike-slip displacement on the Karakoram Fault [*Searle and Phillips*, 2007]. Farther to the west the Hindu Kush mountains are characterized by a similar pre-collisional history as the Karakoram, but subsequently did not experience such dramatic or rapid unroofing [*Hildebrand et al.*, 2001;*Zhuang et al.*, 2018]. In addition, the Western Syntaxis of the mountain chain is marked by the Nanga Parbat Massif (Fig. 1C), characterized by high-grade metamorphic and igneous intrusive rocks that experienced recent, very rapid exhumation [*Zeitler et al.*, 1989]. However, it is unclear exactly when this process began because the rocks now at the surface are very young. Nonetheless, this does not preclude an earlier onset to erosion [*Chirouze et al.*, 2015].

The Greater Himalaya were emplaced along the Main Central Thrust (MCT) after ~24 Ma, placing them over the Lesser Himalaya [*Catlos et al.*, 2001; *Stephenson et al.*, 2001]. These in turn were unroofed and brought to the surface due to motion along the Main Boundary Thrust (MBT) and associated thrust duplexing [*Bollinger et al.*, 2004; *Huyghe et al.*, 2001]. Evidence from the Siwalik Group foreland basin sedimentary strata indicates that the Lesser Himalaya were exposed locally only after 9 Ma and more widely after 6 Ma in NW India [*Najman et al.*, 2009], although the Nd isotopes at Sites U1456 and U1457 imply that widespread unroofing of the Inner (Crystalline) Lesser Himalaya only began at 1.9 Ma [*Clift et al.*, 2019b]. The Siwalik Group rocks themselves have been up-thrusted and are presently eroding, recycling older sediments back into the river system. However, estimates derived from the incision of terraces in the Nepalese frontal Himalaya suggest that the Siwaliks contribute no more than about 15% of the total flux [*Lave and Avouac*, 2000]. The western edge of the Indus drainage basin is characterized by fold and thrust belts (Sulaiman and Kirthar ranges, Fig. 1A), similar to the Siwalik Group in character [*Roddaz et al.*, 2011], but experiencing a more arid climate. Nonetheless, this environment need not limit erosion rates because of the strong erosion associated with occasional flash flooding events in vegetation-poor settings [*Molnar*, 2001], although study of heavy minerals in rivers draining these ranges and the lower Indus indicate that their contribution to the net sediment load is minor [*Garzanti et al.*, 2020].

Other potential sources of sediment delivered into the Laxmi Basin include the Precambrian cratonic rocks of peninsular India and associated Gondwanan sedimentary sequences [*Mukhopadhyay et al.*, 2010; *Yin et al.*, 2010], characterized by old (>500 Ma) bedrock zircon U-Pb ages, similar to those observed in the Himalaya, especially the Lesser Himalaya. Zircon U-Pb dating, given its high closure temperature [*Hodges*, 2003], only records the initial crystallization or high-temperature metamorphism, and thus, does not allow us to

exclude such old grains as having been derived from peninsular India rather than the Himalaya. Sediments eroded from the Deccan Plateau, the latest Cretaceous flood basalt province that dominates the Western Ghats, immediately onshore from the drilling area, were erupted around 65 Ma [*Courtillot et al.*, 2000] over a relatively short period of time. While these would be very distinctive, basalt is characterized by a very low zircon fertility and might not provide significant zircon grains of that age into the adjoining basin. Nd and Sr isotopic evidence suggests enhanced flux in muddy sediments to the Laxmi Basin during interglacial times [*Khim et al.*, 2019]. Low-resolution apatite fission track and zircon U-Pb studies have so far identified just a single sand at the IODP drill sites that was derived from the Indian peninsula [*Zhou et al.*, 2019].

3 Sedimentology and Stratigraphy

Drilling at Sites U1456 and U1457 penetrated ˜1100 m below the seafloor in both locations, with the basement being reached at Site U1457 (Fig. 2)[*Pandey et al.*, 2016b]. Drilling at Site U1456 only just penetrated through the MTC, allowing a very short core of Middle Miocene sandstone to be recovered [*Pandey et al.*, 2016a]. Age assignments at both sites are made by combining biostratigraphy and magnetostratigraphy and we follow the age model of Pandey *et al.* [2016a] for Site U1456 and Pandey *et al.*[2016b] for Site U1457 (Fig. 2), with updates from Routledge*et al.* [2019]. Ages of individual samples are calculated assuming linear sedimentation between the dated points. At Site U1456 the sediments are relatively mud-rich, but with a number of silt and fine sand turbidite interbeds at 460–730 mbsf (meters below seafloor; Fig. 2A), which are overlain by a sequence of mud and carbonate-rich sediments. A thick, sand-rich package was recovered between 360 and 140 mbsf and interpreted as a submarine fan lobe [*Pandey et al.*, 2016a]. Above this sand-rich package, the section is dominated by mud and carbonate, interpreted as the product of hemipelagic sedimentation. Site U1457 is characterized by much lower proportions of sand, reflecting the drilling location on the flanks of the Laxmi Ridge. However, a sand-rich interval between 670 and 810 mbsf is overlain by a carbonate and mud-rich interval between 600 and 670 mbsf. More sand-rich beds were encountered between 470 and 600 mbsf. As at Site U1456, sediments shallower than 200 mbsf at Site U1457, are mud and carbonate-rich (Fig. 2). The coarse-grained intervals are again interpreted as lobe deposits [*Pandey et al.*, 2016b]. The sandy sediments are interpreted to be deposited by turbidity currents, with the muddy sediments representing hemipelagic intervals between depositional events. Changes in grain size might be driven by changes in the erosional power in the source regions, the discharge stream power of the river, or by changes in sea level, but could also reflect avulsion in the main depositional lobes in and out of Laxmi Basin and the main part of the Arabian Sea towards the West. Such auto cyclic behavior is commonly observed in submarine fans [*Deptuck et al.*, 2008;*Shanmugam and Moiola*, 1991].
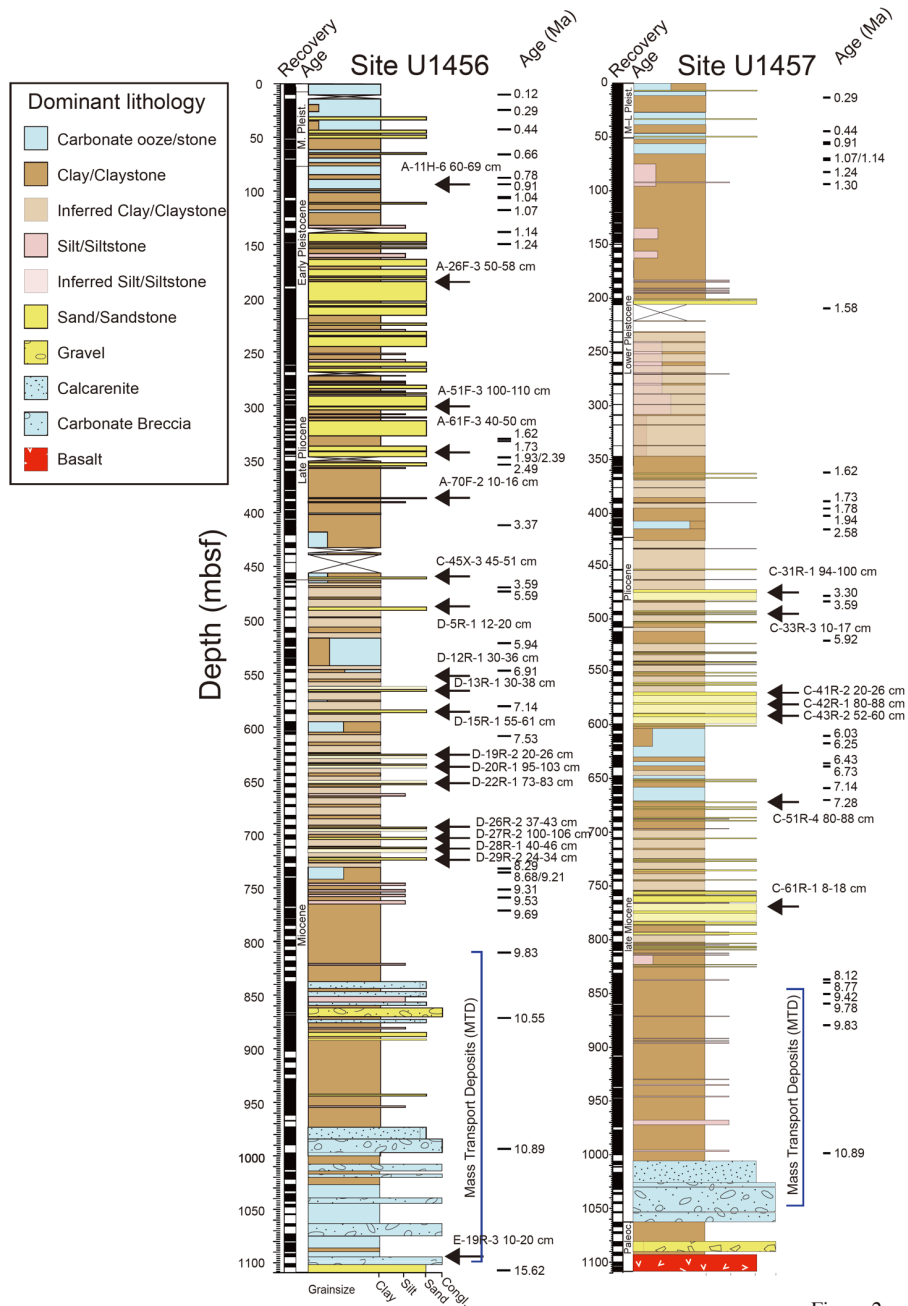
4 Methods

U-Pb geochronology of detrital zircon grains has become a powerful and widely employed tool for discerning provenance in siliciclastic sedimentary systems. The methodology is based on the concept that different bedrock source rocks are characterized by distinct and/or different age populations of zircons. A zircon budget is not the same as an eroded rock budget because of differences in the relative fertility of bedrock sources with regard to zircon. Zr concentrations have been used as a proxy for the relative abundance of zircons in sediment [*Amidon et al.*, 2005], but the reliability of this approach has recently been questioned [*Malusà et al.*, 2016]. Malusà*et al.* [2016] developed a method using mineralogy and density data from the sediment to infer the fertility of the source bedrock. Unfortunately, this approach is not practical for this work because the sample sizes available from IODP were small (<50 cm^3) so that all the material had to be processed for zircon extraction and even required amalgamating neighboring samples in order to generate enough data to make a statistically meaningful result in some cases. We use previously published geochemical data from modern rivers as a guide to zircon fertility as this data already exists and we cross check this prediction against other provenance methods to assess its credibility. Our erosion budgets are however largely zircon based, not bulk sediment.

Zircon is a robust mineral and its grains do not generally experience significant physical abrasion during transport, unless they had previously accumulated major radiation damage. Hence, zircon can undergo multiple episodes of recycling and redeposition. Although the concentration of zircon in any given sediment

can be affected by hydrodynamic sorting, this process may not be a strong influence on the resulting detrital age spectra unless there is a relationship between grain size and crystallization age, which we investigate below. Work on Yangtze River sediments indicates that the typical grain size range analyzed using LA-ICP-MS technology is representative of the overall population in the sediment without a bias related to grains size [*Yang et al.*, 2012]. Detrital zircon U-Pb dating has been widely applied in provenance studies in the Western Himalaya due to the large range of zircon U-Pb age differences between the various source terrains described above. Furthermore, studies of the modern Indus River documented a close correlation between the modern zircon U-Pb age spectra and the bedrock sources, albeit one implying focused erosion in several sub-basins [*Alizai et al.*, 2011; *Zhuang et al.*, 2018]. Several studies have also used detrital zircon dating to investigate the provenance of the Siwalik Group foreland basin sedimentary rocks [*Baral et al.*, 2015; *Bernet et al.*, 2006; *DeCelles et al.*, 2004; *Zhuang et al.*, 2015] and Quaternary sediments in the delta and offshore [*Clift et al.*, 2008a; *Li et al.*, 2019], allowing evolving erosion patterns to be reconstructed.

4.1 Major Element Analyses

In addition to detrital zircon U-Pb dating, bulk sediment samples were analyzed for their major element contents by Inductively Coupled Plasma Emission Spectrometry (ICP-ES) at Boston University (BU), USA. Sediment samples were decarbonated with acetic acid, washed with distilled and deionized water with a purity of 9–12 megaohms, and hand powdered at Louisiana State University (LSU) before total fusion preparation at BU. Glass beads for each sample were made in a muffle furnace under 1050@C by fusing 100 ± 0.5 mg of sample mixed with 400 ± 0.5 mg lithium metaborate ($LiBO_2$). The melted mixture was then dissolved in 5% HNO_3, sonicated, manually shaken until no visible grains were observed, and further diluted for analysis [*Dunlea et al.*, 2015]. Precision for all elements was better than 1% of the measured value, and accuracy was confirmed by repeated analyses of International Standard Reference Materials (Basalt, Hawaiian Volcano Observatory, BHVO-2)[*Wilson*, 1997]. Results of the geochemical measurements are shown in Table 1.

4.2 Grain size Analysis

For quantitative grain size analysis, samples were prepared using standard procedures as described by Howell *et al.* [2014]. We put a small amount of sample into a cleaned 50 ml plastic centrifuge tube and added 5–7 ml of sodium phosphate solution. The tube was capped and vortexed to deflocculate clay-sized sediment and separate organic particles. The sample was poured through an 850 μm sieve and funneled into a 15 ml glass test tube. After centrifuging and removing the clear supernatant, 2–3 ml of sodium phosphate and 5 ml of 30% H2O2 were added. Tubes were vortexed again and then put into a hot bath that was heated to 70@C. This step requires persistent monitoring to prevent loss of reactant by spraying it with acetone until the reaction is stabilized. Reactants then sat overnight to completely oxidize organic matter. Reacted supernatant was removed, and 5 ml of sodium phosphate was added. These treated samples were then rinsed with deionized water, transferred into clean 50 ml plastic centrifuge tubes, and topped with sodium phosphate into a sample solution of up to 40 ml. Samples were vortexed again prior to grain size analysis. Grain size analysis was conducted on a Beckmann Coulter LS13 320 laser diffraction particle size analyzer at LSU. The obscuration of all running samples in the aqueous liquid module (ALM) was between 8–12 %. Result of the analysis are provided in Table 2.

4.3 Zircon U-Pb dating

After standard mineral separation, zircon grains were sprinkle-mounted onto double-sided tape on 1" acrylic discs and analyzed at random using depth-profiling LA-ICP-MS U-Pb geochronology [*Marsh and Stockli*, 2015]. Although this method differs from the more common analysis of cut and polished grains there is no indication that this profiling approach yields results that differ significantly from earlier work, including work done in the Himalaya [*Colleps et al.*, 2019]. For each sample at least 120 zircons were analyzed to obtain provenance datasets that resolve all components that comprise >5% of the total population [*Vermeesch*, 2004]. The analyses were completed using a PhotonMachine Analyte G.2 Excimer laser (30 μm laser spot size) with a large-volume Helex sample cell and a Thermo Element2 ICP-MS using procedures described in Hart *et al.* [2016] at the UTChron facilities at the Jackson School of Geosciences at the University of

Texas at Austin. GJ1 was used as the primary reference standard [*Jackson et al.*, 2004] and a secondary in-house zircon standard (Pak1 with a TIMS^{206}Pb/^{239}U age of 43.0 Ma). The data from the analyses were then reduced using the Iolite data reduction software VizualAge [*Paton et al.*, 2011; *Petrus and Kamber*, 2012]. For analyzed detrital zircons, the^{206}Pb/^{238}U age was used for grains younger than 850 Ma and the^{207}Pb/^{206}Pb age was used for grains older than 850 Ma [*Gehrels et al.*, 2008]. All ages reported use 2σ absolute propagated uncertainties.^{207}Pb/^{206}Pb ages are less than 30% discordant, and ^{206}Pb/^{238}U ages are less than 10% discordant [*Gehrels et al.*, 2011]. The discordance reported is calculated with the^{206}Pb/^{238}U and^{207}Pb/^{235}U ages if <850 Ma and the ^{206}Pb/^{238}U and^{207}Pb/^{206}Pb ages if >850 Ma. Although some studies have suggested older crossovers between the ^{206}Pb/^{238}U and ^{207}Pb/^{235}U ages and the^{206}Pb/^{238}U and^{207}Pb/^{206}Pb ages (e.g., 1.5 Ga [*Spencer et al.*, 2016]) blindly picking a crossover at 1.5 Ga leads to culling of discordant^{206}Pb/^{238}U ages, or unacceptable smearing and loss of age mode definition between 800–1500 Ma for many samples. Picking a 1500 Ma crossover cutoff and a 20% discordance filter would result in the loss of 80% of the data between 850 and 1500 Ma making the data bad provenance proxies. The 850 Ma crossover was chosen in accordance with the approach of Spencer et al. [2016] and Marsh et al. [2019]. The data are reported in Table 3.

When accurately dating a geological event, high concordance is a requirement but when assigning grains to broad age populations for provenance work the emphasis is on high numbers of grains rather than on high precision in order to improve the statistical reliability. The appropriate level of discordance filter needs to be determined for each data set in light of the goals of the study and the complexities encountered. If a study yields a mix of Phanerozoic and Archean ages, and the relative proportions of these ages are important, a generous (e.g., 30%) discordance cutoff is appropriate so that most Precambrian ages are retained [*Gehrels*, 2012].

5 Results

5.1 Grain-size of sediments

The sediments were assessed using the classification scheme of Folk [1974](Fig. 3). Sediments range from silty sand to silt and mud, both the new samples processed here and those from the earlier study we integrate with here {Clift, 2019 #152}. The grain size variation in single samples can be better assessed by plotting the proportion of each grain size fraction as a spectrum (Fig. 4). We see generally good sorting (positive kurtosis) and a negative skew, meaning a dominance of the finer grain sizes and a tail of coarser grains comprising a diminishing proportion of the sediment. This is especially true for the coarsest grained sediments. The vast majority of the sediment considered here is classified as fine sand to silt, with only small amounts of medium and coarse sand in a minority of samples, three from Site U1456 dated at 1.92–1.32 Ma and one from Site U1457 at 3.02 Ma. Three of the new samples do contain significant volumes of medium and even coarse sand (3.39, 7.00 and 7.27 Ma). The spot size of the laser used for the U-Pb dating means that grains smaller than ~30 μm were not considered in this study. Depending on the sample this represents a wide range of the total sediment load. Only 9% of Sample U1456A-51F-3, 100-110 cm was less than 30 μm, while 89% of Sample U1456A-70F-2, 10-16 cm is smaller than that threshold. See Table 2 for full results.

5.2 Bulk Sediment Chemistry

The general geochemical character of the sediments can be seen on a CN-A-K ternary diagram [*Fedo et al.*, 1995](Fig. 5A). The IODP samples plot in an array with a Chemical Index of Alteration (CIA) of ~65 to 73 [*Nesbitt et al.*, 1980]. They form a roughly linear array trending towards the illite end member and suggestive of its progressive involvement as the primary mineral breakdown product. The Laxmi Basin samples can be compared with sediments from the Quaternary Indus delta [*Clift et al.*, 2010], Indus Canyon [*Li et al.*, 2018], the Indus Marine A-1 borehole, as well as modern sediments from the western Indian shelf and slope between the Saurashtra peninsula and Bhatikal [*Kurian et al.*, 2013](Fig. 1). Rivers south of Bhatikal have a different composition and are unlikely to be sources to the Laxmi Basin sites.

The Laxmi Basin sands have very similar bulk compositions to the Quaternary Indus canyon and delta, as well as the Indus Marine A-1 samples (Fig. 5A), but plot below or to the right of the array of the

7

western Indian shelf sediments. Only the shelf sample taken near Bhatikal (the southernmost shelf sample that overlies the Precambrian crystalline basement of India, rather than the Deccan Traps), plots below the Laxmi Basin sediments, with a lower CIA value. This plot confirms that the analyzed sands have little in common with material eroded from peninsular India and appear consistent with an Indus River origin. Likewise, the sediments plot close to the Quaternary Indus sediments and those of Indus Marine A-1 on the discrimination diagram of Herron [1988](Fig. 5B). The IODP samples plot with slightly lower Fe_2O_3/K_2O values compared to the proximal sediments. The Laxmi Basin sediments form an array defined as shales and wackes, while the western Indian shelf sediments fall into the Fe shale, litharenite, sublitharenite and Fe sand fields.

We further assess whether grain size has any relationship to zircon concentrations by plotting Zr contents against median grain size (Fig. 6). Although the original source characteristics and hydrodynamic sorting of the sediment might be expected to concentrate zircons in certain size fractions this does not appear to be a significant factor within the range of grain sizes considered here.

5.3 Detrital Zircon U-Pb

We examined the range of zircon U-Pb ages using a kernel density estimate (KDE) diagram (Fig. 7) to assess similarities between different sampled sediments and potential source regions (Fig. 7). All of the sediments analyzed in this study show a significant zircon U-Pb component younger than 200 Ma. In addition, we see significant components dated at 350–1250 Ma and 1500–2300 Ma. The abundance of these older age components overall increases with decreasing sample depositional age. The 350–1250 Ma age component appears to increase in all sediment samples dated at 5.87 Ma or younger compared to the older sediments. A particularly prominent age mode at ˜1800 Ma first occurs in sediments deposited at 3.43 Ma and becomes extremely prominent in all samples younger than 1.92 Ma. This age mode is also observed in the modern sediment from the Indus river mouth [*Clift et al.*, 2004].

Examining the <200 Ma zircon U-Pb ages in detail, we see that the vast majority of grains are younger than 120 Ma with prominent age peaks at around 100–120 Ma and 40–70 Ma (Fig. 8). In the youngest samples, especially those deposited starting at 3.02 Ma, we see another age mode at ˜20 Ma, although this is also seen in the sample dated at 5.78 Ma. One sample deposited at 3.17 Ma differs in its <200 Ma age spectra from the other samples as it is characterized by a prominent age peak at 100–120 Ma, with a general lack of other young zircon grains.

6 Discussion

Major element discrimination diagrams (Fig. 5) suggest that the Laxmi Basin sediments are most similar to deposits found in the Quaternary and modern Indus River/delta/canyon, as well as the older sedimentary rocks from Indus Marine A-1 (Fig. 5). However, they are distinctly different from sediments sampled from the modern western Indian shelf, and largely derived from the Deccan Plateau and underlying units [*Kurian et al.*, 2013]. These geochemical data suggest that the Laxmi Basin sediments, most likely originated from the Indus River mouth.

We assessed the overall geochemical characteristics of the sediments by plotting the major element composition of each sample normalized to the upper continental crust (UCC; Fig. 9)[*Taylor and McLennan*, 1995]. Most of the samples display a relatively uniform topology in these diagrams and are broadly similar to both post-LGM sediments from the Indus Delta (KB-40-4), the Holocene delta (TH-10-1) and, the modern Indus river (Thatta TH-1). Most of the samples show a similar major element composition compared to the UCC, with a consistent enrichment in TiO_2, suggestive of a higher content of Ti-bearing heavy minerals (e.g., rutile, anatase, brookite, ilmenite, titanite). This enrichment is particularly strong in the 0.93 Ma sample which apatite fission track data indicate to have a unique provenance [*Zhou et al.*, 2019]. There are also relative depletions in CaO and Na_2O, as well as P_2O_5, implying both a lower plagioclase and apatite content relative to the UCC. This relative depletion in CaO is strongest in the modern river mouth sediment and weakest in the post-glacial delta sediments, with the fan sediments plotting between these extremes. The systematically lower abundance of plagioclase and apatite likely reflects chemical weathering in the flood-

8

plains prior to deposition in the ocean, because these phases are less stable under conditions dominated by chemical weathering [*Guidry and Mackenzie*, 2000; *White and Brantley*, 1995]. However, all samples show this effect and there is a general consistency in the overall composition, we conclude that we are comparing sediments of a similar bulk character. All fan sediments show Zr abundances relatively close to the UCC average
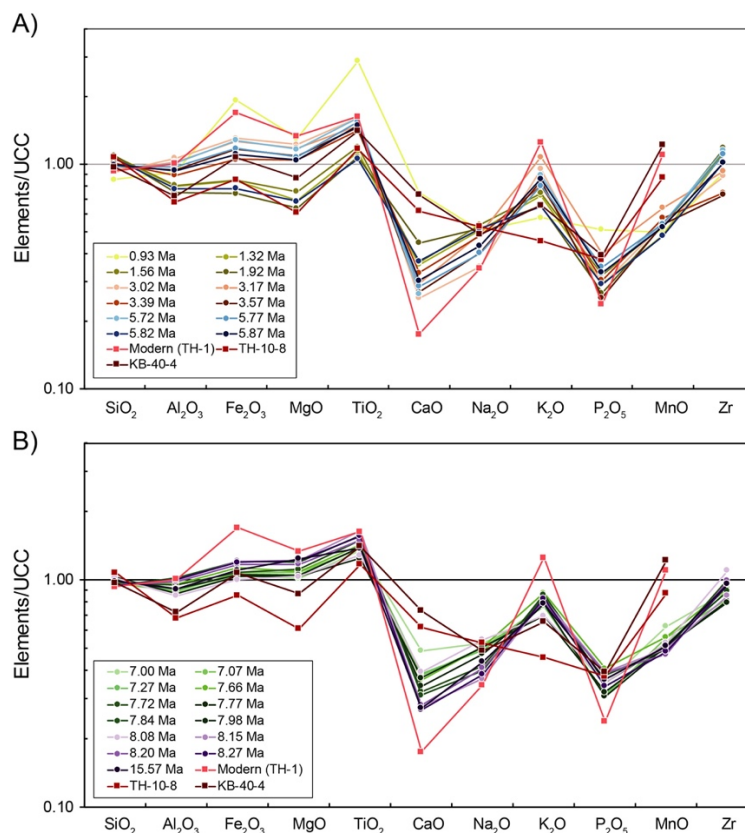
6.1 Changing Provenance

Before using the changing zircon U-Pb age spectra to infer changing sediment provenance we examine the possible role of grain size in controlling the results. Sediment grains are fractionated during transport because different densities and shapes affect their settling characteristics [*Garzanti et al.*, 2009]. Zircons all have the same density but the size and shape of the grains from a given source may vary and influence the final conclusions. If one source is associated with smaller or larger grains compared to other sources then this may prejudice the analysis, especially if the grains are too small to be analyzed. Garzanti *et al.* [2009] concluded that this effect was moderate in the Ganges-Brahmaputra catchment, which has strong similarities to the Indus. We plot major, provenance-related age populations (0–25, 40–70, 70–120, 300–750, 750–1250 and 1500–2300 Ma) against median grain size for all samples considered here to see if grain size plays a strong role in controlling the age spectra. Figure 10 shows that there is not a strong correlation between sediment median grain size and the proportion of various provenance-sensitive age groups. However, we note that the four coarsest sediments (>100 µm) do contain more 750–1250 and 1500–2300 Ma grains compared to the 40–70 and 70–120 Ma groups. The effect is especially strong with the 1500–2300 Ma group. In contrast to work on the Amazon River by Lawrence *et al.* [2011] who showed that older grains were significantly smaller than younger ones, the reverse may be true in the Indus. It is however noteworthy that the coarser sediments are all young 3.02 Ma and younger and as demonstrated below the provenance inferred from similar aged finer sediment is not greatly different and also consistent with neighboring bulk sediment Nd isotope constraints. We conclude that there may be a grain size issue with the coarsest sediment, but that this is not dominant in controlling the U-Pb age spectra.

The zircon U-Pb age spectra are used to track the source evolution of sediment reaching the Arabian Sea and compared to bedrock zircon U-Pb age signatures of possible source areas (Fig. 7). The abundance of grains younger than 200 Ma correlates well with young bedrock from the Indus Suture Zone, particularly in Kohistan, the Transhimalaya and Karakoram, as well as Nanga Parbat (Fig. 8). The abundance of these young zircon grains clearly points to sediment being supplied by the Indus River and not by peninsular India, where no magmatism <200 Ma is known outside the Deccan Plateau. Detrital zircon grains older than 350 Ma also largely correlate with various bedrock sources known in the Himalaya. Detrital zircon age modes between 350 and 750 Ma have been correlated with bedrock sources in the Tethyan Himalaya [*Alizai et al.*, 2011], although it is generally agreed that there is little real difference in terms of U-Pb ages, between Tethyan and Greater Himalaya zircon signatures [*Gehrels et al.*, 2011], and these are in any case not always mapped consistently by different groups [*Webb*, 2013]. Consequently, zircons with ages between 350 and 1250 Ma could be derived from either source. The older samples show relatively low abundance of grains in this age range, but these increased significantly starting at 5.87 Ma and become very abundant in the last few million years. Older grains, dating between 1500 and 2300 Ma, are particularly common in Lesser Himalayan sources, although they are also present in smaller amounts in the Tethyan and Greater Himalaya [*DeCelles et al.*, 2000; *Gehrels et al.*, 2011]. These mainly Paleoproterozoic zircon grains are almost entirely absent from the Laxmi Basin Miocene samples, but show a marked increase beginning at 5.72 Ma, and becoming very abundant beginning at 1.56 Ma (Fig. 7). We therefore interpret these patterns to indicate a progressive increase in erosion from the Himalaya starting after 7.0 Ma, and especially starting at 5.72 Ma, with strong erosion from the Tethyan and Greater Himalaya. After 3.02 Ma there is a dramatic increase in erosional flux from the Lesser Himalaya, which have had a strong influence on the river system since the onset of the Holocene [*Clift et al.*, 2004; *Clift et al.*, 2008a].
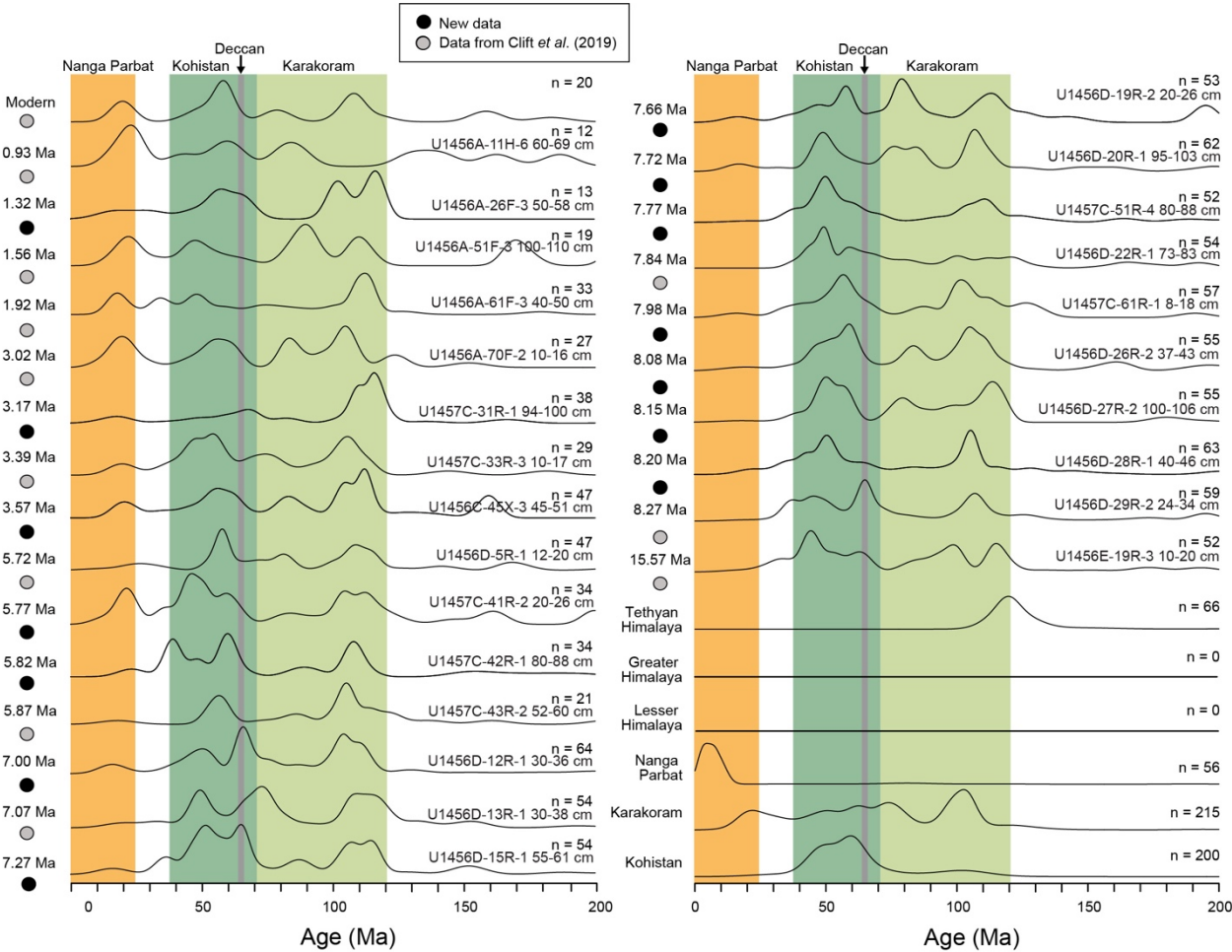
If we only consider the zircon grains younger than 200 Ma then we can see that there is evidence of erosion, from both Kohistan and from the Karakoram, in most of the samples analyzed (Fig. 8). Kohistan is

particularly noteworthy for having zircon dated between 40 and 70 Ma [*Alizai et al.*, 2011; *Zhuang et al.*, 2018], although there are similar aged units in the Karakoram as well. However, zircon grains older than 70 Ma but younger than 120 Ma are almost exclusively known only from Karakoram bedrock sources [*Searle*, 1996]. The 3.17 Ma sample does not show the younger 40–70 Ma population, suggesting that it did not receive any significant material from Kohistan/Ladakh.

The youngest (<25 Ma) zircon grains are more enigmatic in terms of their provenance. While very young zircons are known from the present-day Nanga Parbat massif, these are generally younger even than the 25 Ma zircon U-Pb age component observed in many of the samples [*Zeitler et al.*, 1993]. Our new data also show an increased influx from bedrock sources with very young zircon starting at 3.02 Ma, as well as a brief appearance at around 5.78 Ma. It is possible that this increase starting at 3.02 Ma reflects the emergence of Nanga Parbat, although we cannot exclude the influence of other young sources in the southern Karakoram metamorphic belt, which also contains rocks of this age and have experienced very rapid exhumation in the last few million years [*Wallis et al.*, 2016]. Because the Deccan Plateau volcanic rocks were erupted rather quickly around 65 Ma, it is hard to completely exclude their influence because grains of a similar age are also known in Kohistan, and in the Karakoram. However, the erosion from the Deccan Plateau would not account for the other young grains and an influx from that area should result in a clear peak age at 65 Ma, which is not observed.

We also assessed the evolving provenance patterns of sediments in Laxmi Basin using a multidimensional scalar (MDS) analysis of the detrital zircon U-Pb dates [*Vermeesch et al.*, 2016]. In this plot, which is a type of principle component analysis, samples with similar age spectra plot close to one another, while distinct samples are far separated. Figure 11A shows all the detrital samples data, along with a modern river mouth and a delta sample (KB-40) dating from shortly after the LGM [*Clift et al.*, 2008a]. The MDS analysis shows clear and coherent patterns. Samples deposited at and after 1.56 Ma, are relatively similar to the modern river. In contrast, the oldest samples plot in a cluster suggesting a similar Miocene provenance and a subsequent progressive shift from right to left with decreasing depositional age, although with some reversals, most notably at 3.17 and 3.57 Ma. This reflects an overall shift in the zircon age spectra through time. Nonetheless, the LGM sample has stronger similarities with sediments deposited on the fan during the Late Miocene. Earlier work implied that erosion during the LGM was focused in the Karakoram [*Clift et al.*, 2008a] compared to the modern river or during the Holocene when the summer monsoon was strong [*Caley et al.*, 2014; *Fleitmann et al.*, 2003; *Gupta et al.*, 2003]. The new data indicate that older Miocene samples were also deriving their material from Karakoram sources, and this was followed by a shift to more Himalayan sources, especially in the last few million years. The plot implies that the change might be step wise, with a change starting between 7.0 and 5.87 Ma and again at 1.56 Ma.

The fact that the youngest turbidite sands are most similar to the modern interglacial river, and not the compositions of the Indus shortly after the LGM, also implies that most of the sediment deposited in the Indus Fan has been eroded during interglacial times when the monsoon was strong, even if final deposition did not occur until the sea level fell during the onset of the subsequent glaciation. We envisage fast interglacial erosion generating great volumes of sediment, which is then mobilized, transported, and delivered to the delta as the rains strengthened [*Jonell et al.*, 2017]. The sediment would then be stored on the shelf or in the upper canyon during sea level high stands before being eroded and redeposited as sea level fell [*Li et al.*, 2018]. This emphasizes the importance of monsoon intensity in controlling erosion and sediment delivery in the Western Himalaya.

We also compared the Arabian Sea sediments with known zircon ages from bedrock sources themselves. Figure 11B shows the progressive changes from the Miocene to the present and emphasizes the fact that the stratigraphically oldest detrital zircon samples plot closest to sources in the Karakoram and have similarities with analyses from the trunk stream (upper reaches) of the main Indus River, before it mixes with the Himalaya-draining Eastern tributaries, such as the Jhellum, Chenab, Ravi, Sutlej and Beas (Fig. 1). Conversely, the stratigraphically youngest sediments plot on this diagram closest to Himalayan sources and have greater similarity not only to the modern river mouth, but also Himalayan tributaries such as the Ravi,

Chenab and Jhellum rivers.

These data also imply that Nanga Parbat has not been a very important contributor to the bulk sediment flux. Whether this is actually true or not is not entirely apparent because the bedrock analyses from Nanga Parbat were focused on igneous rocks in the center of that metamorphic massif, and might not be representative of the net erosional flux from this particular source. However, the relationships displayed in Figure 11B can be readily explained as a simple mixing between Karakoram and Himalayan sources, with a progressive shift towards the Himalaya through time.

6.2 Unmixing Sources

In order to further characterize the evolving source of sediments to the Indus Fan we employ the unmixing software of Sundell and Saylor [2017], which analyzes the U-Pb age spectra from each of the samples and compares them with the defined end-member compositions of the different source ranges compiled from the published literature. This approach works particularly well in the western Himalaya where the sources are well defined and often unique. Data from the Tethyan, Greater and Lesser Himalaya were compiled from DeCelles *et al.*[2004]. Data from the Karakoram are from Le Fort *et al.*[1983], Parrish and Tirrul [1989], Schärer *et al.*[1990], Fraser *et al.* [2001] and Ravikant *et al.*[2009]. Data from Nanga Parbat are from Zeitler and Chamberlain [1991] and Zeitler *et al.* [1993]. Data from the Transhimalayan are from Honegger *et al.* [1982], Schärer*et al.* [1984], Krol *et al.* [1996], Weinberg and Dunlap [2000], Zeilinger *et al.* [2001], Dunlap and Wysoczanski [2002], Singh *et al.* [2007], and Ravikant*et al.* [2009].

This unmixing method uses a Monte Carlo approach to estimate the contributions from the different sources that would be required to generate the modes and modal abundances of U-Pb ages seen in the sediment samples. Because this is relatively objective the method is considered robust for analyzing potential source contributions, assuming that the sources themselves have been well characterized. The bedrock sources of the Indus catchment have significant differences between many of them and are some of the best characterized worldwide. Results of the Monte Carlo simulation are provided in Table 4, showing the output using all three statistical comparison methods, cross-correlation, the best V value in the Kuiper test. as well as the best D value in the K-S test. The method involves creating 10,000 model mixed sediments using the defined bedrock source end members. The DZMix software then compares the model with the measured spectra and retains the best 1% of these models in order to estimate which sources were contributing the sampled material. We favor the unmixing models derived from the cross-correlation approach as being geological reasonable and favored by Sundell and Saylor [2017].

The results of our unmixing calculations show a progressive provenance evolution that is consistent with that seen in the MDS diagram (Figs. 11 and 12). The very oldest sample deposited at 15.5 Ma shows a dominance of sediment eroded from the Karakoram and from the Tethyan and Greater Himalaya. Most of the Miocene samples dated between 8.2 and 7.0 Ma are more dominated by material from the Karakoram but also usually show significant Tethyan and Greater Himalayan contributions. This Himalayan component is particularly noteworthy at 7.99, 7.84, 7.78, 7.66, and 7.0 Ma during this interval. The proportion of Karakoram zircons shows a significant decrease starting no later than 5.72 Ma and again at 3.02 Ma. The sediment deposited at 3.17 Ma shows the greatest amount of modeled erosion from Karakoram sources of any sample.

From 3.02 Ma onwards the Himalaya dominate as sources to the submarine fan, with significant amounts of material from the Lesser Himalaya first appearing at 1.56 Ma. The sample dated as being deposited at 0.93 Ma is anomalous for being very similar in source signature to Tethyan and Greater Himalayan bed rocks sources. However, we note that fission track data indicate that this sample was derived from peninsular India [*Zhou et al.* , 2019]. The unmixing analysis largely mirrors the pattern shown by the MDS diagram, in showing a progressive long-term increase in erosion from the Himalaya relative to the Karakoram, although with significant steps making the evolution nonlinear. All of the samples contain a small amount of very young <25 Ma zircons. None of the samples analyzed show a close similarity with post-LGM river compositions. Delta samples deposited at 6.6 and 15 ka are strongly enriched in Karakoram-derived grains compared to fan sediments deposited at and after 3.02 Ma. This short term variability is interpreted to reflect the short-term

changes in erosion patterns linked to monsoon strength, modulated by glacial cycles since the onset of the NHG.

6.3 Relationships to Climate Change and Tectonics

The progressive increase in the relative flux from the Himalaya since the Middle Miocene represents the progressive unroofing of these units. Structural reconstructions of the Western Himalaya predict that prior to 5.4 Ma the Greater and Lesser Himalaya were not exposed [*Webb* , 2013] implying that the Himalayan contribution was derived entirely from the Tethyan Himalaya during the Miocene. As we are not able to distinguish between Tethyan and Greater Himalaya derived sediment we focused on the first appearance of significant amounts of 1500–2300 Ma, Inner Lesser Himalayan detritus starting at 1.56 Ma. Previous studies considered these ranges to have been exposed somewhat before 1.6 Ma. Study of the Siwalik Group in the area of the Beas River Valley indicated an initial exposure of these units around 9 Ma and significant exposure by 6 Ma based on Nd isotope data [*Najman et al.* , 2009]. Our data support the findings of Clift *et al* . [2019b] that this exposure may only reflect the local situation in the paleo-Beas River area, but that widespread regional exposure of the Inner Lesser Himalayan units comes somewhat later. While Clift *et al* . [2019b]favored increased Inner Lesser Himalaya erosion starting at 1.9 Ma our new zircon data imply that 1.56 Ma is a more accurate age for this this transition.

Our result also contrasts with the suggestion by Myrow *et al.*[2015] that the Inner Lesser Himalaya were widely exposed and eroding by 16 Ma. Although we cannot exclude this from happening further east in the Ganges Basin our data do not support this over a wide area of the western Himalaya until much later.

The timing of Lesser Himalayan unroofing may reflect the development of the thrust duplex, which characterizes the structure of the Lesser Himalaya in this area [*Huyghe et al.* , 2001; *Webb* , 2013]. Integrated metamorphic and geochronologic data indicate rapid cooling of the Inner Lesser Himalaya before 6 Ma, following peak metamorphism around 10 Ma [*Caddick et al.* , 2007; *Thiede et al.* , 2009]}. We note that rapid cooling does not however require synchronous unroofing. The first major flux of Himalayan zircons to the submarine fan is dated at 7.99 to 7.78 Ma, although widespread Himalayan unroofing may not have started until 5.72 Ma, followed by Inner Lesser Himalayan unroofing starting around 1.56 Ma. This timing is younger than reconstructed by Colleps *et al.* [2018] who favor exposure of the Outer Lesser Himalaya after 16 Ma and of the Inner Lesser Himalaya after 11 Ma, although that study was again located in an area father east, within the wetter Ganges catchment, and need not apply to the drier Indus basin. A more erosive climate further east might favor earlier unroofing in that area. The erosion data support the concept of significant along strike diachroneity of unroofing.

Uplift of the Lesser Himalayan Duplex would have created a topographic barrier, susceptible to erosion as monsoon rains were focused along this topographic front. The increasing Himalayan character of the total zircon input comes at a time when the summer monsoon rains were generally weakening after ˜8 Ma [*Dettman et al.* , 2001], or after 7.7 Ma based on new environmental data from Site U1456 [*Clift et al.* , 2019a](Fig. 13). Moisture delivery to this area from the winter westerlies has also been shown to have reduced around 7 Ma [*Vögeli et al.* , 2017]. In the recent geologic past, since the LGM, strong Himalayan rather than Karakoram erosion has occurred when the summer monsoon was strong, during interglacial times and not when it was weak during glacial times [*Clift et al.* , 2008a]. The increase in Himalayan erosion over longer periods of time, correlating with the weakening monsoon, is the opposite of this shorter-term trend. It is possible that solid Earth tectonic forces, rather than climate, have dominated the long-term evolution of erosion, although the temporal correlation of provenance and aridity is suggestive of a climatic control.

All of the samples show the presence of very young zircons (<25 Ma) that possibly correlate with bedrock dates from Nanga Parbat, although these are never very numerous. It is also possible that some of these young ages may in fact be derived from erosion of fast exhuming rocks in parts of the southern Karakoram [*Wallis et al.* , 2014]. However, even if that this material was derived from Nanga Parbat, the low abundance of such zircon grains in the Laxmi Basin sediments would suggest that this massif was not generating very high proportions of sediment in the trunk Indus river, unlike the situation in the eastern syntaxis [*Garzanti*

et al. , 2004; *Stewart et al.* , 2008]. This is consistent with the U-Pb zircon ages in the modern Indus River downstream of Nanga Parbat [*Alizai et al.* , 2011] that show neither many <25 Ma zircons or older 1500–2300 Ma grains that would be associated with less deeply buried rocks but with the Lesser Himalayan affiliation typically made with Nanga Parbat [*Whittington et al.* , 1999].

We compare our detrital zircon budget with that of the Nd budget published by Clift *et al.* [2019b]. Translating zircon budgets into rock erosion budgets is not easy due to bedrock zircon fertility variations. However, whole-rock geochemical analysis of Alizai *et al.* [2012] suggested that on average the eastern, Himalaya-draining tributaries are around 2.2 times more fertile in zircon than the trunk Indus. If we simply use the source percentages from the zircon unmixing calculation described above and the average ε_{Nd} values for these different units then it is possible to predict the average composition of the bulk sediment through time. We use an ε_{Nd} value of -14.6 for the Greater and Tethyan Himalaya, -21.7 for the Lesser Himalaya, -9.3 for the Karakoram, -20 for Nanga Parbat and +5.1 for Kohistan and the Transhimalaya based on synthesis of the bedrock data, but especially the composition of river sediments that are derived from wide areas of these ranges [*Clift et al.* , 2002b]. Transhimalaya Nd data are from Rolland *et al.*[2002], Singh *et al.* [2002], and Khan *et al.*[1997]. Greater and Lesser Himalayan data are from Ahmad *et al.* [2000], Deniel *et al.* [1987], Inger *et al.*[1993] and Parrish and Hodges [1996]. Karakoram data are from Crawford and Searle [1992] and Schärer *et al.* [1990].

The results of this estimate are shown next to the smoothed long-term Nd isotope evolution from bulk sediment analysis [*Clift et al.* , 2019b] (Fig. 13). We account for the ±1 ε_{Nd}uncertainty value estimated from the Indus Quaternary [*Jonell et al.* , 2018]. We note that before 6 Ma the estimates overlap with the bulk sediment record that was derived from muddy lithologies, suggesting similar sources. After this time both the estimated and measured ε_{Nd} values became more negative. However, the predicted Nd isotope compositions are always more negative than those measured from the bulk sediment and this implies an over estimation in the flux from isotopically negative sources, i.e. the Himalaya, using the zircon method. This is consistent with the geochemical data indicating that the Himalaya are more abundant in zircon than the Karakoram, but have similar concentrations in Nd [*Alizai et al.* , 2011]. As a result, our zircon budget (Fig. 13) represents an overestimate of the influence of the Himalaya compared the Karakoram through time in terms of total rock eroded. Nonetheless, the overall trends in the two data sets are consistent and the reconstruction of increasing Himalayan erosion since the 5.72 Ma may be considered robust.

7. Conclusions

Sandy and silty sediments recovered from the Laxmi Basin in the Eastern Arabian Sea provide a relatively continuous erosional record derived from the Indus River and spanning the last 15.5 m.y. In this study samples were taken from IODP Sites U1456 and U1457 for geochemical and geochronological analyses. Detrital zircon grains were dated by U-Pb methods to determine their provenance. The sediments themselves are defined as wackes and are relatively immature in composition, with bulk sediment characters similar to those found in the Quaternary delta of the Indus and in its submarine Canyon. They are readily distinguishable from sediments on the Western Indian Shelf, confirming their derivation from the Indus River and not the peninsula with one exception. The sediments are mostly of silty sand to silt size, with only a few being classified as fine sand. Although the sediments are relatively depleted in Ca, Na and P relative to the upper continental crust this reflects chemical weathering during transport and does not affect the provenance analysis conducted here.

Detrital zircon U-Pb ages fall into a number of categories which can be correlated with bedrock sources in the Himalaya. The ubiquitous presence of zircon grains younger than 200 Ma requires the sediments to be the erosional products of the Himalaya/Karakoram and not peninsular India. The progressive increase in zircon grains dating at 350–1250 Ma, as well as 1500–2300 Ma, indicates that the erosional flux from the Himalaya increased through the studied time interval. Almost all the samples contain grains that could be derived from the Karakoram or from Kohistan, and there is an appearance of very young zircon grains, younger than 25 Ma, that is especially marked since 3.17 Ma. Such young zircon grains may be from Nanga Parbat or parts of the eastern Karakoram. Statistical analysis shows that there are a number of groupings and an increase

in Himalayan erosion through time. High flux from the Himalaya was noted at 7.99–7.78 Ma and starting between 7.0 and 5.87 Ma. Since 1.32 Ma the sediments are similar to the modern Indus River, but not like the glacial-era river, which has more similarities with the Miocene Laxmi Basin samples and with enhanced erosion in the Karakoram. Detrital zircon population unmixing techniques allow us to objectively confirm the progressive increase of Himalayan erosion relative to the Karakoram, and the sharp jump in erosion from the Inner Lesser Himalayas starting at 1.56 Ma. This is somewhat younger than the anticipated unroofing of these ranges derived from earlier foreland studies, although much of the earlier data comes from further east in the Ganges catchment. The shift to more Himalayan erosion through time occurs as the monsoon climate weakened, as well as when the Lesser Himalayan Duplex formed. This suggests that the changing patterns of erosion could be largely a function of solid Earth tectonic forces building topography, although the correlation of unroofing to the Late Miocene drying trend does raise the possible role for climate too, albeit in the opposite fashion to that seen since the LGM, when more Himalayan erosion correlates with strong summer monsoon rains.

References

Ahmad, T., N. Harris, M. Bickle, H. Chapman, J. Bunbury, and C. Prince (2000), Isotopic constraints on the structural relationships between the Lesser Himalayan Series and the High Himalayan Crystalline Series, Garhwal Himalaya, *Geol. Soc. Am. Bull.* , *112* (3), 467-477.

Alizai, A., A. Carter, P. D. Clift, S. VanLaningham, J. C. Williams, and R. Kumar (2011), Sediment provenance, reworking and transport processes in the Indus River by U-Pb dating of detrital zircon grains, *Global Planet. Change* , *76* , 33-55, doi:10.1016/j.gloplacha.2010.11.008.

Alizai, A., S. Hillier, P. D. Clift, and L. Giosan (2012), Clay mineral variations in Holocene terrestrial sediments from the Indus Basin; a response to SW Asian Monsoon variability, *Quat. Res.* , *77* (3), 368–381, doi:10.1016/j.yqres.2012.01.008.

Amidon, W. H., D. W. Burbank, and G. E. Gehrels (2005), U-Pb zircon ages as a sediment mixing tracer in the Nepal Himalaya, *Earth Planet. Sci. Letts.* , *235* (1-2), 244-260.

Baral, U., D. Lin, and D. Chamlagain (2015), Detrital zircon U–Pb geochronology of the Siwalik Group of the Nepal Himalaya: implications for provenance analysis, *Intern. J. Earth Sci.* , 1-19, doi;10.1007/s00531-015-1198-7.

Bernet, M., P. van der Beek, R. Pik, P. Huyghe, J.-L. Mugnier, E. Labrin, et al. (2006), Miocene to Recent exhumation of the central Himalaya determined from combined detrital zircon fission-track and U/Pb analysis of Siwalik sediments, western Nepal, *Basin Res.* , *18* , 393–412, doi: 10.1111/j.1365-2117.2006.00303.x.

Bhattacharya, G. C. B., A. K. Chaubey, G. P. S. Murty, S. Srinivas, K. V. Sarma, V. Subrahmanyam, et al. (1994), Evidence for seafoor spreading in the Laxmi Basin, northeastern Indian Ocean, *Earth Planet. Sci. Letts.* , *125* , 211-220.

Bollinger, L., J. P. Avouac, O. Beyssac, E. J. Catlos, T. M. Harrison, M. Grove, et al. (2004), Thermal structure and exhumation history of the Lesser Himalaya in central Nepal, *Tectonics* , *23* (5), 19, doi:10.1029/2003TC001564.

Bookhagen, B., R. C. Thiede, and M. R. Strecker (2005), Late Quaternary intensified monsoon phases control landscape evolution in the northwest Himalaya, *Geology* , *33* (2), 149-152, doi:10.1130/G20982.1.

Burbank, D. W., A. E. Blythe, J. Putkonen, B. Pratt-Sitaula, E. Gabet, M. Oskins, et al. (2003), Decoupling of erosion and precipitation in the Himalayas, *Nature* , *426* , 652–655.

Caddick, M. J., M. J. Bickle, N. B. W. Harris, T. J. B. Holland, M. S. A. Horstwood, R. R. Parrish, et al. (2007), Burial and exhumation history of a Lesser Himalayan schist: Recording the formation of an inverted metamorphic sequence in NW India, *Earth Planet. Sci. Letts.* , *264* (3–4), 375–390, doi:10.1016/j.epsl.2007.09.011.

Caley, T., D. M. Roche, and H. Renssen (2014), Orbital Asian summer monsoon dynamics revealed using an isotope-enabled global climate model, *Nature Comm.* , *5* , 5371, doi:10.1038/ncomms6371.

Calvès, G., M. Huuse, P. D. Clift, and S. Brusset (2015), Giant fossil mass wasting off the coast of West India: The Nataraja submarine slide, *Earth Planet. Sci. Letts.* , *432* , 265–272, doi:10.1016/j.epsl.2015.10.022.

Catlos, E. J., T. M. Harrison, M. J. Kohn, M. Grove, F. J. Ryerson, C. E. Manning, et al. (2001), Geochronologic and thermobarometric constraints on the evolution of the Main Central Thrust, central Nepal Himalaya, *J. Geophys. Res.* , *106* (B8), 16,177-116,204.

Chirouze, F., P. Huyghe, C. Chauvel, P. van der Beek, M. Bernet, and J.-L. Mugnier (2015), Stable Drainage Pattern and Variable Exhumation in the Western Himalaya since the Middle Miocene, *J. Geol.* , *123* , 1–20, doi:10.1086/679305.

Clift, P., C. Gaedicke, R. Edwards, J. Lee, II, P. Hildebrand, S. Amjad, et al. (2002a), The stratigraphic evolution of the Indus Fan and the history of sedimentation in the Arabian Sea, *Mar. Geophys. Res.* , *23* (3), 223-245.

Clift, P. D. (2006), Controls on the erosion of Cenozoic Asia and the flux of clastic sediment to the ocean, *Earth Planet. Sci. Letts.* , *241* (3-4), 571-580.

Clift, P. D., and J. S. Blusztajn (2005), Reorganization of the western Himalayan river system after five million years ago, *Nature* , *438* (7070), 1001-1003.

Clift, P. D., I. H. Campbell, M. S. Pringle, A. Carter, X. Zhang, K. V. Hodges, et al. (2004), Thermochronology of the modern Indus River bedload; new insight into the control on the marine stratigraphic record, *Tectonics* , *23* (TC5013), doi:10.1029/2003TC001559.

Clift, P. D., L. Giosan, J. Blusztajn, I. H. Campbell, C. M. Allen, M. Pringle, et al. (2008a), Holocene erosion of the Lesser Himalaya triggered by intensified summer monsoon, *Geology* , *36* (1), 79–82, doi: 10.1130/G24315A.1.

Clift, P. D., L. Giosan, A. Carter, E. Garzanti, V. Galy, A. R. Tabrez, et al. (2010), Monsoon control over erosion patterns in the Western Himalaya: possible feed-backs into the tectonic evolution, in *Monsoon evolution and tectonic-climate linkage in Asia* , edited by P. D. Clift, R. Tada and H. Zheng, pp. 181–213, Geological Society, London.

Clift, P. D., K. Hodges, D. Heslop, R. Hannigan, L. V. Hoang, and G. Calves (2008b), Greater Himalayan exhumation triggered by Early Miocene monsoon intensification, *Nature Geosci.* , *1* , 875-880, doi:10.1038/ngeo351.

Clift, P. D., D. K. Kulhanek, P. Zhou, M. G. Bowen, S. M. Vincent, M. Lyle, et al. (2019a), Chemical Weathering and Erosion Responses to Changing Monsoon Climate in the Late Miocene of Southwest Asia, *Geol. Mag.* , doi:10.1017/S0016756819000608.

Clift, P. D., J. I. Lee, P. Hildebrand, N. Shimizu, G. D. Layne, J. Blusztajn, et al. (2002b), Nd and Pb isotope variability in the Indus River system; implications for sediment provenance and crustal heterogeneity in the western Himalaya, *Earth Planet. Sci. Letts.* , *200* (1-2), 91-106, doi:10.1016/S0012-821X(02)00620-9.

Clift, P. D., N. Shimizu, G. Layne, C. Gaedicke, H. U. Schlüter, M. K. Clark, et al. (2001), Development of the Indus Fan and its significance for the erosional history of the western Himalaya and Karakoram, *Geol. Soc. Am. Bull.* , *113* , 1039–1051.

Clift, P. D., P. Zhou, D. F. Stockli, and J. Blusztajn (2018), Regional Pliocene Exhumation of the Lesser Himalaya in the Indus Drainage, *Solid Earth* , doi:10.5194/se-2018-132.

Clift, P. D., P. Zhou, D. F. Stockli, and J. Blusztajn (2019b), Regional Pliocene Exhumation of the Lesser Himalaya in the Indus Drainage, *Solid Earth* , *10* , 647–661, doi:10.5194/se-10-647-2019.

Colleps, C. L., R. N. McKenzie, D. F. Stockli, N. C. Hughes, B. P. Singh, A. A. G. Webb, et al. (2018), Zircon (U-Th)/He thermochronometric constraints on Himalayan thrust belt exhumation, bedrock weathering, and Cenozoic seawater chemistry, *Geochem. Geophys. Geosyst.* , *19* , 257– 271, doi:10.1002/2017GC007191.

Colleps, C. L., D. F. Stockli, N. R. McKenzie, A. G. Webb, and B. K. Horton (2019), Neogene kinematic evolution and exhumation of the NW India Himalaya: Zircon geo-/thermochronometric insights from the fold-thrust belt and foreland basin, *Tectonics* , *38* , 2059–2086, 10.1029/2018TC005304.

Courtillot, V., Y. Gallet, R. Rocchia, G. Féraud, E. Robin, C. Hofmann, et al. (2000), Cosmic markers, 40Ar/39Ar dating and paleomagnetism of the KT sections in the Anjar Area of the Deccan large igneous province, *Earth Planet. Sci. Letts.* , *182* , 137-156.

Crawford, M. B., and M. P. Searle (1992), Field relationships and geochemistry of pre-collisional (India-Asia) granitoid magmatism in the central Karakoram, northern Pakistan, *Tectonophysics* , *206* (1-2), 171-192.

Dailey, S. K., P. D. Clift, D. K. Kulhanek, J. Blusztajn, C. M. Routledge, G. Calvès, et al. (2019), Large-scale Mass Wasting on the Miocene Continental Margin of Western India, *Geol. Soc. Am. Bull.* , doi:/10.1130/B35158.1.

DeCelles, P. G., G. E. Gehrels, Y. Najman, A. J. Martin, A. Carter, and E. Garzanti (2004), Detrital geochronology and geochemistry of Cretaceous-Early Miocene strata of Nepal: implications for timing and diachroneity of initial Himalayan orogenesis, *Earth Planet. Sci. Letts.* , *227* (3-4), 313-330.

DeCelles, P. G., G. E. Gehrels, J. Quade, B. LaReau, and M. Spurlin (2000), Tectonic implications of U-Pb zircon ages of the Himalayan orogenic belt in Nepal, *Science* , *288* (5465), 497-499, doi:10.1126/science.288.5465.497.

Deniel, C., P. Vidal, A. Fernandez, P. Fort, and J.-J. Peucat (1987), Isotopic study of the Manaslu granite (Himalaya, Nepal): inferences on the age and source of Himalayan leucogranites, *Contribs. Min. Petrol.* , *96* (1), 78-92.

Deptuck, M. E., D. J. Piper, B. Savoye, and A. Gervais (2008), Dimensions and architecture of late Pleistocene submarine lobes off the northern margin of East Corsica, *Sedimentology* , *55* (4), 869-898.

Dettman, D. L., M. J. Kohn, J. Quade, F. J. Ryerson, T. P. Ojha, and S. Hamidullah (2001), Seasonal stable isotope evidence for a strong Asian monsoon throughout the past 10.7 m.y, *Geology* , *29* (1), 31-34.

Dunlap, W. J., and R. Wysoczanski (2002), Thermal evidence for Early Cretaceous metamorphism in the Shyok suture zone and age of the Khardung volcanic rocks, Ladakh, India, *J. Asian Earth Sci.* , *20* (5), 481-490.

Dunlea, A. G., R. W. Murray, J. Sauvage, A. J. Spivack, R. N. Harris, and S. D'Hondt (2015), Dust, volcanic ash, and the evolution of the South Pacific Gyre through the Cenozoic, *Paleocean.* , *30* (8), 1078-1099, doi:10.1002/2015PA002829.

Fedo, C. M., H. W. Nesbitt, and G. M. Young (1995), Unraveling the effects of potassium metasomatism in sedimentary rocks and paleosols, with implications for paleoweathering conditions and provenance, *Geology* , *23* , 921–924.

Fleitmann, D., S. J. Burns, M. Mudelsee, U. Neff, J. Kramers, A. Mangini, et al. (2003), Holocene forcing of the Indian monsoon recorded in a stalagmite from southern Oman, *Science* , *300* (5626), 1737-1739.

Folk, R. L. (1974), *Petrology of Sedimentary Rocks* , 182 pp., Hemphill Press, Austin, Texas.

Fraser, J. E., M. P. Searle, R. R. Parrish, and S. R. Noble (2001), Chronology of deformation, metamorphism, and magmatism in the southern Karakoram Mountains, *Geol. Soc. Am. Bull.* , *113* (11), 1443-1455.

Gaedicke, C., H.-U. Schlueter, H.-A. Roeser, A. Prexl, B. Schreckenberger, H. Meyer, et al. (2002), Origin of the northern Indus Fan and Murray Ridge, northern Arabian Sea; interpretation from seismic and magnetic imaging, *Tectonophysics* , *355* , 127-143.

Garzanti, E., S. Andò, and G. Vezzoli (2009), Grain-size dependence of sediment composition and environmental bias in provenance studies, *Earth Planet. Sci. Letts.* , *277* (3-4), 422-432.

Garzanti, E., A. Baud, and G. Mascle (1987), Sedimentary record of the northward flight of India and its collision with Eurasia (Ladakh Himalaya, India), *Geodin. Acta* , *1* (4/5), 297–312.

Garzanti, E., W. Liang, S. Andò, P. D. Clift, A. Resentini, P. Vermeesch, et al. (2020), Provenance of Thal Desert sand: Focused erosion in the western Himalayan syntaxis and foreland-basin deposition driven by latest Quaternary climate change, *Earth Sci. Rev.* , *207* , 103220, doi:10.1016/j.earscirev.2020.103220.

Garzanti, E., G. Vezzoli, S. Ando, C. France-Lanord, S. K. Singh, and G. Foster (2004), Sand petrology and focused erosion in collision orogens: the Brahmaputra case, *Earth Planet. Sci. Letts.* , *220* (1-2), 157-174.

Garzanti, E., G. Vezzoli, S. Ando, P. Paparella, and P. D. Clift (2005), Petrology of Indus River sands; a key to interpret erosion history of the western Himalayan syntaxis, *Earth Planet. Sci. Letts.* , *229* (3-4), 287-302, doi: 10.1016/j.epsl.2004.11.008.

Gehrels, G. (2012), Detrital Zircon U-Pb Geochronology: Current Methods and New Opportunities, in *Tectonics of Sedimentary Basins* , edited by C. Busby and A. Azor, pp. 47-62, Wiley, doi:10.1002/9781444347166.ch2.

Gehrels, G. E., P. Kapp, P. DeCelles, A. Pullen, R. Blakely, A. Weislgel, et al. (2011), Detrital zircon geochronology of pre-Tertiary strata in the Tibetan-Himalayan orogen, *Tectonics* , *30* (TC5016), doi:10.1029/2011TC002868.

Gehrels, G. E., V. Valencia, and J. Ruiz (2008), Enhanced precision, accuracy, efficiency, and spatial resolution of U-Pb ages by laser ablation–multicollector–inductively coupled plasma–mass spectrometry, *Geochem. Geophys. Geosyst.* , *9* (Q03017), doi:10.1029/2007GC001805.

Guidry, M. W., and F. T. Mackenzie (2000), Apatite weathering and the Phanerozoic phosphorus cycle, *Geology* , *28* (7), 631-634.

Gupta, A. K., D. M. Anderson, and J. T. Overpeck (2003), Abrupt changes in the Asian southwest monsoon during the Holocene and their links to the North Atlantic Ocean, *Nature* , *421* , 354–356.

Hart, N. R., D. F. Stockli, and N. W. Hayman (2016), Provenance evolution during progressive rifting and hyperextension using bedrock and detrital zircon U-Pb geochronology, Mauleon Basin, western Pyrenees, *Geosphere* , *12* (4), 1166-1186, doi:10.1130/GES01273.1.

Herron, M. M. (1988), Geochemical classification of terrigenous sands and shales from core or log data, *J. Sed. Petrol.* , *58* , 820–829.

Hildebrand, P. R., S. R. Noble, M. P. Searle, D. J. Waters, and R. R. Parrish (2001), Old origin for an active mountain range; geology and geochronology of the eastern Hindu Kush, Pakistan, *Geol. Soc. Am. Bull.* , *113* (5), 625-639.

Hodges, K. (2003), Geochronology and thermochronology in orogenic systems, in *The Crust* , edited by R. Rudnick, pp. 263-292, Elsevier-Science, Amsterdam.

Hodges, K. V. (2000), Tectonics of the Himalaya and southern Tibet from two perspectives, *Geol. Soc. Am. Bull.* , *112* (3), 324-350.

Honegger, K., V. Dietrich, W. Frank, A. Gansser, M. Thoni, and V. F. Trommsdorf (1982), Magmatism and metamorphism in the Ladakh Himalayas (The Indus-Tsangpo suture zone), *Earth Planet. Sci. Letts.* ,*60* , 178-194.

Howell, A. L., S. J. Bentley, K. Xu, R. E. Ferrell, Z. Muhammad, and E. Septama (2014), Fine sediment mineralogy as a tracer of latest Quaternary sediment delivery to a dynamic continental margin: Pandora Trough, Gulf of Papua, Papua New Guinea, *Mar. Geol.* , *357* , 108-122, doi:10.1016/j.margeo.2014.08.003.

Hu, X., E. Garzanti, J. Wang, W. Huang, W. An, and A. Webb (2016), The timing of India-Asia collision onset – Facts, theories, controversies,*Earth Sci. Rev.* , *160* , 264-299, doi:10.1016/j.earscirev.2016.07.014.

Huyghe, P., A. Galy, J.-L. Mugnier, and C. France-Lanord (2001), Propagation of the thrust system and erosion in the Lesser Himalaya: Geochemical and sedimentological evidence, *Geology* ,*29* (11), 1007–1010.

Inger, S., and N. Harris (1993), Geochemical constraints on leucogranite magmatism in the Langtang Valley, Nepal Himalaya, *J. Petrol.* ,*34* (2), 345-368.

Jackson, S. E., N. J. Pearson, W. L. Griffin, and E. A. Belousova (2004), The application of laser ablation-inductively coupled plasma-mass spectrometry (LA-ICP-MS) to in situ U–Pb zircon geochronology, *Chem. Geol.* , *211* , 47–69.

Jaeger, J.-J., V. Courtillot, and P. Tapponnier (1989), Paleontological view of the ages of the Deccan Traps, the Cretaceous/Tertiary boundary, and the India-Asia collision, *Geology* , *17* (4), 316-319, doi:10.1130/0091-7613(1989)017<0316:Pvotao>2.3.Co;2.

Jonell, T. N., A. Carter, P. Boning, K. Pahnke, and P. D. Clift (2017), Climatic and glacial impact on erosion patterns and sediment provenance in the Himalayan rain shadow, Zanskar River, NW India, *Geol. Soc. Am. Bull.* , *129* (7-8), 820-836, doi:10.1130/B31573.

Jonell, T. N., Y. Li, J. Blusztajn, L. Giosan, and P. D. Clift (2018), Signal or noise? Isolating grain size effects on Nd and Sr isotope variability in Indus delta sediment provenance, *Chem. Geol.* ,*485* , 56–73, doi:10.1016/j.chemgeo.2018.03.036.

Khan, M. A., R. J. Stern, R. F. Gribble, and B. F. Windley (1997), Geochemical and isotopic constraints on subduction polarity, magma sources, and palaeogeography of the Kohistan intra-oceanic arc, northern Pakistan Himalaya, *J. Geol. Soc.* , *154* , 935–946.

Khim, B.-K., K. Horikawa, Y. Asahara, J.-E. Kim, and M. Ikehara (2019), Detrital Sr-Nd isotopes, sediment provenances, and depositional processes in the Laxmi Basin of the Arabian Sea during the last 800 kyrs, *Geol. Mag.* , 1-13, doi:10.1017/S0016756818000596.

Klootwijk, C. T., J. S. Gee, J. W. Peirce, G. M. Smith, and P. L. McFadden (1992), An early India-Asia contact: Paleomagnetic constraints from Ninetyeast Ridge, ODP Leg 121, *Geology* , *20* (5), 395-398, DOI: 10.1130/0091-7613(1992)020.

Kolla, V., and F. Coumes (1987), Morphology, internal structure, seismic stratigraphy, and sedimentation of Indus Fan, *AAPG Bull.* ,*71* , 650–677.

Krol, M. A., P. K. Zeitler, and P. Copeland (1996), Episodic unroofing of the Kohistan Batholith, Pakistan: Implications from K-feldspar thermochronology, *J. Geophys. Res.-Solid Earth* , *101* (B12), 28149-28164.

Kurian, S., B. N. Nath, N. C. Kumar, and K. K. C. Nair (2013), Geochemical and Isotopic Signatures of Surficial Sediments from the Western Continental Shelf of India: Inferring Provenance, Weathering, and the Nature of Organic Matter Geochemical and Isotopic Signatures of Sediments From The Indian West Coast, *J. Sed. Res.* , *83* (6), 427-442, doi:10.2110/jsr.2013.36.

Lave, J., and J. P. Avouac (2000), Active folding of fluvial terraces across the Siwaliks Hills (Himalayas of central Nepal), *J. Geophys. Res.* , *105* , 5735–5770, doi: 10.1029/1999JB900292.

Lawrence, R. L., R. Cox, R. W. Mapes, and D. S. Coleman (2011), Hydrodynamic fractionation of zircon age populations, *GSA Bulletin* , *123* (1-2), 295-305, doi:10.1130/B30151.1.

Le Fort, P., F. Debon, and J. Sonet (1983), Petrography, geochemistry and geochronology of some samples from the Karakoram Batholith (N. Pakistan), in *Granites of the Himalayas, Karakoram and Hindu Kush* , edited by F. A. Shams, pp. 377–387, Punjab University, Lahore, Pakistan.

Li, Y., P. D. Clift, P. Böning, J. Blusztajn, R. W. Murray, T. Ireland, et al. (2018), Continuous Signal Propagation in the Indus Submarine Canyon since the Last Deglacial, *Mar. Geol.* , *406* , 159–176, doi:10.1016/j.margeo.2018.09.011.

Li, Y., P. D. Clift, and P. O'Sullivan (2019), Millennial and Centennial Variations in Zircon U-Pb and Apatite Fission Track Ages in the Quaternary Indus Submarine Canyon, *Basin Res.* , *31* , 155–170, doi:10.1111/bre.12313.

Malusà, M. G., A. Resentini, and E. Garzanti (2016), Hydraulic sorting and mineral fertility bias in detrital geochronology, *Gondwana Res.* , *31* , 1-19, doi:10.1016/j.gr.2015.09.002.

Marsh, A. D., W. G. Parker, D. F. Stockli, and J. W. Martz (2019), Regional correlation of the Sonsela Member (Upper Triassic Chinle Formation) and detrital U-Pb zircon data from the Sonsela Sandstone bed near the Sonsela Buttes, northeastern Arizona, USA, support the presence of a distributive fluvial system, *Geosphere* , *15* (4), 1128-1139, doi:10.1130 /GES02004.1.

Marsh, J. H., and D. F. Stockli (2015), Zircon U–Pb and trace element zoning characteristics in an anatectic granulite domain: Insights from LASS-ICP-MS depth profiling, *Lithos* , *239* , 170-185, doi:10.1016/j.lithos.2015.10.017.

Molnar, P. (2001), Climate change, flooding in arid environments, and erosion rates, *Geology* , *29* (12), 1071-1074.

Mukhopadhyay, G., S. Mukhopadhyay, M. Roychowdhury, and P. Parui (2010), Stratigraphic correlation between different Gondwana basins of India,*J. Geol. Soc. India* , *76* (3), 251-266.

Myrow, P. M., N. C. Hughes, L. A. Derry, R. N. McKenzie, G. Jiang, A. A. G. Webb, et al. (2015), Neogene marine isotopic evolution and the erosion of Lesser Himalayan strata: Implications for Cenozoic tectonic history, *Earth Planet. Sci. Letts.* , *417* , 142-150, doi:10.1016/j.epsl.2015.02.016.

Najman, Y. (2006), The detrital record of orogenesis: A review of approaches and techniques used in the Himalayan sedimentary basins,*Earth Sci. Rev.* , *74* (1-2), 1-72.

Najman, Y., E. Appel, M. Boudagher-Fadel, P. Bown, A. Carter, E. Garzanti, et al. (2010), Timing of India-Asia collision: Geological, biostratigraphic, and palaeomagnetic constraints, *J. Geophys. Res.* , *115* (B12416), doi:10.1029/2010JB007673.

Najman, Y., M. Bickle, E. Garzanti, M. Pringle, D. Barfod, N. Brozovic, et al. (2009), Reconstructing the exhumation history of the Lesser Himalaya, NW India, from a multitechnique provenance study of the foreland basin Siwalik Group, *Tectonics* , *28* (TC5018), doi:10.1029/2009TC002506.

Najman, Y., D. Jenks, L. Godin, M. Boudagher-Fadel, I. Millar, E. Garzanti, et al. (2017), The Tethyan Himalayan detrital record shows that India–Asia terminal collision occurred by 54 Ma in the Western Himalaya, *Earth Planet. Sci. Letts.* , *459* , 301-310, doi:10.1016/j.epsl.2016.11.036.

Nesbitt, H. W., G. Markovics, and R. C. Price (1980), Chemical processes affecting alkalis and alkaline earths during continental weathering,*Geochim. Cosmochim. Acta* , *44* , 1659–1666.

Pandey, D. K., P. D. Clift, D. K. Kulhanek, S. Ando, J. A. P. Bendle, S. Bratenkov, et al. (2016a), Site U1456, in *Arabian Sea Monsoon. Proceedings of the International Ocean Discovery Program* , edited by D. K. Pandey, P. D. Clift and D. K. Kulhanek, International Ocean Discovery Program, College Station, TX, doi:10.14379/iodp.proc.355.103.2016.

Pandey, D. K., P. D. Clift, D. K. Kulhanek, S. Ando, J. A. P. Bendle, S. Bratenkov, et al. (2016b), Site U1457, in *Arabian Sea Monsoon. Proceedings of the International Ocean Discovery Program* , edited by D. K. Pandey, P. D. Clift and D. K. Kulhanek, International Ocean Discovery Program, College Station, TX, doi:10.14379/iodp.proc.355.104.2016.

Pandey, D. K., P. D. Clift, D. K. Kulhanek, and Expedition 355 Scientists (2016c), Arabian Sea Monsoon, *Proc. Int. Ocean Disc. Prog.* , *355* , doi:10.14379/iodp.proc.355.2016.

Pandey, D. K., P. D. Clift, D. K. Kulhanek, and Expedition 355 Scientists (2016d), Arabian Sea Monsoon: Expedition Summary, *Proc. Int. Ocean Disc. Prog.* , *355* , 1-32, doi:10.14379/iodp.proc.355.101.2016.

Pandey, O. P., P. K. Agrawal, and J. G. Negi (1995), Lithospheric structure beneath Laxmi Ridge and late Cretaceous geodynamic events,*Geo-Mar. Lett.* , *15* , 85-91.

Parrish, R. R., and K. V. Hodges (1996), Isotopic constraints on the age and provenance of the Lesser and Greater Himalayan sequences, Nepalese Himalaya, *Geol. Soc. Am. Bull.* , *108* (7), 904-911.

Parrish, R. R., and R. Tirrul (1989), U-Pb age of the Baltoro Granite, Northwest Himalaya, and implications for monazite U-Pb systematics,*Geology* , *17* , 1076–1079.

Paton, C., J. Hellstrom, B. Paul, J. Woodhead, and J. Hergt (2011), Iolite: Freeware for the visualisation and processing of mass spectrometric data, *J. Analyt. Atom. Spect.* , *26* (12), 2508–2518.

Petrus, J. A., and B. S. Kamber (2012), VizualAge: A novel approach to laser ablation ICP-MS U-Pb geochronology data reduction, *Geostand. Geoanalyt. Res.* , *36* (3), 247–270.

Quade, J., T. E. Cerling, and J. R. Bowman (1989), Development of Asian monsoon revealed by marked ecological shift during the latest Miocene in northern Pakistan, *Nature* , *342* (6246), 163-166.

Ravikant, V., F. Y. Wu, and W. Q. Ji (2009), Zircon U-Pb and Hf isotopic constraints on petrogenesis of the Cretaceous-Tertiary granites in eastern Karakoram and Ladakh, India, *Lithos* , *110* , 153-166.

Roddaz, M., A. Said, S. p. Guillot, P. O. Antoine, J. M. Montel, F. Martin, et al. (2011), Provenance of Cenozoic sedimentary rocks from the Sulaiman fold and thrust belt, Pakistan: implications for the palaeo-geography of the Indus drainage system, *J. Geol. Soc.* ,*168* , 499-516 doi: 10.1144/0016-76492010-100.

Rolland, Y., C. Picard, A. Pecher, H. Lapierre, D. Bosch, and F. Keller (2002), The Cretaceous Ladakh arc of NW himalaya—slab melting and melt–mantle interaction during fast northward drift of Indian Plate,*Chem. Geol.* , *182* , 139–178.

Routledge, C. M., D. K. Kulhanek, L. Tauxe, G. Scardia, A. D. Singh, S. Steinke, et al. (2019), Revised geological timescale for IODP Sites U1456 and U1457, *Geol. Mag.* , doi:10.1017/S0016756819000104.

Scharer, U., P. Copeland, T. M. Harrison, and M. P. Searle (1990), Age, cooling history, and origin of post-collisional leucogranites in the Karakoram Batholith; a multi-system isotope study, *J. Geol.* ,*98* (2), 233-251.

Scharer, U., R.-H. Xu, and C. J. Allegre (1984), U-Pb geochronology of Gangdese (Transhimalaya) plutonism in the Lhasa-Xigaze region, Tibet,*Earth Planet. Sci. Letts.* , *69* (2), 311-320.

Searle, M. P. (1996), Cooling history, erosion, exhumation and kinematics of the Himalaya-Karakoram-Tibet orogenic belt, in *The Tectonic Evolution of Asia* , edited by A. Yin and T. M. Harrison, pp. 110-137, Cambridge University Press, Cambridge.

Searle, M. P., and R. J. Phillips (2007), Relationships between right-lateral shear along the Karakoram Fault and metamorphism, magmatism, exhumation and uplift; evidence from the K2-Gasherbrum-Pangong ranges, north Pakistan and Ladakh, *J. Geol. Soc.* , *164* (2), 439-450.

Searle, M. P., A. J. Rex, R. Tirrul, D. C. Rex, A. Barnicoat, and B. F. Windley (1989), Metamorphic, magmatic and tectonic evolution of the Central Karakoram in the Biafo-Baltoro-Hushe regions of north Pakistan,*Geol. Soc. America Spec. Pap.* , *232* , 47-73.

Shanmugam, G., and R. Moiola (1991), Types of submarine fan lobes: models and implications (1), *AAPG Bull.* , *75* (1), 156-179.

Shuaib, S. M. (1982), Geology and hydrocarbon potential of offshore Indus Basin, Pakistan, *AAPG Bull.* , *66* , 940–946.

Singh, S., R. Kumar, M. E. Barley, and A. K. Jain (2007), SHRIMP U–Pb ages and depth of emplacement of Ladakh batholith, eastern Ladakh, India, *J. Asian Earth Sci.* , *30* (3), 490–503.

Singh, S., B. Parkash, A. K. Awasthi, and S. Kumar (2011), Late Miocene record of palaeovegetation from Siwalik palaeosols of the Ramnagar sub-basin, India, *Current Sci.* , *100* (2), 213-222.

Singh, S. K., and C. France-Lanord (2002), Tracing the distribution of erosion in the Brahmaputra watershed from isotopic compositions of stream sediments, *Earth Planet. Sci. Letts.* , *202* (3-4), 645-662.

Spencer, C. J., C. L. Kirkland, and R. J. M. Taylor (2016), Strategies towards statistically robust interpretations of in situ U–Pb zircon geochronology, *Geoscience Frontiers* , *7* (4), 581-589, doi:10.1016/j.gsf.2015.11.006.

Stephenson, B. J., M. P. Searle, D. J. Waters, and D. C. Rex (2001), Structure of the Main Central Thrust zone and extrusion of the High Himalayan deep crustal wedge, Kishtwar-Zanskar Himalaya, *J. Geol. Soc.* , *158* (4), 637-652.

Stewart, R. J., B. Hallet, P. K. Zeitler, M. A. Malloy, C. M. Allen, and D. Trippett (2008), Brahmaputra sediment flux dominated by highly localized rapid erosion from the easternmost Himalaya, *Geology* ,*36* (9), 711–714, doi: 10.1130/G24890A.1.

Sundell, K., and J. E. Saylor (2017), Unmixing detrital geochronology age distributions, *Geochem. Geophys. Geosyst.* , *18* , 2872–2886.

Taylor, S. R., and S. M. McLennan (1995), The geochemical evolution of the continental crust, *Rev. Geophys.* , *33* , 241–265.

Thiede, R. C., B. Bookhagen, J. R. Arrowsmith, E. R. Sobel, and M. R. Strecker (2004), Climatic control on rapid exhumation along the Southern Himalayan Front, *Earth Planet. Sci. Letts.* , *222* (3-4), 791-806.

Thiede, R. C., T. A. Ehlers, B. Bookhagen, and M. R. Strecker (2009), Erosional variability along the northwest Himalaya, *J. Geophys. Res.* , *114* (F01015), doi:10.1029/2008JF001010.

Vermeesch, P. (2004), How many grains are needed for a provenance study?, *Earth Planet. Sci. Letts.* , *224* , 351–441.

Vermeesch, P., A. Resentini, and E. Garzanti (2016), An R package for statistical provenance analysis, *Sed. Geol.* , *336* , 14-25, doi:10.1016/j.sedgeo.2016.01.009.

Vogeli, N., Y. Najman, P. van der Beek, P. Huyghe, P. M. Wynn, G. Govin, et al. (2017), Lateral variations in vegetation in the Himalaya since the Miocene and implications for climate evolution, *Earth Planet. Sci. Letts.* , *471* , 1–9, doi:10.1016/j.epsl.2017.04.037.

Wallis, D., A. Carter, R. J. Phillips, A. J. Parsons, and M. P. Searle (2016), Spatial variation in exhumation rates across Ladakh and the Karakoram: New apatite fission track data from the Eastern Karakoram, NW India, *Tectonics* , *35* , 704–721, doi:10.1002/2015TC003943.

Wallis, D., R. J. Phillips, and G. E. Lloyd (2014), Evolution of the Eastern Karakoram Metamorphic Complex, Ladakh, NW India, and its relationship to magmatism and regional tectonics, *Tectonophysics*, *626*, 41–52, doi:10.1016/j.tecto.2014.03.023.

Webb, A. A. G. (2013), Preliminary palinspastic reconstruction of Cenozoic deformation across the Himachal Himalaya (northwestern India), *Geosphere*, *9*, 572-587.

Weinberg, R. F., and W. J. Dunlap (2000), Growth and Deformation of the Ladakh Batholith, Northwest Himalayas: Implications for Timing of Continental Collision and Origin of Calc-Alkaline Batholiths, *J. Geol.*, *108*, 303–320, DOI: 10.1086/314405.

Whipple, K. X. (2009), The influence of climate on the tectonic evolution of mountain belts *Nature Geosci.*, *2*, 1-8, doi: 10.1038/ngeo413.

White, A. F., and S. L. Brantley (1995), *Chemical weathering rates of silicate minerals*, 581 pp., Mineralogical Society of America.

Whittington, A., G. Foster, N. Harris, D. Vance, and M. Ayres (1999), Lithostratigraphic correlations in the western Himalaya - An isotopic approach, *Geology*, *27* (7), 585-588.

Wilson, S. A. (1997), Data compilation for USGS reference material BHVO-2, Hawaiian Basalt, *U.S. Geol. Surv. Open-File Rept*.

Wobus, C. W., K. V. Hodges, and K. X. Whipple (2003), Has focused denudation sustained active thrusting at the Himalayan topographic front?, *Geology*, *31* (10), 861-864.

Yang, S., F. Zhang, and Z. Wang (2012), Grain size distribution and age population of detrital zircons from the Changjiang (Yangtze) River system, China, *Chem. Geol.*, *296-297*, 26-38.

Yin, A., C. S. Dubey, T. K. Kelty, A. A. G. Webb, T. M. Harrison, C. Y. Chou, et al. (2010), Geologic correlation of the Himalayan orogen and Indian craton: Part 2. Structural geology, geochronology, and tectonic evolution of the Eastern Himalaya, *GSA Bulletin*, *122* (3-4), 360-395, 10.1130/B26461.1.

Zeilinger, G., J. P. Burg, U. Schaltegger, and D. Seward (2001), New U/Pb and fission track ages and their implication for the tectonic history of the lower Kohistan Arc Complex, northern Pakistan, *J. Asian Earth Sci.*, *19* (3S), 79-81.

Zeitler, P. K., and C. P. Chamberlain (1991), Petrogenetic and Tectonic Significance of Young Leukogranites from the Northwestern Himalaya, Pakistan, *Tectonics*, *10* (4), 729-741.

Zeitler, P. K., C. P. Chamberlain, and H. A. Smith (1993), Synchronous Anatexis, Metamorphism, and Rapid Denudation at Nanga-Parbat (Pakistan Himalaya), *Geology*, *21* (4), 347-350.

Zeitler, P. K., J. F. Sutter, I. S. Williams, R. E. Zartman, and R. A. K. Tahirkheli (1989), Geochronology and temperature history of the Nanga Parbat-Haramosh Massif, Pakistan, in *Tectonics of the western Himalayas*, edited by L. L. Malinconico and R. J. Lillie, pp. 1–22, Geological Society of America, Boulder, CO.

Zhou, P., A. Carter, Y. Li, and P. D. Clift (2019), Slowing Rates of Regional Exhumation in the Western Himalaya: Fission Track Evidence from the Indus Fan, *Geol. Mag.*, doi:10.1017/S001675681900092X.

Zhuang, G., Y. Najman, S. Guillot, M. Roddaz, P.-O. Antoine, G. Metaise, et al. (2015), Constraints on the collision and the pre-collision tectonic configuration between India and Asia from detrital geochronology, thermochronology, and geochemistry studies in the lower Indus basin, Pakistan, *Earth Planet. Sci. Letts.*, *432*, 363–373, doi:10.1016/j.epsl.2015.10.026.

Zhuang, G., Y. Najman, Y. Tian, A. Carter, L. Gemignani, J. Wijbrans, et al. (2018), Insights into the evolution of the Hindu Kush-Kohistan-Karakoram from modern river sand detrital geo- and thermochronological studies, *J. Geol. Soc.*, doi:10.1144/jgs2018-007.

Figure Captions

Figure 1. A) Shaded bathymetric and topographic map of the Arabian Sea and surrounding area showing the location of the drilling sites considered by this study. Map also shows the major tributary systems of the Indus River, as well as smaller peninsular India rivers and their source mountains. B) Inset map shows detail of the Laxmi Basin and location of the drill sites considered in this study. Numbered red circles indicate existing scientific boreholes from Deep Sea Drilling Project (DSDP) and Ocean Drilling Program (ODP). KK = Karakoram; NP = Nanga Parbat. C) Geological map of the western Himalaya showing the major tectonic units that are eroded by the Indus River and its tributaries. Map is modified after Garzanti *et al.* [2005]. Rivers as shown in thick black lines. ISZ = Indus Suture Zone, MCT = Main Central Thrust, MBT = Main Boundary Thrust and MFT = Main Frontal Thrust. Thick black line shows the boundary of the Indus drainage, while thinner lines demark the limits of the major Himalayan tributaries. Figure is modified from Clift *et al.* [2019b].

Figure 2. Simplified lithologic logs of the two drill sites considered in this study. Black arrows show the location of the samples analyzed. Modified from Pandey *et al.* [2016c]. Pale shaded intervals show inferred lithologies based on small amounts of recovered core. Because induration is progressive and there is no sharp division, we make no attempt to distinguish between sediments and indurated rocks. Numerical ages are from Pandey *et al.* [2016a] for Site U1456 and from Pandey *et al.* [2016b] for Site U1457, with updates from Routledge *et al.* [2019].

Figure 3. Grainsize range of all samples analyzed for U-Pb zircon dating from the Laxmi Basin shown on the scheme of Folk [1974]. Samples are marked to show those published by Clift *et al.* [2019b], rather than presented new here (Table 2). Note the dominance of silty sand and sandy silt in the analyzed samples.

Figure 4. Detailed grain size spectra showing the range of sizes of the different samples considered within this study. Most of the sediment is fine sand to coarse silt in size and typically shows a coarse-skewed. A) Samples younger than 7 Ma, b) samples older than 7 Ma. Samples are marked to show those published by Clift *et al.*[2019b](gray text labels and white ringed symbol), rather than presented new here (Table 2) (black text labels and black ringed symbol).

Figure 5. (A) Geochemical signature of the analyzed samples illustrated by a CN-A-K ternary diagram [Fedo *et al.* , 1995]. CN denotes the mole weight of Na_2O and CaO* (CaO* represent the CaO associated with silicate, excluding all the carbonate). A and K indicate the content of Al_2O_3 and K_2O respectively. Samples closer to A are rich in kaolinite, chlorite and/or gibbsite (representing by kao, chl and gib). CIA values are also calculated and shown on the left side, with its values are correlated with the CN-A-K. Samples from the delta have the lowest values of CIA and indicates high contents of CaO and Na_2O and plagioclase. Abbreviations: sm (smectite), pl (plagioclase), ksp (K-feldspar), il (illite), m (muscovite). B) Geochemical classification of sediments from this study as well as those from the Indus delta [*Clift et al.* , 2010], Indus Canyon [Li *et al.* , 2018] and western Indian shelf [Kurian *et al.* , 2013] following the scheme of Herron [1988].

Figure 6. Cross plot of Zr concentration against median sample grain size. No strong correlation is observed.

Figure 7. Kernal density estimate (KDE) diagram showing the range of the zircon U-Pb ages for individual sand grains back to 3000 Ma. Colored strips show the range of populations with diagnostic links to critical source terrains in the headwaters of the Indus. Data from the Siwaliks, as well as the Tethyan, Greater and Lesser Himalaya are compiled from DeCelles *et al.* [2004]. Karakoram data is from is from Le Fort *et al.* [1983], Parrish and Tirrul [1989], Scharer *et al.* [1990], Fraser *et al.* [2001] and Ravikant *et al.* [2009]. Nanga Parbat data is from Zeitler and Chamberlain [1991] and Zeitler *et al.* [1993]. Transhimalayan data is from Honegger *et al.* [1982], Scharer*et al.* [1984], Krol *et al.* [1996], Weinberg and Dunlap [2000], Zeilinger *et al.* [2001], Dunlap and Wysoczanski [2002], Singh *et al.* [2007], and Ravikant*et al.* [2009]. Samples are marked to show those published by Clift *et al.* [2019b], and those presented new here.

Figure 8. Kernal density estimate (KDE) diagram showing the range of the zircon U-Pb ages for individual sand grains back to 200 Ma. Colored strips show the range of populations with diagnostic links to critical source terrains in the headwaters. See Figure 6 caption for data sources.

23

Figure 9. Upper continental crust normalized compositions of the sediments whose zircons are the focus of the study. Bulk settlement compositions are normalized according to the average of the continental crust from Taylor and McLennan [1995].

Figure 10. Plots of relative abundance of provenance sensitive zircon age populations in individual samples compared with sample median grain size. The coarsest samples show preference for the oldest U-Pb ages and a relative lack of the younger populations.

Figure 11. Multidimensional scalar (MDS) diagrams made from zircon U-Pb age data showing (A) how the different sediment samples from IODP Expedition 355 compare with one another and post-glacial sediments from the Indus delta (TH-10-8 and KB-40-4) and (B) with the major source terranes in the Indus catchment, as well as the modern rivers of the Indus catchment, i.e., the main or trunk stream of the Indus, upstream of Attock, and its major eastern tributaries. Solid lines join sediments to their most similar neighbor, while dashed lines join the next most similar. Sources of bedrock age data come from the literature, as described in Figure 6. River data is from Alizai *et al.*[2011]. Note that sediments older than 5 Ma plot towards the right in Figure 10B, in the direction of Karakoram bedrock sources, whereas there is a progressive migration towards the left, towards Himalayan sources after that time. Diagram was constructed using the statistical package of Vermeesch *et al.* [2016].

Figure 12. Pie diagrams showing the predicted source compositions of the zircon populations in sands from the Laxmi Basin as unmixed using the software of Sundell and Saylor [2017]. Note the significant reduction in flux from the Karakoram starting ~5.72 and again at 3.02 Ma. Samples are marked to show those published by Clift *et al.* [2019b], and those presented new here.

Figure 13. Comparison of climate, erosion and exhumation proxies in the Himalaya. (a) Smoothed Nd isotope history for the Indus River with grey background showing effective uncertainties from Clift *et al.* [2018]. (b) Breakdown of the sources of detrital zircons based on the unmixing procedure of Sundell and Saylor [2017]. (c) Carbon isotope character of pedogenic carbonate in Pakistan as an indicator of dominant vegetation in the Potwar Plateau of Pakistan [Quade *et al.* , 1989], and NW India [*Singh et al.* , 2011]. (d) Relative exhumation rates of the Greater Himalaya tracked by bedrock Ar-Ar dating [*Clift et al.* , 2008b] and zircon fission track from foreland basin sediment [Chirouze *et al.* , 2015]. (e) Rates of sediment supply to the Arabian Sea calculated from regional seismic [*Clift* , 2006].

Table Captions

Table 1. Major elements major elements geochemical analysis of the samples considered in this study.

Table 2. Analytical results from the laser particle size analyzer for all bulk samples considered in this study.

Table 3. Analytical data for the zircon U-Pb dating of grains presented in this work.

Table 4. Results of the mixing modelling performed by the DZMix software of Sundell and Saylor [2017] on the detrital samples from the Laxmi Basin.

1   **Zircon U-Pb Age Constraints on the Exhumation of the Lesser Himalayas from the**
2   **Laxmi Basin, Arabian Sea**
3

4   **Peng Zhou[1,2], Daniel F. Stockli[3], Thomas Ireland[4], Richard W. Murray[5], Peter D. Clift[1]**

5

6   [1] Department of Geology and Geophysics, Louisiana State University, Baton Rouge, LA 70803,
7   USA

8   [2] Department of Physics, Geology, and Engineering Technology, Northern Kentucky University,
9   Highland Heights, KY 41099, USA

10 [3] Department of Geological Sciences, Jackson School of Geosciences, University of Texas,
11 Austin, TX 78712-1722, USA

12 [4] Department of Earth and Environment, Boston University, Boston, MA 02215, USA

13 [5] Woods Hole Oceanographic Institution, Woods Hole, MA 02543, USA

14

15 Corresponding author: Peter Clift (pclift@lsu.edu)

16 **Key Points:**

17 • First basin-wide study of how regional erosion patterns have changed through time since
18   15.5 Ma in the Western Himalaya and Karakoram.

19 • Geochemical and geochronological analyses show increased relative erosion from the
20   Himalaya compared to the Karakoram at 7.99–7.78 Ma.

21 • Changing patterns of erosion correlate with climatic drying at ~7.7–6.3 Ma, and relate to
22   solid Earth tectonic forces building topography.
23

24

25   **Abstract**

26   The Indus Fan, located in the Arabian Sea, contains the bulk of the sediment eroded from the
27   Western Himalaya and Karakoram. Scientific drilling in the Laxmi Basin by the International
28   Ocean Discovery Program (IODP) provides an erosional record from the Indus River drainage
29   dating back to 10.8 Ma, and with a single sample from 15.5 Ma. We dated detrital zircon grains
30   by U-Pb geochronology to reconstruct how erosion patterns changed through time. Long-term
31   increases in detrital zircon U-Pb components of 750–1200 Ma and 1500–2300 Ma show
32   increasing preferential erosion of the Himalaya relative to the Karakoram at 7.99–7.78 Ma and
33   more consistently starting by 5.87 Ma. An increase in the contribution of 1500–2300 Ma zircons
34   starting by 1.56 Ma indicates significant unroofing of the Inner Lesser Himalaya (ILH) by that
35   time. The trend in zircon U-Pb age populations is consistent with bulk sediment Nd isotope data
36   implies greater zircon fertility in Himalayan bedrock compared to the Karakoram and
37   Transhimalaya. The initial change in spatial erosion patterns at 7.0–5.87 Ma occurred during a
38   time of drying climate in the Indus foreland. The increase in ILH erosion postdates the onset of
39   dry-wet glacial-interglacial cycles suggesting some role for climate control. However, erosion
40   driven by rising topography in response to formation of the Lesser Himalayan thrust duplex,
41   especially during the Pliocene may also be important. The influence of the Nanga Parbat Massif
42   to the bulk sediment flux is modest, in contrast to the situation in the eastern Himalaya syntaxis.

43   Keywords: Erosion, zircon, monsoon, Himalaya.

44   **1 Introduction**

45   Collision between India and Eurasia, starting about 50–60 Ma [*Garzanti et al.*, 1987;
46   *Jaeger et al.*, 1989; *Klootwijk et al.*, 1992; *Najman et al.*, 2010], has resulted in the formation the
47   largest mountain ranges on Earth. The timing of collision remains controversial but is best
48   addressed by consideration of the stratigraphic record that shows the onset of mixed Indian-
49   Eurasian sediments. Sedimentary rocks in the central and eastern Himalaya imply initial collision
50   at 59 ± 1 Ma [*Hu et al.*, 2016]. Recent work combining Hf isotopes with U-Pb ages in zircon
51   grains from the Tethyan Himalaya now show that sediment eroded from Eurasia, rather than
52   oceanic island arcs, was reaching NW India by 54 Ma, requiring India-Eurasia collision before
53   than time [*Najman et al.*, 2017]. The Himalaya have continued to evolve both in topography and
54   structure as a result of ongoing tectonic deformation coupled with erosion, largely modulated by
55   the strength of summer monsoon rains [*Bookhagen et al.*, 2005; *Clift et al.*, 2008b; *Wobus et al.*,
56   2003]. Sediments eroded from the Western Himalaya has been deposited in the Arabian Sea
57   where they form the second largest sediment body on Earth, the Indus submarine fan [*Clift et al.*,
58   2001; *Kolla and Coumes*, 1987].

59   The sedimentary deposits of the Indus submarine fan represent an archive of the erosion
60   and weathering processes in the Western Himalaya since the onset of continental collision, at
61   least since ~45 Ma [*Clift et al.*, 2001]. While bedrocks exposed at the surface in the mountains
62   can be used to reconstruct the uplift and exhumation of those particular rock formations, the
63   submarine fan sedimentary record captures spatial and temporal variations of the long-term
64   history of denudation, albeit one buffered by sediment transport processes. Because older
65   portions of bedrocks have been completely removed by erosion and their exhumation history no

66 longer accessible, the sedimentary record becomes the only record of the earlier erosion and
67 exhumation history. Although this record is partially available in the Himalayan foreland basin,
68 these proximal, continental syn-tectonic deposits are more difficult to date at high resolution, and
69 the sequence is truncated by significant unconformities, and deformed by progressive
70 incorporation into the sub-Himalayan fold and thrust belt [*Najman*, 2006]. Moreover, any given
71 section in the accreted foreland basin can only represent the sediment deposited from paleo-
72 rivers that once flowed in front of the mountains in that region. As such a given section would
73 preserve a history of erosion in a limited catchment of a particular part of the mountains, but
74 does not provide a more integrated orogen-scale overview.

75   Sediments from the western Himalaya are delivered to the Arabian Sea by the Indus
76 River and its eastern tributaries in the Punjab (Fig. 1A). The Indus is particularly sensitive to
77 variations in the strength of the Asian monsoon because it lies on the western edge of the zone
78 affected by this climatic phenomenon. As a result, variations in monsoon strength can have a
79 major impact on both patterns and rates of erosion in the various ranges that comprise the
80 western end of the Himalayan mountain chain (Fig. 1B). A number of studies have suggested
81 that changes in monsoon intensity have significantly impacted the erosion history of the western
82 Himalaya [*Bookhagen et al.*, 2005; *Clift et al.*, 2008a; *Clift et al.*, 2008b].

83   Debate continues regarding what controls the erosion of the Himalaya, with some
84 workers favoring tectonic processes that drive rock uplift [*Burbank et al.*, 2003], as being the
85 critical control, while others have argued for a dominance by monsoon rainfall and/or glaciation
86 [*Whipple*, 2009; *Wobus et al.*, 2003]. These focus the sediment producing regions across a
87 relatively narrow band of the range front and in turn drive exhumation of deep buried rocks
88 [*Thiede et al.*, 2004]. It is however known that the erosion of the Himalaya is sensitive to climate
89 change because sediment supply during and shortly after the Last Glacial Maximum (LGM) was
90 preferentially focused in the Karakoram, while the strongest erosion has shifted into the Lesser
91 Himalaya since the onset of the Holocene [*Clift et al.*, 2008a].

92   In this study we focus on the Late Miocene-Recent history and examine evidence for
93 coupling between the tectonic evolution and the changing strength of summer monsoon rains.
94 We take advantage of recently recovered sediments collected by the International Ocean
95 Discovery Program (IODP) in 2015 from the Eastern Arabian Sea, which provide a record of
96 erosion extending back to ~10.8 Ma, with one sample dated at ~15.5 Ma [*Pandey et al.*, 2016d].
97 An earlier lower-resolution study using detrital zircon grains and numerous bulk sediment Nd
98 and Sr isotopes argued that changes in erosion across the Indus Basin were unconnected to
99 climate change and largely manifest as increasing erosion of the Lesser Himalaya, especially
100 starting at 1.9 Ma [*Clift et al.*, 2019b]. We test this model using an expanded set of new U-Pb
101 ages from detrital zircon sand grains (1882 new ages from 15 additional samples, compared to
102 1335 ages from ten samples in the earlier work) coupled with a more sophisticated statistical
103 treatment of the total data set in order to reconstruct the evolving patterns of erosion.

104

Figure 1. A) Shaded bathymetric and topographic map of the Arabian Sea and surrounding area
showing the location of the drilling sites considered by this study. Map also shows the major
tributary systems of the Indus River, as well as smaller peninsular India rivers and their source
mountains. B) Inset map shows detail of the Laxmi Basin and location of the drill sites
considered in this study. Numbered red circles indicate existing scientific boreholes from Deep
Sea Drilling Project (DSDP) and Ocean Drilling Program (ODP). KK = Karakoram; NP = Nanga

111   Parbat. C) Geological map of the western Himalaya showing the major tectonic units that are
112   eroded by the Indus River and its tributaries. Map is modified after Garzanti *et al.* [2005]. Rivers
113   as shown in thick black lines. ISZ = Indus Suture Zone, MCT = Main Central Thrust, MBT =
114   Main Boundary Thrust and MFT = Main Frontal Thrust. Thick black line shows the boundary of
115   the Indus drainage, while thinner lines demark the limits of the major Himalayan tributaries.
116   Figure is modified from Clift *et al.* [2019b].

117

2 Geologic Setting

119   The sediments analyzed in this study were retrieved from the Laxmi Basin in the Eastern
120   Arabian Sea (Fig. 1A and 1B). This basin is separated from the rest of the Arabian Sea by a
121   continental block known as Laxmi Ridge [*Pandey et al.*, 1995]. Rifting in Laxmi Basin preceded
122   the breakup of the main Arabian basin, west of Laxmi Ridge, and likely occurred in the latest
123   Cretaceous [*Bhattacharya et al.*, 1994]. Since that time 2–3 km of sediment have accumulated in
124   the Laxmi Basin. Initial provenance investigation of these sediments using Nd isotopes and
125   limited zircon U-Pb dating indicates that while some fine-grained material might be derived in
126   from peninsular India, immediately to the east of the Laxmi Basin, most of the sediment was
127   sourced from the Indus Delta, located around 800 km towards the north [*Clift et al.*, 2019b].
128   Continuous sedimentation in Laxmi Basin was interrupted by the emplacement of a large mass
129   transport complex (MTC) just before 10.8 Ma, which eroded most of the Middle Miocene at Site
130   U1456 [*Calvès et al.*, 2015; *Dailey et al.*, 2019]. At Site U1457 the MTC removed almost the
131   entire sediment fill from the edge of Laxmi Ridge leaving only a thin deposit of red Paleocene
132   mudstones [*Pandey et al.*, 2016b].

133   We also compare our sediments with those recovered as drill cuttings from the industrial
134   borehole Indus Marine A-1 located on the Indus shelf (Fig. 1A). Because Indus Marine A-1 is
135   located close to the Indus River mouth the source of sediment is more straight forward, and
136   cannot have involved influence from the Indian Peninsula, as might be the case in the Laxmi
137   Basin. This site penetrated into the Middle Miocene [*Shuaib*, 1982] and drill cuttings have been
138   used to look at the evolving provenance using Nd isotope methods, going back further in time
139   than possible at the IODP sites [*Clift and Blusztajn*, 2005; *Clift et al.*, 2019b]. The Indus Marine
140   A-1 drill site is located on the relatively flat continental shelf and is only affected by growth
141   faulting, but has otherwise escaped major tectonic deformation since the breakup of the Arabian
142   Sea, except along its western edge adjacent to the Murray Ridge [*Clift et al.*, 2002a; *Gaedicke et*
143   *al.*, 2002]. Unfortunately, the recovered sediments from Indus Marine A-1 are fine-grained and
144   are not conducive to detrital zircon U-Pb dating in this proximal area. We examined the major
145   element chemistry of the sediments at Indus Marine A-1 for comparison with the more distal
146   drill sites sampled by IODP in order to demonstrate their Indus provenance. Neodymium isotope
147   data indicate that Indus Marine A-1 sediments were derived from the Indus River, consistent
148   with their proximal location, providing a useful comparison with the deep-water materials [*Clift*
149   *and Blusztajn*, 2005].

150   Determining the provenance of the sediment delivered to the Arabian Sea is facilitated by
151   the leverage of the significant spatial diversity of bedrock ages and lithologies within the Indus

152 drainage basin [*Hodges*, 2000; *Searle*, 1996]. Geochemical and isotopic differences between
153 bedrock sources are transferred to the eroded sediment and although grains may be altered during
154 the transport process, many of these differences are preserved in the final deposited sediment,
155 allowing us to deconvolve the sources and variations using appropriate proxies. Figure 1C shows
156 the various mountain ranges that comprise the main distinct source regions to the modern Indus
157 River, including the Greater and Lesser Himalaya, the Tethyan Himalaya that lie further north,
158 and that represent the telescoped, passive continental margin of Greater India [*Garzanti et al.*,
159 1987]. This unit is separated by the Indus Suture Zone from magmatic arc rocks of the
160 Transhimalaya and Kohistan (Fig. 1C) that were largely emplaced in the Cretaceous and
161 Paleogene [*Khan et al.*, 1997; *Rolland et al.*, 2002]. Further north, across the Shyok Suture Zone,
162 lie the Karakoram, the old active margin of continental Eurasia, which also comprises Mesozoic
163 arc rocks, and experienced magmatism after India-Euasia collision, most notably in the form of
164 the Early Miocene Karakoram Batholith [*Ravikant et al.*, 2009; *Searle et al.*, 1989]. The
165 Karakoram region was uplifted in response to both compressional tectonics and strike-slip
166 displacement on the Karakoram Fault [*Searle and Phillips*, 2007]. Farther to the west the Hindu
167 Kush mountains are characterized by a similar pre-collisional history as the Karakoram, but
168 subsequently did not experience such dramatic or rapid unroofing [*Hildebrand et al.*, 2001;
169 *Zhuang et al.*, 2018]. In addition, the Western Syntaxis of the mountain chain is marked by the
170 Nanga Parbat Massif (Fig. 1C), characterized by high-grade metamorphic and igneous intrusive
171 rocks that experienced recent, very rapid exhumation [*Zeitler et al.*, 1989]. However, it is unclear
172 exactly when this process began because the rocks now at the surface are very young.
173 Nonetheless, this does not preclude an earlier onset to erosion [*Chirouze et al.*, 2015].

174   The Greater Himalaya were emplaced along the Main Central Thrust (MCT) after ~24
175 Ma, placing them over the Lesser Himalaya [*Catlos et al.*, 2001; *Stephenson et al.*, 2001]. These
176 in turn were unroofed and brought to the surface due to motion along the Main Boundary Thrust
177 (MBT) and associated thrust duplexing [*Bollinger et al.*, 2004; *Huyghe et al.*, 2001]. Evidence
178 from the Siwalik Group foreland basin sedimentary strata indicates that the Lesser Himalaya
179 were exposed locally only after 9 Ma and more widely after 6 Ma in NW India [*Najman et al.*,
180 2009], although the Nd isotopes at Sites U1456 and U1457 imply that widespread unroofing of
181 the Inner (Crystalline) Lesser Himalaya only began at 1.9 Ma [*Clift et al.*, 2019b]. The Siwalik
182 Group rocks themselves have been up-thrusted and are presently eroding, recycling older
183 sediments back into the river system. However, estimates derived from the incision of terraces in
184 the Nepalese frontal Himalaya suggest that the Siwaliks contribute no more than about 15% of
185 the total flux [*Lavé and Avouac*, 2000]. The western edge of the Indus drainage basin is
186 characterized by fold and thrust belts (Sulaiman and Kirthar ranges, Fig. 1A), similar to the
187 Siwalik Group in character [*Roddaz et al.*, 2011], but experiencing a more arid climate.
188 Nonetheless, this environment need not limit erosion rates because of the strong erosion
189 associated with occasional flash flooding events in vegetation-poor settings [*Molnar*, 2001],
190 although study of heavy minerals in rivers draining these ranges and the lower Indus indicate that
191 their contribution to the net sediment load is minor [*Garzanti et al.*, 2020].

192   Other potential sources of sediment delivered into the Laxmi Basin include the
193 Precambrian cratonic rocks of peninsular India and associated Gondwanan sedimentary
194 sequences [*Mukhopadhyay et al.*, 2010; *Yin et al.*, 2010], characterized by old (>500 Ma)
195 bedrock zircon U-Pb ages, similar to those observed in the Himalaya, especially the Lesser

196   Himalaya. Zircon U-Pb dating, given its high closure temperature [*Hodges*, 2003], only records
197   the initial crystallization or high-temperature metamorphism, and thus, does not allow us to
198   exclude such old grains as having been derived from peninsular India rather than the Himalaya.
199   Sediments eroded from the Deccan Plateau, the latest Cretaceous flood basalt province that
200   dominates the Western Ghats, immediately onshore from the drilling area, were erupted around
201   65 Ma [*Courtillot et al.*, 2000] over a relatively short period of time. While these would be very
202   distinctive, basalt is characterized by a very low zircon fertility and might not provide significant
203   zircon grains of that age into the adjoining basin. Nd and Sr isotopic evidence suggests enhanced
204   flux in muddy sediments to the Laxmi Basin during interglacial times [*Khim et al.*, 2019]. Low-
205   resolution apatite fission track and zircon U-Pb studies have so far identified just a single sand at
206   the IODP drill sites that was derived from the Indian peninsula [*Zhou et al.*, 2019].

207   **3 Sedimentology and Stratigraphy**

208   Drilling at Sites U1456 and U1457 penetrated ~1100 m below the seafloor in both
209   locations, with the basement being reached at Site U1457 (Fig. 2)[*Pandey et al.*, 2016b]. Drilling
210   at Site U1456 only just penetrated through the MTC, allowing a very short core of Middle
211   Miocene sandstone to be recovered [*Pandey et al.*, 2016a]. Age assignments at both sites are
212   made by combining biostratigraphy and magnetostratigraphy and we follow the age model of
213   Pandey *et al.* [2016a] for Site U1456 and Pandey *et al.* [2016b] for Site U1457 (Fig. 2), with
214   updates from Routledge *et al.* [2019]. Ages of individual samples are calculated assuming linear
215   sedimentation between the dated points. At Site U1456 the sediments are relatively mud-rich, but
216   with a number of silt and fine sand turbidite interbeds at 460–730 mbsf (meters below seafloor;
217   Fig. 2A), which are overlain by a sequence of mud and carbonate-rich sediments. A thick, sand-
218   rich package was recovered between 360 and 140 mbsf and interpreted as a submarine fan lobe
219   [*Pandey et al.*, 2016a]. Above this sand-rich package, the section is dominated by mud and
220   carbonate, interpreted as the product of hemipelagic sedimentation. Site U1457 is characterized
221   by much lower proportions of sand, reflecting the drilling location on the flanks of the Laxmi
222   Ridge. However, a sand-rich interval between 670 and 810 mbsf is overlain by a carbonate and
223   mud-rich interval between 600 and 670 mbsf. More sand-rich beds were encountered between
224   470 and 600 mbsf. As at Site U1456, sediments shallower than 200 mbsf at Site U1457, are mud
225   and carbonate-rich (Fig. 2). The coarse-grained intervals are again interpreted as lobe deposits
226   [*Pandey et al.*, 2016b]. The sandy sediments are interpreted to be deposited by turbidity currents,
227   with the muddy sediments representing hemipelagic intervals between depositional events.
228   Changes in grain size might be driven by changes in the erosional power in the source regions,
229   the discharge stream power of the river, or by changes in sea level, but could also reflect
230   avulsion in the main depositional lobes in and out of Laxmi Basin and the main part of the
231   Arabian Sea towards the West. Such auto cyclic behavior is commonly observed in submarine
232   fans [*Deptuck et al.*, 2008; *Shanmugam and Moiola*, 1991].

233

Figure 2. Simplified lithologic logs of the two drill sites considered in this study. Black arrows show the location of the samples analyzed. Modified from Pandey *et al.* [2016c]. Pale shaded intervals show inferred lithologies based on small amounts of recovered core. Because induration is progressive and there is no sharp division, we make no attempt to distinguish between sediments and indurated rocks. Numerical ages are from Pandey *et al.* [2016a] for Site U1456 and from Pandey *et al.* [2016b] for Site U1457, with updates from Routledge *et al.* [2019].

240

4 Methods

241 **4 Methods**

242   U-Pb geochronology of detrital zircon grains has become a powerful and widely
243 employed tool for discerning provenance in siliciclastic sedimentary systems. The methodology
244 is based on the concept that different bedrock source rocks are characterized by distinct and/or
245 different age populations of zircons. A zircon budget is not the same as an eroded rock budget
246 because of differences in the relative fertility of bedrock sources with regard to zircon. Zr
247 concentrations have been used as a proxy for the relative abundance of zircons in sediment
248 [*Amidon et al.*, 2005], but the reliability of this approach has recently been questioned [*Malusà et
249 al.*, 2016]. Malusà *et al.* [2016] developed a method using mineralogy and density data from the
250 sediment to infer the fertility of the source bedrock. Unfortunately, this approach is not practical
251 for this work because the sample sizes available from IODP were small (<50 cm^3) so that all the
252 material had to be processed for zircon extraction and even required amalgamating neighboring
253 samples in order to generate enough data to make a statistically meaningful result in some cases.
254 We use previously published geochemical data from modern rivers as a guide to zircon fertility
255 as this data already exists and we cross check this prediction against other provenance methods
256 to assess its credibility. Our erosion budgets are however largely zircon based, not bulk
257 sediment.

258   Zircon is a robust mineral and its grains do not generally experience significant physical
259 abrasion during transport, unless they had previously accumulated major radiation damage.
260 Hence, zircon can undergo multiple episodes of recycling and redeposition. Although the
261 concentration of zircon in any given sediment can be affected by hydrodynamic sorting, this
262 process may not be a strong influence on the resulting detrital age spectra unless there is a
263 relationship between grain size and crystallization age, which we investigate below. Work on
264 Yangtze River sediments indicates that the typical grain size range analyzed using LA-ICP-MS
265 technology is representative of the overall population in the sediment without a bias related to
266 grains size [*Yang et al.*, 2012]. Detrital zircon U-Pb dating has been widely applied in
267 provenance studies in the Western Himalaya due to the large range of zircon U-Pb age
268 differences between the various source terrains described above. Furthermore, studies of the
269 modern Indus River documented a close correlation between the modern zircon U-Pb age spectra
270 and the bedrock sources, albeit one implying focused erosion in several sub-basins [*Alizai et al.*,
271 2011; *Zhuang et al.*, 2018]. Several studies have also used detrital zircon dating to investigate the
272 provenance of the Siwalik Group foreland basin sedimentary rocks [*Baral et al.*, 2015; *Bernet et
273 al.*, 2006; *DeCelles et al.*, 2004; *Zhuang et al.*, 2015] and Quaternary sediments in the delta and
274 offshore [*Clift et al.*, 2008a; *Li et al.*, 2019], allowing evolving erosion patterns to be
275 reconstructed.

276   *4.1 Major Element Analyses*

277   In addition to detrital zircon U-Pb dating, bulk sediment samples were analyzed for their
278 major element contents by Inductively Coupled Plasma Emission Spectrometry (ICP-ES) at
279 Boston University (BU), USA. Sediment samples were decarbonated with acetic acid, washed
280 with distilled and deionized water with a purity of 9–12 megaohms, and hand powdered at
281 Louisiana State University (LSU) before total fusion preparation at BU. Glass beads for each
282 sample were made in a muffle furnace under 1050˚C by fusing 100 ± 0.5 mg of sample mixed

9

283 with 400 ± 0.5 mg lithium metaborate (LiBO$_2$). The melted mixture was then dissolved in 5%
284 HNO$_3$, sonicated, manually shaken until no visible grains were observed, and further diluted for
285 analysis [*Dunlea et al.*, 2015]. Precision for all elements was better than 1% of the measured
286 value, and accuracy was confirmed by repeated analyses of International Standard Reference
287 Materials (Basalt, Hawaiian Volcano Observatory, BHVO-2)[*Wilson*, 1997]. Results of the
288 geochemical measurements are shown in Table 1.

289 *4.2 Grain size Analysis*

290   For quantitative grain size analysis, samples were prepared using standard procedures as
291 described by Howell *et al.* [2014]. We put a small amount of sample into a cleaned 50 ml plastic
292 centrifuge tube and added 5–7 ml of sodium phosphate solution. The tube was capped and
293 vortexed to deflocculate clay-sized sediment and separate organic particles. The sample was
294 poured through an 850 µm sieve and funneled into a 15 ml glass test tube. After centrifuging and
295 removing the clear supernatant, 2–3 ml of sodium phosphate and 5 ml of 30% H2O2 were added.
296 Tubes were vortexed again and then put into a hot bath that was heated to 70˚C. This step
297 requires persistent monitoring to prevent loss of reactant by spraying it with acetone until the
298 reaction is stabilized. Reactants then sat overnight to completely oxidize organic matter. Reacted
299 supernatant was removed, and 5 ml of sodium phosphate was added. These treated samples were
300 then rinsed with deionized water, transferred into clean 50 ml plastic centrifuge tubes, and
301 topped with sodium phosphate into a sample solution of up to 40 ml. Samples were vortexed
302 again prior to grain size analysis. Grain size analysis was conducted on a Beckmann Coulter
303 LS13 320 laser diffraction particle size analyzer at LSU. The obscuration of all running samples
304 in the aqueous liquid module (ALM) was between 8–12 %. Result of the analysis are provided in
305 Table 2.

306   *4.3 Zircon U-Pb dating*

307   After standard mineral separation, zircon grains were sprinkle-mounted onto double-
308 sided tape on 1" acrylic discs and analyzed at random using depth-profiling LA-ICP-MS U-Pb
309 geochronology [*Marsh and Stockli*, 2015]. Although this method differs from the more common
310 analysis of cut and polished grains there is no indication that this profiling approach yields
311 results that differ significantly from earlier work, including work done in the Himalaya [*Colleps*
312 *et al.*, 2019]. For each sample at least 120 zircons were analyzed to obtain provenance datasets
313 that resolve all components that comprise >5% of the total population [*Vermeesch*, 2004]. The
314 analyses were completed using a PhotonMachine Analyte G.2 Excimer laser (30 µm laser spot
315 size) with a large-volume Helex sample cell and a Thermo Element2 ICP-MS using procedures
316 described in Hart *et al.* [2016] at the UTChron facilities at the Jackson School of Geosciences at
317 the University of Texas at Austin. GJ1 was used as the primary reference standard [*Jackson et*
318 *al.*, 2004] and a secondary in-house zircon standard (Pak1 with a TIMS ^{206}Pb/^{239}U age of 43.0
319 Ma). The data from the analyses were then reduced using the Iolite data reduction software
320 VizualAge [*Paton et al.*, 2011; *Petrus and Kamber*, 2012]. For analyzed detrital zircons, the
321 ^{206}Pb/^{238}U age was used for grains younger than 850 Ma and the ^{207}Pb/^{206}Pb age was used for
322 grains older than 850 Ma [*Gehrels et al.*, 2008]. All ages reported use 2σ absolute propagated
323 uncertainties. ^{207}Pb/^{206}Pb ages are less than 30% discordant, and ^{206}Pb/^{238}U ages are less than
324 10% discordant [*Gehrels et al.*, 2011]. The discordance reported is calculated with the ^{206}Pb/^{238}U

325 and $^{207}Pb/^{235}U$ ages if <850 Ma and the $^{206}Pb/^{238}U$ and $^{207}Pb/^{206}Pb$ ages if >850 Ma. Although
326 some studies have suggested older crossovers between the $^{206}Pb/^{238}U$ and $^{207}Pb/^{235}U$ ages and the
327 $^{206}Pb/^{238}U$ and $^{207}Pb/^{206}Pb$ ages (e.g., 1.5 Ga [*Spencer et al.*, 2016]) blindly picking a crossover at
328 1.5 Ga leads to culling of discordant $^{206}Pb/^{238}U$ ages, or unacceptable smearing and loss of age
329 mode definition between 800–1500 Ma for many samples. Picking a 1500 Ma crossover cutoff
330 and a 20% discordance filter would result in the loss of 80% of the data between 850 and 1500
331 Ma making the data bad provenance proxies. The 850 Ma crossover was chosen in accordance
332 with the approach of Spencer et al. [2016] and Marsh et al. [2019]. The data are reported in
333 Table 3.

334   When accurately dating a geological event, high concordance is a requirement but when
335 assigning grains to broad age populations for provenance work the emphasis is on high numbers
336 of grains rather than on high precision in order to improve the statistical reliability. The
337 appropriate level of discordance filter needs to be determined for each data set in light of the
338 goals of the study and the complexities encountered. If a study yields a mix of Phanerozoic and
339 Archean ages, and the relative proportions of these ages are important, a generous (e.g., 30%)
340 discordance cutoff is appropriate so that most Precambrian ages are retained [*Gehrels*, 2012].

341 **5 Results**

342   *5.1 Grain-size of sediments*

343   The sediments were assessed using the classification scheme of Folk [1974](Fig. 3).
344 Sediments range from silty sand to silt and mud, both the new samples processed here and those
345 from the earlier study we integrate with here {Clift, 2019 #152}. The grain size variation in
346 single samples can be better assessed by plotting the proportion of each grain size fraction as a
347 spectrum (Fig. 4). We see generally good sorting (positive kurtosis) and a negative skew,
348 meaning a dominance of the finer grain sizes and a tail of coarser grains comprising a
349 diminishing proportion of the sediment. This is especially true for the coarsest grained
350 sediments. The vast majority of the sediment considered here is classified as fine sand to silt,
351 with only small amounts of medium and coarse sand in a minority of samples, three from Site
352 U1456 dated at 1.92–1.32 Ma and one from Site U1457 at 3.02 Ma. Three of the new samples do
353 contain significant volumes of medium and even coarse sand (3.39, 7.00 and 7.27 Ma). The spot
354 size of the laser used for the U-Pb dating means that grains smaller than ~30 μm were not
355 considered in this study. Depending on the sample this represents a wide range of the total
356 sediment load. Only 9% of Sample U1456A-51F-3, 100-110 cm was less than 30 μm, while 89%
357 of Sample U1456A-70F-2, 10-16 cm is smaller than that threshold. See Table 2 for full results.

Figure 3. Grainsize range of all samples analyzed for U-Pb zircon dating from the Laxmi Basin shown on the scheme of Folk [1974]. Samples are marked to show those published by Clift *et al.* [2019b], rather than presented new here (Table 2). Note the dominance of silty sand and sandy silt in the analyzed samples.

Figure 4. Detailed grain size spectra showing the range of sizes of the different samples considered within this study. Most of the sediment is fine sand to coarse silt in size and typically shows a coarse-skewed. A) Samples younger than 7 Ma, b) samples older than 7 Ma. Samples are marked to show those published by Clift *et al.* [2019b](gray text labels and white ringed symbol), rather than presented new here (Table 2) (black text labels and black ringed symbol).

370   *5.2 Bulk Sediment Chemistry*

371   The general geochemical character of the sediments can be seen on a CN-A-K ternary
372   diagram [*Fedo et al.*, 1995](Fig. 5A). The IODP samples plot in an array with a Chemical Index
373   of Alteration (CIA) of ~65 to 73 [*Nesbitt et al.*, 1980]. They form a roughly linear array trending
374   towards the illite end member and suggestive of its progressive involvement as the primary
375   mineral breakdown product. The Laxmi Basin samples can be compared with sediments from the
376   Quaternary Indus delta [*Clift et al.*, 2010], Indus Canyon [*Li et al.*, 2018], the Indus Marine A-1
377   borehole, as well as modern sediments from the western Indian shelf and slope between the
378   Saurashtra peninsula and Bhatikal [*Kurian et al.*, 2013](Fig. 1). Rivers south of Bhatikal have a
379   different composition and are unlikely to be sources to the Laxmi Basin sites.

380

381   **Figure 5.** (A) Geochemical signature of the analyzed samples illustrated by a CN-A-K ternary
382   diagram [Fedo *et al.*, 1995]. CN denotes the mole weight of Na$_2$O and CaO* (CaO* represent the
383   CaO associated with silicate, excluding all the carbonate). A and K indicate the content of Al$_2$O$_3$
384   and K$_2$O respectively. Samples closer to A are rich in kaolinite, chlorite and/or gibbsite
385   (representing by kao, chl and gib). CIA values are also calculated and shown on the left side,

386   with its values are correlated with the CN-A-K. Samples from the delta have the lowest values of
387   CIA and indicates high contents of CaO and Na$_2$O and plagioclase. Abbreviations: sm (smectite),
388   pl (plagioclase), ksp (K-feldspar), il (illite), m (muscovite). B) Geochemical classification of
389   sediments from this study as well as those from the Indus delta [*Clift et al.*, 2010], Indus Canyon
390   [Li *et al.*, 2018] and western Indian shelf [Kurian *et al.*, 2013] following the scheme of Herron
391   [1988].

392

393   The Laxmi Basin sands have very similar bulk compositions to the Quaternary Indus
394   canyon and delta, as well as the Indus Marine A-1 samples (Fig. 5A), but plot below or to the
395   right of the array of the western Indian shelf sediments. Only the shelf sample taken near
396   Bhatikal (the southernmost shelf sample that overlies the Precambrian crystalline basement of
397   India, rather than the Deccan Traps), plots below the Laxmi Basin sediments, with a lower CIA
398   value. This plot confirms that the analyzed sands have little in common with material eroded
399   from peninsular India and appear consistent with an Indus River origin. Likewise, the sediments
400   plot close to the Quaternary Indus sediments and those of Indus Marine A-1 on the
401   discrimination diagram of Herron [1988](Fig. 5B). The IODP samples plot with slightly lower
402   Fe$_2$O$_3$/K$_2$O values compared to the proximal sediments. The Laxmi Basin sediments form an
403   array defined as shales and wackes, while the western Indian shelf sediments fall into the Fe
404   shale, litharenite, sublitharenite and Fe sand fields.

405   We further assess whether grain size has any relationship to zircon concentrations by
406   plotting Zr contents against median grain size (Fig. 6). Although the original source
407   characteristics and hydrodynamic sorting of the sediment might be expected to concentrate
408   zircons in certain size fractions this does not appear to be a significant factor within the range of
409   grain sizes considered here.

410

411   **Figure 6.** Cross plot of Zr concentration against median sample grain size. No strong correlation
412   is observed.

15

413

414   *5.3 Detrital Zircon U-Pb*

415   We examined the range of zircon U-Pb ages using a kernel density estimate (KDE)
416   diagram (Fig. 7) to assess similarities between different sampled sediments and potential source
417   regions (Fig. 7). All of the sediments analyzed in this study show a significant zircon U-Pb
418   component younger than 200 Ma. In addition, we see significant components dated at 350–1250
419   Ma and 1500–2300 Ma. The abundance of these older age components overall increases with
420   decreasing sample depositional age. The 350–1250 Ma age component appears to increase in all
421   sediment samples dated at 5.87 Ma or younger compared to the older sediments. A particularly
422   prominent age mode at ~1800 Ma first occurs in sediments deposited at 3.43 Ma and becomes
423   extremely prominent in all samples younger than 1.92 Ma. This age mode is also observed in the
424   modern sediment from the Indus river mouth [*Clift et al.*, 2004].

425   Examining the <200 Ma zircon U-Pb ages in detail, we see that the vast majority of
426   grains are younger than 120 Ma with prominent age peaks at around 100–120 Ma and 40–70 Ma
427   (Fig. 8). In the youngest samples, especially those deposited starting at 3.02 Ma, we see another
428   age mode at ~20 Ma, although this is also seen in the sample dated at 5.78 Ma. One sample
429   deposited at 3.17 Ma differs in its <200 Ma age spectra from the other samples as it is
430   characterized by a prominent age peak at 100–120 Ma, with a general lack of other young zircon
431   grains.

432

Figure 7. Kernal density estimate (KDE) diagram showing the range of the zircon U-Pb ages for individual sand grains back to 3000 Ma. Colored strips show the range of populations with diagnostic links to critical source terrains in the headwaters of the Indus. Data from the Siwaliks, as well as the Tethyan, Greater and Lesser Himalaya are compiled from DeCelles *et al.* [2004]. Karakoram data is from is from Le Fort *et al.* [1983], Parrish and Tirrul [1989], Schärer *et al.* [1990], Fraser *et al.* [2001] and Ravikant *et al.* [2009]. Nanga Parbat data is from Zeitler and Chamberlain [1991] and Zeitler *et al.* [1993]. Transhimalayan data is from Honegger *et al.* [1982], Schärer *et al.* [1984], Krol *et al.* [1996], Weinberg and Dunlap [2000], Zeilinger *et al.* [2001], Dunlap and Wysoczanski [2002], Singh *et al.* [2007], and Ravikant *et al.* [2009]. Samples are marked to show those published by Clift *et al.* [2019b], and those presented new here.

6 Discussion

Major element discrimination diagrams (Fig. 5) suggest that the Laxmi Basin sediments are most similar to deposits found in the Quaternary and modern Indus River/delta/canyon, as well as the older sedimentary rocks from Indus Marine A-1 (Fig. 5). However, they are distinctly

17

449   different from sediments sampled from the modern western Indian shelf, and largely derived
450   from the Deccan Plateau and underlying units [*Kurian et al.*, 2013]. These geochemical data
451   suggest that the Laxmi Basin sediments, most likely originated from the Indus River mouth.

452   We assessed the overall geochemical characteristics of the sediments by plotting the
453   major element composition of each sample normalized to the upper continental crust (UCC; Fig.
454   9)[*Taylor and McLennan*, 1995]. Most of the samples display a relatively uniform topology in
455   these diagrams and are broadly similar to both post-LGM sediments from the Indus Delta (KB-
456   40-4), the Holocene delta (TH-10-1) and, the modern Indus river (Thatta TH-1). Most of the
457   samples show a similar major element composition compared to the UCC, with a consistent
458   enrichment in TiO_2, suggestive of a higher content of Ti-bearing heavy minerals (e.g., rutile,
459   anatase, brookite, ilmenite, titanite). This enrichment is particularly strong in the 0.93 Ma sample
460   which apatite fission track data indicate to have a unique provenance [*Zhou et al.*, 2019]. There
461   are also relative depletions in CaO and Na_2O, as well as P_2O_5, implying both a lower plagioclase
462   and apatite content relative to the UCC. This relative depletion in CaO is strongest in the modern
463   river mouth sediment and weakest in the post-glacial delta sediments, with the fan sediments
464   plotting between these extremes. The systematically lower abundance of plagioclase and apatite
465   likely reflects chemical weathering in the floodplains prior to deposition in the ocean, because
466   these phases are less stable under conditions dominated by chemical weathering [*Guidry and*
467   *Mackenzie*, 2000; *White and Brantley*, 1995]. However, all samples show this effect and there is
468   a general consistency in the overall composition, we conclude that we are comparing sediments
469   of a similar bulk character. All fan sediments show Zr abundances relatively close to the UCC
470   average.

471

18

472 **Figure 9.** Upper continental crust normalized compositions of the sediments whose zircons are
473 the focus of the study. Bulk settlement compositions are normalized according to the average of
474 the continental crust from Taylor and McLennan [1995].

475

476 *6.1 Changing Provenance*

477 Before using the changing zircon U-Pb age spectra to infer changing sediment
478 provenance we examine the possible role of grain size in controlling the results. Sediment grains
479 are fractionated during transport because different densities and shapes affect their settling
480 characteristics [*Garzanti et al.*, 2009]. Zircons all have the same density but the size and shape of
481 the grains from a given source may vary and influence the final conclusions. If one source is
482 associated with smaller or larger grains compared to other sources then this may prejudice the
483 analysis, especially if the grains are too small to be analyzed. Garzanti *et al.* [2009] concluded
484 that this effect was moderate in the Ganges-Brahmaputra catchment, which has strong
485 similarities to the Indus. We plot major, provenance-related age populations (0–25, 40–70, 70–
486 120, 300–750, 750–1250 and 1500–2300 Ma) against median grain size for all samples
487 considered here to see if grain size plays a strong role in controlling the age spectra. Figure 10
488 shows that there is not a strong correlation between sediment median grain size and the
489 proportion of various provenance-sensitive age groups. However, we note that the four coarsest
490 sediments (>100 μm) do contain more 750–1250 and 1500–2300 Ma grains compared to the 40–
491 70 and 70–120 Ma groups. The effect is especially strong with the 1500–2300 Ma group. In
492 contrast to work on the Amazon River by Lawrence *et al.* [2011] who showed that older grains
493 were significantly smaller than younger ones, the reverse may be true in the Indus. It is however
494 noteworthy that the coarser sediments are all young 3.02 Ma and younger and as demonstrated
495 below the provenance inferred from similar aged finer sediment is not greatly different and also
496 consistent with neighboring bulk sediment Nd isotope constraints. We conclude that there may
497 be a grain size issue with the coarsest sediment, but that this is not dominant in controlling the U-
498 Pb age spectra.

499

Figure 10. Plots of relative abundance of provenance sensitive zircon age populations in individual samples compared with sample median grain size. The coarsest samples show preference for the oldest U-Pb ages and a relative lack of the younger populations.

The zircon U-Pb age spectra are used to track the source evolution of sediment reaching the Arabian Sea and compared to bedrock zircon U-Pb age signatures of possible source areas (Fig. 7). The abundance of grains younger than 200 Ma correlates well with young bedrock from the Indus Suture Zone, particularly in Kohistan, the Transhimalaya and Karakoram, as well as Nanga Parbat (Fig. 8). The abundance of these young zircon grains clearly points to sediment being supplied by the Indus River and not by peninsular India, where no magmatism <200 Ma is known outside the Deccan Plateau. Detrital zircon grains older than 350 Ma also largely correlate with various bedrock sources known in the Himalaya. Detrital zircon age modes between 350 and 750 Ma have been correlated with bedrock sources in the Tethyan Himalaya [*Alizai et al.*, 2011], although it is generally agreed that there is little real difference in terms of U-Pb ages, between Tethyan and Greater Himalaya zircon signatures [*Gehrels et al.*, 2011], and these are in any case not always mapped consistently by different groups [*Webb*, 2013]. Consequently, zircons with ages between 350 and 1250 Ma could be derived from either source. The older samples show relatively low abundance of grains in this age range, but these increased significantly starting at 5.87 Ma and become very abundant in the last few million years. Older grains, dating between 1500 and 2300 Ma, are particularly common in Lesser Himalayan sources, although they are also present in smaller amounts in the Tethyan and Greater Himalaya [*DeCelles et al.*, 2000; *Gehrels et al.*, 2011]. These mainly Paleoproterozoic zircon grains are almost entirely absent from the Laxmi Basin Miocene samples, but show a marked increase beginning at 5.72 Ma, and becoming very abundant beginning at 1.56 Ma (Fig. 7). We therefore interpret these patterns to indicate a progressive increase in erosion from the Himalaya starting

20

525 after 7.0 Ma, and especially starting at 5.72 Ma, with strong erosion from the Tethyan and
526 Greater Himalaya. After 3.02 Ma there is a dramatic increase in erosional flux from the Lesser
527 Himalaya, which have had a strong influence on the river system since the onset of the Holocene
528 [*Clift et al.*, 2004; *Clift et al.*, 2008a].

530 **Figure 8.** Kernal density estimate (KDE) diagram showing the range of the zircon U-Pb ages for
531 individual sand grains back to 200 Ma. Colored strips show the range of populations with
532 diagnostic links to critical source terrains in the headwaters. See Figure 6 caption for data
533 sources.

534

535   If we only consider the zircon grains younger than 200 Ma then we can see that there is
536 evidence of erosion, from both Kohistan and from the Karakoram, in most of the samples
537 analyzed (Fig. 8). Kohistan is particularly noteworthy for having zircon dated between 40 and 70
538 Ma [*Alizai et al.*, 2011; *Zhuang et al.*, 2018], although there are similar aged units in the
539 Karakoram as well. However, zircon grains older than 70 Ma but younger than 120 Ma are
540 almost exclusively known only from Karakoram bedrock sources [*Searle*, 1996]. The 3.17 Ma

541 sample does not show the younger 40–70 Ma population, suggesting that it did not receive any
542 significant material from Kohistan/Ladakh.

543 The youngest (<25 Ma) zircon grains are more enigmatic in terms of their provenance.
544 While very young zircons are known from the present-day Nanga Parbat massif, these are
545 generally younger even than the 25 Ma zircon U-Pb age component observed in many of the
546 samples [*Zeitler et al.*, 1993]. Our new data also show an increased influx from bedrock sources
547 with very young zircon starting at 3.02 Ma, as well as a brief appearance at around 5.78 Ma. It is
548 possible that this increase starting at 3.02 Ma reflects the emergence of Nanga Parbat, although
549 we cannot exclude the influence of other young sources in the southern Karakoram metamorphic
550 belt, which also contains rocks of this age and have experienced very rapid exhumation in the
551 last few million years [*Wallis et al.*, 2016]. Because the Deccan Plateau volcanic rocks were
552 erupted rather quickly around 65 Ma, it is hard to completely exclude their influence because
553 grains of a similar age are also known in Kohistan, and in the Karakoram. However, the erosion
554 from the Deccan Plateau would not account for the other young grains and an influx from that
555 area should result in a clear peak age at 65 Ma, which is not observed.

556 We also assessed the evolving provenance patterns of sediments in Laxmi Basin using a
557 multidimensional scalar (MDS) analysis of the detrital zircon U-Pb dates [*Vermeesch et al.*,
558 2016]. In this plot, which is a type of principle component analysis, samples with similar age
559 spectra plot close to one another, while distinct samples are far separated. Figure 11A shows all
560 the detrital samples data, along with a modern river mouth and a delta sample (KB-40) dating
561 from shortly after the LGM [*Clift et al.*, 2008a]. The MDS analysis shows clear and coherent
562 patterns. Samples deposited at and after 1.56 Ma, are relatively similar to the modern river. In
563 contrast, the oldest samples plot in a cluster suggesting a similar Miocene provenance and a
564 subsequent progressive shift from right to left with decreasing depositional age, although with
565 some reversals, most notably at 3.17 and 3.57 Ma. This reflects an overall shift in the zircon age
566 spectra through time. Nonetheless, the LGM sample has stronger similarities with sediments
567 deposited on the fan during the Late Miocene. Earlier work implied that erosion during the LGM
568 was focused in the Karakoram [*Clift et al.*, 2008a] compared to the modern river or during the
569 Holocene when the summer monsoon was strong [*Caley et al.*, 2014; *Fleitmann et al.*, 2003;
570 *Gupta et al.*, 2003]. The new data indicate that older Miocene samples were also deriving their
571 material from Karakoram sources, and this was followed by a shift to more Himalayan sources,
572 especially in the last few million years. The plot implies that the change might be step wise, with
573 a change starting between 7.0 and 5.87 Ma and again at 1.56 Ma.

22

574

Figure 11. Multidimensional scalar (MDS) diagrams made from zircon U-Pb age data showing
(A) how the different sediment samples from IODP Expedition 355 compare with one another
and post-glacial sediments from the Indus delta (TH-10-8 and KB-40-4) and (B) with the major
source terranes in the Indus catchment, as well as the modern rivers of the Indus catchment, i.e.,
the main or trunk stream of the Indus, upstream of Attock, and its major eastern tributaries. Solid
lines join sediments to their most similar neighbor, while dashed lines join the next most similar.
Sources of bedrock age data come from the literature, as described in Figure 6. River data is
from Alizai *et al.* [2011]. Note that sediments older than 5 Ma plot towards the right in Figure
10B, in the direction of Karakoram bedrock sources, whereas there is a progressive migration
towards the left, towards Himalayan sources after that time. Diagram was constructed using the
statistical package of Vermeesch *et al.* [2016].

23

586

587   The fact that the youngest turbidite sands are most similar to the modern interglacial
588   river, and not the compositions of the Indus shortly after the LGM, also implies that most of the
589   sediment deposited in the Indus Fan has been eroded during interglacial times when the monsoon
590   was strong, even if final deposition did not occur until the sea level fell during the onset of the
591   subsequent glaciation. We envisage fast interglacial erosion generating great volumes of
592   sediment, which is then mobilized, transported, and delivered to the delta as the rains
593   strengthened [*Jonell et al.*, 2017]. The sediment would then be stored on the shelf or in the upper
594   canyon during sea level high stands before being eroded and redeposited as sea level fell [*Li et
595   al.*, 2018]. This emphasizes the importance of monsoon intensity in controlling erosion and
596   sediment delivery in the Western Himalaya.

597   We also compared the Arabian Sea sediments with known zircon ages from bedrock
598   sources themselves. Figure 11B shows the progressive changes from the Miocene to the present
599   and emphasizes the fact that the stratigraphically oldest detrital zircon samples plot closest to
600   sources in the Karakoram and have similarities with analyses from the trunk stream (upper
601   reaches) of the main Indus River, before it mixes with the Himalaya-draining Eastern tributaries,
602   such as the Jhellum, Chenab, Ravi, Sutlej and Beas (Fig. 1). Conversely, the stratigraphically
603   youngest sediments plot on this diagram closest to Himalayan sources and have greater similarity
604   not only to the modern river mouth, but also Himalayan tributaries such as the Ravi, Chenab and
605   Jhellum rivers.

606   These data also imply that Nanga Parbat has not been a very important contributor to the
607   bulk sediment flux. Whether this is actually true or not is not entirely apparent because the
608   bedrock analyses from Nanga Parbat were focused on igneous rocks in the center of that
609   metamorphic massif, and might not be representative of the net erosional flux from this
610   particular source. However, the relationships displayed in Figure 11B can be readily explained as
611   a simple mixing between Karakoram and Himalayan sources, with a progressive shift towards
612   the Himalaya through time.

613   *6.2 Unmixing Sources*

614   In order to further characterize the evolving source of sediments to the Indus Fan we
615   employ the unmixing software of Sundell and Saylor [2017], which analyzes the U-Pb age
616   spectra from each of the samples and compares them with the defined end-member compositions
617   of the different source ranges compiled from the published literature. This approach works
618   particularly well in the western Himalaya where the sources are well defined and often unique.
619   Data from the Tethyan, Greater and Lesser Himalaya were compiled from DeCelles *et al.* [2004].
620   Data from the Karakoram are from Le Fort *et al.* [1983], Parrish and Tirrul [1989], Schärer *et al.*
621   [1990], Fraser *et al.* [2001] and Ravikant *et al.* [2009]. Data from Nanga Parbat are from Zeitler
622   and Chamberlain [1991] and Zeitler *et al.* [1993]. Data from the Transhimalayan are from
623   Honegger *et al.* [1982], Schärer *et al.* [1984], Krol *et al.* [1996], Weinberg and Dunlap [2000],
624   Zeilinger *et al.* [2001], Dunlap and Wysoczanski [2002], Singh *et al.* [2007], and Ravikant *et al.*
625   [2009].

626 This unmixing method uses a Monte Carlo approach to estimate the contributions from
627 the different sources that would be required to generate the modes and modal abundances of U-
628 Pb ages seen in the sediment samples. Because this is relatively objective the method is
629 considered robust for analyzing potential source contributions, assuming that the sources
630 themselves have been well characterized. The bedrock sources of the Indus catchment have
631 significant differences between many of them and are some of the best characterized worldwide.
632 Results of the Monte Carlo simulation are provided in Table 4, showing the output using all three
633 statistical comparison methods, cross-correlation, the best V value in the Kuiper test. as well as
634 the best D value in the K-S test. The method involves creating 10,000 model mixed sediments
635 using the defined bedrock source end members. The DZMix software then compares the model
636 with the measured spectra and retains the best 1% of these models in order to estimate which
637 sources were contributing the sampled material. We favor the unmixing models derived from the
638 cross-correlation approach as being geological reasonable and favored by Sundell and Saylor
639 [2017].

640 The results of our unmixing calculations show a progressive provenance evolution that is
641 consistent with that seen in the MDS diagram (Figs. 11 and 12). The very oldest sample
642 deposited at 15.5 Ma shows a dominance of sediment eroded from the Karakoram and from the
643 Tethyan and Greater Himalaya. Most of the Miocene samples dated between 8.2 and 7.0 Ma are
644 more dominated by material from the Karakoram but also usually show significant Tethyan and
645 Greater Himalayan contributions. This Himalayan component is particularly noteworthy at 7.99,
646 7.84, 7.78, 7.66, and 7.0 Ma during this interval. The proportion of Karakoram zircons shows a
647 significant decrease starting no later than 5.72 Ma and again at 3.02 Ma. The sediment deposited
648 at 3.17 Ma shows the greatest amount of modeled erosion from Karakoram sources of any
649 sample.

Legend:
- ● New data
- ○ Previously published data

Modern River — 0.0 Ma ○
TH10-8 — 6.6 Ka ○
KB40 — 15 Ka ○
U1456A-11H-6 60-69cm — 0.93 Ma ○
U1456A-26F-3 50-58 cm — 1.32 Ma ●

U1456A-51F-3 100-110 cm — 1.56 Ma ○
U1456A-61F-3 40-50 cm — 1.92 Ma ○
U1456A-70F-2 10-16 cm — 3.02 Ma ○
U1457C-31R-1 94-100 cm — 3.17 Ma ●
U1457C-33R-3 10-17 cm — 3.39 Ma ○

U1456C-45X-3 45-51 cm — 3.57 Ma ●
U1456D-5R-1 12-20 cm — 5.72 Ma ○
U1457C-41R-2 20-26 cm — 5.77 Ma ●
U1457C-42R-1 80-88 cm — 5.82 Ma ●
U1457C-43R-2 55-63 cm — 5.87 Ma ○

U1456D-12R-1 30-36 cm — 7.0 Ma ●
U1456D-13R-1 30-38 cm — 7.07 Ma ○
U1456D-15R-1 55-61 cm — 7.27 Ma ●
U1456D-19R-2 20-26 cm — 7.66 Ma ●
U1456D-20R-1 95-103 cm — 7.72 Ma ●

U1457C-51R-4 80-88 cm — 7.77 Ma ●
U1456D-22R-1 73-83 cm — 7.84 Ma ○
U1457C-61R-1 8-18 cm — 7.98 Ma ●
U1456D-26R-2 37-43 cm — 8.08 Ma ●
U1456D-27R-2 100-106 cm — 8.15 Ma ●

U1456D-28R-1 40-46 cm — 8.2 Ma ●
U1456D-29R-2 24-34 cm — 8.27 Ma ○
U1456E-19R-3 10-20 cm — 15.57 Ma ○

Legend (provenance):
- Tethyan & Greater Himalaya
- Lesser Himalaya
- Karakoram
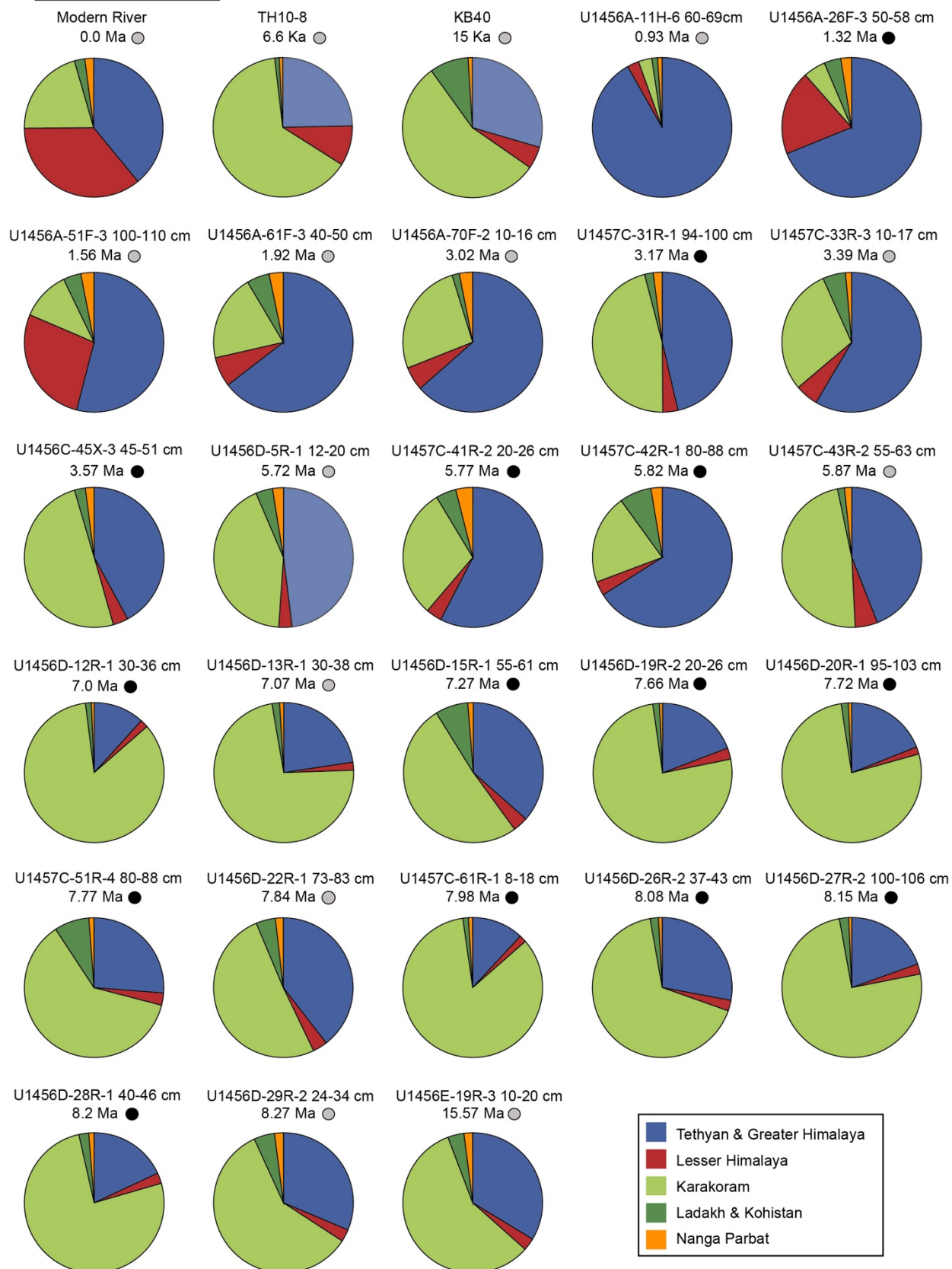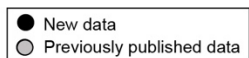- Ladakh & Kohistan
- Nanga Parbat

650

26

651 **Figure 12.** Pie diagrams showing the predicted source compositions of the zircon populations in
652 sands from the Laxmi Basin as unmixed using the software of Sundell and Saylor [2017]. Note
653 the significant reduction in flux from the Karakoram starting ~5.72 and again at 3.02 Ma.
654 Samples are marked to show those published by Clift *et al.* [2019b], and those presented new
655 here.

656

657   From 3.02 Ma onwards the Himalaya dominate as sources to the submarine fan, with
658 significant amounts of material from the Lesser Himalaya first appearing at 1.56 Ma. The sample
659 dated as being deposited at 0.93 Ma is anomalous for being very similar in source signature to
660 Tethyan and Greater Himalayan bed rocks sources. However, we note that fission track data
661 indicate that this sample was derived from peninsular India [*Zhou et al.*, 2019]. The unmixing
662 analysis largely mirrors the pattern shown by the MDS diagram, in showing a progressive long-
663 term increase in erosion from the Himalaya relative to the Karakoram, although with significant
664 steps making the evolution nonlinear. All of the samples contain a small amount of very young
665 <25 Ma zircons. None of the samples analyzed show a close similarity with post-LGM river
666 compositions. Delta samples deposited at 6.6 and 15 ka are strongly enriched in Karakoram-
667 derived grains compared to fan sediments deposited at and after 3.02 Ma. This short term
668 variability is interpreted to reflect the short-term changes in erosion patterns linked to monsoon
669 strength, modulated by glacial cycles since the onset of the NHG.

670   *6.3 Relationships to Climate Change and Tectonics*

671   The progressive increase in the relative flux from the Himalaya since the Middle
672 Miocene represents the progressive unroofing of these units. Structural reconstructions of the
673 Western Himalaya predict that prior to 5.4 Ma the Greater and Lesser Himalaya were not
674 exposed [*Webb*, 2013] implying that the Himalayan contribution was derived entirely from the
675 Tethyan Himalaya during the Miocene. As we are not able to distinguish between Tethyan and
676 Greater Himalaya derived sediment we focused on the first appearance of significant amounts of
677 1500–2300 Ma, Inner Lesser Himalayan detritus starting at 1.56 Ma. Previous studies considered
678 these ranges to have been exposed somewhat before 1.6 Ma. Study of the Siwalik Group in the
679 area of the Beas River Valley indicated an initial exposure of these units around 9 Ma and
680 significant exposure by 6 Ma based on Nd isotope data [*Najman et al.*, 2009]. Our data support
681 the findings of Clift *et al*. [2019b] that this exposure may only reflect the local situation in the
682 paleo-Beas River area, but that widespread regional exposure of the Inner Lesser Himalayan
683 units comes somewhat later. While Clift *et al*. [2019b]favored increased Inner Lesser Himalaya
684 erosion starting at 1.9 Ma our new zircon data imply that 1.56 Ma is a more accurate age for this
685 this transition.

686   Our result also contrasts with the suggestion by Myrow *et al.* [2015] that the Inner Lesser
687 Himalaya were widely exposed and eroding by 16 Ma. Although we cannot exclude this from
688 happening further east in the Ganges Basin our data do not support this over a wide area of the
689 western Himalaya until much later.

690   The timing of Lesser Himalayan unroofing may reflect the development of the thrust
691   duplex, which characterizes the structure of the Lesser Himalaya in this area [*Huyghe et al.*,
692   2001; *Webb*, 2013]. Integrated metamorphic and geochronologic data indicate rapid cooling of
693   the Inner Lesser Himalaya before 6 Ma, following peak metamorphism around 10 Ma [*Caddick*
694   *et al.*, 2007; *Thiede et al.*, 2009]}. We note that rapid cooling does not however require
695   synchronous unroofing. The first major flux of Himalayan zircons to the submarine fan is dated
696   at 7.99 to 7.78 Ma, although widespread Himalayan unroofing may not have started until 5.72
697   Ma, followed by Inner Lesser Himalayan unroofing starting around 1.56 Ma. This timing is
698   younger than reconstructed by Colleps *et al.* [2018] who favor exposure of the Outer Lesser
699   Himalaya after 16 Ma and of the Inner Lesser Himalaya after 11 Ma, although that study was
700   again located in an area father east, within the wetter Ganges catchment, and need not apply to
701   the drier Indus basin. A more erosive climate further east might favor earlier unroofing in that
702   area. The erosion data support the concept of significant along strike diachroneity of unroofing.

703   Uplift of the Lesser Himalayan Duplex would have created a topographic barrier,
704   susceptible to erosion as monsoon rains were focused along this topographic front. The
705   increasing Himalayan character of the total zircon input comes at a time when the summer
706   monsoon rains were generally weakening after ~8 Ma [*Dettman et al.*, 2001], or after 7.7 Ma
707   based on new environmental data from Site U1456 [*Clift et al.*, 2019a](Fig. 13). Moisture
708   delivery to this area from the winter westerlies has also been shown to have reduced around 7
709   Ma [*Vögeli et al.*, 2017]. In the recent geologic past, since the LGM, strong Himalayan rather
710   than Karakoram erosion has occurred when the summer monsoon was strong, during interglacial
711   times and not when it was weak during glacial times [*Clift et al.*, 2008a]. The increase in
712   Himalayan erosion over longer periods of time, correlating with the weakening monsoon, is the
713   opposite of this shorter-term trend. It is possible that solid Earth tectonic forces, rather than
714   climate, have dominated the long-term evolution of erosion, although the temporal correlation of
715   provenance and aridity is suggestive of a climatic control.

716

Figure 13. Comparison of climate, erosion and exhumation proxies in the Himalaya. (a)
Smoothed Nd isotope history for the Indus River with grey background showing effective
uncertainties from Clift *et al.* [2018]. (b) Breakdown of the sources of detrital zircons based on
the unmixing procedure of Sundell and Saylor [2017]. (c) Carbon isotope character of pedogenic
carbonate in Pakistan as an indicator of dominant vegetation in the Potwar Plateau of Pakistan
[Quade *et al.*, 1989], and NW India [*Singh et al.*, 2011]. (d) Relative exhumation rates of the
Greater Himalaya tracked by bedrock Ar-Ar dating [*Clift et al.*, 2008b] and zircon fission track
from foreland basin sediment [Chirouze *et al.*, 2015]. (e) Rates of sediment supply to the Arabian
Sea calculated from regional seismic [*Clift*, 2006].

All of the samples show the presence of very young zircons (<25 Ma) that possibly
correlate with bedrock dates from Nanga Parbat, although these are never very numerous. It is
also possible that some of these young ages may in fact be derived from erosion of fast
exhuming rocks in parts of the southern Karakoram [*Wallis et al.*, 2014]. However, even if that
this material was derived from Nanga Parbat, the low abundance of such zircon grains in the
Laxmi Basin sediments would suggest that this massif was not generating very high proportions
of sediment in the trunk Indus river, unlike the situation in the eastern syntaxis [*Garzanti et al.*,
2004; *Stewart et al.*, 2008]. This is consistent with the U-Pb zircon ages in the modern Indus
River downstream of Nanga Parbat [*Alizai et al.*, 2011] that show neither many <25 Ma zircons
or older 1500–2300 Ma grains that would be associated with less deeply buried rocks but with
the Lesser Himalaya affiliation typically made with Nanga Parbat [*Whittington et al.*, 1999].

738   We compare our detrital zircon budget with that of the Nd budget published by Clift *et al.*
739   [2019b]. Translating zircon budgets into rock erosion budgets is not easy due to bedrock zircon
740   fertility variations. However, whole-rock geochemical analysis of Alizai *et al.* [2012] suggested
741   that on average the eastern, Himalaya-draining tributaries are around 2.2 times more fertile in
742   zircon than the trunk Indus. If we simply use the source percentages from the zircon unmixing
743   calculation described above and the average ϵ_{Nd} values for these different units then it is possible
744   to predict the average composition of the bulk sediment through time. We use an ϵ_{Nd} value of -
745   14.6 for the Greater and Tethyan Himalaya, -21.7 for the Lesser Himalaya, -9.3 for the
746   Karakoram, -20 for Nanga Parbat and +5.1 for Kohistan and the Transhimalaya based on
747   synthesis of the bedrock data, but especially the composition of river sediments that are derived
748   from wide areas of these ranges [*Clift et al.*, 2002b]. Transhimalaya Nd data are from Rolland *et*
749   *al.* [2002], Singh *et al.* [2002], and Khan *et al.* [1997]. Greater and Lesser Himalayan data are
750   from Ahmad *et al.* [2000], Deniel *et al.* [1987], Inger *et al.* [1993] and Parrish and Hodges
751   [1996]. Karakoram data are from Crawford and Searle [1992] and Schärer *et al.* [1990].

752   The results of this estimate are shown next to the smoothed long-term Nd isotope
753   evolution from bulk sediment analysis [*Clift et al.*, 2019b] (Fig. 13). We account for the ±1 ϵ_{Nd}
754   uncertainty value estimated from the Indus Quaternary [*Jonell et al.*, 2018]. We note that before
755   6 Ma the estimates overlap with the bulk sediment record that was derived from muddy
756   lithologies, suggesting similar sources. After this time both the estimated and measured ϵ_{Nd}
757   values became more negative. However, the predicted Nd isotope compositions are always more
758   negative than those measured from the bulk sediment and this implies an over estimation in the
759   flux from isotopically negative sources, i.e. the Himalaya, using the zircon method. This is
760   consistent with the geochemical data indicating that the Himalaya are more abundant in zircon
761   than the Karakoram, but have similar concentrations in Nd [*Alizai et al.*, 2011]. As a result, our
762   zircon budget (Fig. 13) represents an overestimate of the influence of the Himalaya compared the
763   Karakoram through time in terms of total rock eroded. Nonetheless, the overall trends in the two
764   data sets are consistent and the reconstruction of increasing Himalayan erosion since the 5.72 Ma
765   may be considered robust.

7. Conclusions

767   Sandy and silty sediments recovered from the Laxmi Basin in the Eastern Arabian Sea
768   provide a relatively continuous erosional record derived from the Indus River and spanning the
769   last 15.5 m.y. In this study samples were taken from IODP Sites U1456 and U1457 for
770   geochemical and geochronological analyses. Detrital zircon grains were dated by U-Pb methods
771   to determine their provenance. The sediments themselves are defined as wackes and are
772   relatively immature in composition, with bulk sediment characters similar to those found in the
773   Quaternary delta of the Indus and in its submarine Canyon. They are readily distinguishable from
774   sediments on the Western Indian Shelf, confirming their derivation from the Indus River and not
775   the peninsula with one exception. The sediments are mostly of silty sand to silt size, with only a
776   few being classified as fine sand. Although the sediments are relatively depleted in Ca, Na and P
777   relative to the upper continental crust this reflects chemical weathering during transport and does
778   not affect the provenance analysis conducted here.

779   Detrital zircon U-Pb ages fall into a number of categories which can be correlated with
780   bedrock sources in the Himalaya. The ubiquitous presence of zircon grains younger than 200 Ma
781   requires the sediments to be the erosional products of the Himalaya/Karakoram and not
782   peninsular India. The progressive increase in zircon grains dating at 350–1250 Ma, as well as
783   1500–2300 Ma, indicates that the erosional flux from the Himalaya increased through the studied
784   time interval. Almost all the samples contain grains that could be derived from the Karakoram or
785   from Kohistan, and there is an appearance of very young zircon grains, younger than 25 Ma, that
786   is especially marked since 3.17 Ma. Such young zircon grains may be from Nanga Parbat or
787   parts of the eastern Karakoram. Statistical analysis shows that there are a number of groupings
788   and an increase in Himalayan erosion through time. High flux from the Himalaya was noted at
789   7.99–7.78 Ma and starting between 7.0 and 5.87 Ma. Since 1.32 Ma the sediments are similar to
790   the modern Indus River, but not like the glacial-era river, which has more similarities with the
791   Miocene Laxmi Basin samples and with enhanced erosion in the Karakoram. Detrital zircon
792   population unmixing techniques allow us to objectively confirm the progressive increase of
793   Himalayan erosion relative to the Karakoram, and the sharp jump in erosion from the Inner
794   Lesser Himalayas starting at 1.56 Ma. This is somewhat younger than the anticipated unroofing
795   of these ranges derived from earlier foreland studies, although much of the earlier data comes
796   from further east in the Ganges catchment. The shift to more Himalayan erosion through time
797   occurs as the monsoon climate weakened, as well as when the Lesser Himalayan Duplex formed.
798   This suggests that the changing patterns of erosion could be largely a function of solid Earth
799   tectonic forces building topography, although the correlation of unroofing to the Late Miocene
800   drying trend does raise the possible role for climate too, albeit in the opposite fashion to that seen
801   since the LGM, when more Himalayan erosion correlates with strong summer monsoon rains.
802

812   **References**

813   Ahmad, T., N. Harris, M. Bickle, H. Chapman, J. Bunbury, and C. Prince (2000), Isotopic
814   constraints on the structural relationships between the Lesser Himalayan Series and the
815   High Himalayan Crystalline Series, Garhwal Himalaya, *Geol. Soc. Am. Bull.*, *112*(3), 467-
816   477.
817   Alizai, A., A. Carter, P. D. Clift, S. VanLaningham, J. C. Williams, and R. Kumar (2011),
818   Sediment provenance, reworking and transport processes in the Indus River by U-Pb dating
819   of detrital zircon grains, *Global Planet. Change*, *76*, 33-55,
820   doi:10.1016/j.gloplacha.2010.11.008.
821   Alizai, A., S. Hillier, P. D. Clift, and L. Giosan (2012), Clay mineral variations in Holocene
822   terrestrial sediments from the Indus Basin; a response to SW Asian Monsoon variability,
823   *Quat. Res.*, *77*(3), 368–381, doi:10.1016/j.yqres.2012.01.008.
824   Amidon, W. H., D. W. Burbank, and G. E. Gehrels (2005), U-Pb zircon ages as a sediment
825   mixing tracer in the Nepal Himalaya, *Earth Planet. Sci. Letts.*, *235*(1-2), 244-260.
826   Baral, U., D. Lin, and D. Chamlagain (2015), Detrital zircon U–Pb geochronology of the Siwalik
827   Group of the Nepal Himalaya: implications for provenance analysis, *Intern. J. Earth Sci.*,
828   1-19, doi;10.1007/s00531-015-1198-7.
829   Bernet, M., P. van der Beek, R. Pik, P. Huyghe, J.-L. Mugnier, E. Labrin, et al. (2006), Miocene
830   to Recent exhumation of the central Himalaya determined from combined detrital zircon
831   fission-track and U/Pb analysis of Siwalik sediments, western Nepal, *Basin Res.*, *18*, 393–
832   412, doi: 10.1111/j.1365-2117.2006.00303.
833   Bhattacharya, G. C. B., A. K. Chaubey, G. P. S. Murty, S. Srinivas, K. V. Sarma, V.
834   Subrahmanyam, et al. (1994), Evidence for seafoor spreading in the Laxmi Basin,
835   northeastern Indian Ocean, *Earth Planet. Sci. Letts.*, *125*, 211-220.
836   Bollinger, L., J. P. Avouac, O. Beyssac, E. J. Catlos, T. M. Harrison, M. Grove, et al. (2004),
837   Thermal structure and exhumation history of the Lesser Himalaya in central Nepal,
838   *Tectonics*, *23*(5), 19, doi:10.1029/2003TC001564.
839   Bookhagen, B., R. C. Thiede, and M. R. Strecker (2005), Late Quaternary intensified monsoon
840   phases control landscape evolution in the northwest Himalaya, *Geology*, *33*(2), 149-152,
841   doi:10.1130/G20982.1.
842   Burbank, D. W., A. E. Blythe, J. Putkonen, B. Pratt-Sitaula, E. Gabet, M. Oskins, et al. (2003),
843   Decoupling of erosion and precipitation in the Himalayas, *Nature*, *426*, 652–655.
844   Caddick, M. J., M. J. Bickle, N. B. W. Harris, T. J. B. Holland, M. S. A. Horstwood, R. R.
845   Parrish, et al. (2007), Burial and exhumation history of a Lesser Himalayan schist:
846   Recording the formation of an inverted metamorphic sequence in NW India, *Earth Planet.*
847   *Sci. Letts.*, *264*(3–4), 375–390, doi:10.1016/j.epsl.2007.09.011.
848   Caley, T., D. M. Roche, and H. Renssen (2014), Orbital Asian summer monsoon dynamics
849   revealed using an isotope-enabled global climate model, *Nature Comm.*, *5*, 5371,
850   doi:10.1038/ncomms6371.
851   Calvès, G., M. Huuse, P. D. Clift, and S. Brusset (2015), Giant fossil mass wasting off the coast
852   of West India: The Nataraja submarine slide, *Earth Planet. Sci. Letts.*, *432*, 265–272,
853   doi:10.1016/j.epsl.2015.10.022.
854   Catlos, E. J., T. M. Harrison, M. J. Kohn, M. Grove, F. J. Ryerson, C. E. Manning, et al. (2001),
855   Geochronologic and thermobarometric constraints on the evolution of the Main Central
856   Thrust, central Nepal Himalaya, *J. Geophys. Res.*, *106*(B8), 16,177-116,204.

857   Chirouze, F., P. Huyghe, C. Chauvel, P. van der Beek, M. Bernet, and J.-L. Mugnier (2015),
858   Stable Drainage Pattern and Variable Exhumation in the Western Himalaya since the
859   Middle Miocene, *J. Geol.*, *123*, 1–20, doi:10.1086/679305.
860   Clift, P., C. Gaedicke, R. Edwards, J. Lee, II, P. Hildebrand, S. Amjad, et al. (2002a), The
861   stratigraphic evolution of the Indus Fan and the history of sedimentation in the Arabian
862   Sea, *Mar. Geophys. Res.*, *23*(3), 223-245.
863   Clift, P. D. (2006), Controls on the erosion of Cenozoic Asia and the flux of clastic sediment to
864   the ocean, *Earth Planet. Sci. Letts.*, *241*(3-4), 571-580.
865   Clift, P. D., and J. S. Blusztajn (2005), Reorganization of the western Himalayan river system
866   after five million years ago, *Nature*, *438*(7070), 1001-1003.
867   Clift, P. D., I. H. Campbell, M. S. Pringle, A. Carter, X. Zhang, K. V. Hodges, et al. (2004),
868   Thermochronology of the modern Indus River bedload; new insight into the control on the
869   marine stratigraphic record, *Tectonics*, *23*(TC5013), doi:10.1029/2003TC001559.
870   Clift, P. D., L. Giosan, J. Blusztajn, I. H. Campbell, C. M. Allen, M. Pringle, et al. (2008a),
871   Holocene erosion of the Lesser Himalaya triggered by intensified summer monsoon,
872   *Geology*, *36*(1), 79–82, doi: 10.1130/G24315A.1.
873   Clift, P. D., L. Giosan, A. Carter, E. Garzanti, V. Galy, A. R. Tabrez, et al. (2010), Monsoon
874   control over erosion patterns in the Western Himalaya: possible feed-backs into the
875   tectonic evolution, in *Monsoon evolution and tectonic-climate linkage in Asia*, edited by P.
876   D. Clift, R. Tada and H. Zheng, pp. 181–213, Geological Society, London.
877   Clift, P. D., K. Hodges, D. Heslop, R. Hannigan, L. V. Hoang, and G. Calves (2008b), Greater
878   Himalayan exhumation triggered by Early Miocene monsoon intensification, *Nature*
879   *Geosci.*, *1*, 875-880, doi:10.1038/ngeo351.
880   Clift, P. D., D. K. Kulhanek, P. Zhou, M. G. Bowen, S. M. Vincent, M. Lyle, et al. (2019a),
881   Chemical Weathering and Erosion Responses to Changing Monsoon Climate in the Late
882   Miocene of Southwest Asia, *Geol. Mag.*, doi:10.1017/S0016756819000608.
883   Clift, P. D., J. I. Lee, P. Hildebrand, N. Shimizu, G. D. Layne, J. Blusztajn, et al. (2002b), Nd
884   and Pb isotope variability in the Indus River system; implications for sediment provenance
885   and crustal heterogeneity in the western Himalaya, *Earth Planet. Sci. Letts.*, *200*(1-2), 91-
886   106, doi:10.1016/S0012-821X(02)00620-9.
887   Clift, P. D., N. Shimizu, G. Layne, C. Gaedicke, H. U. Schlüter, M. K. Clark, et al. (2001),
888   Development of the Indus Fan and its significance for the erosional history of the western
889   Himalaya and Karakoram, *Geol. Soc. Am. Bull.*, *113*, 1039–1051.
890   Clift, P. D., P. Zhou, D. F. Stockli, and J. Blusztajn (2018), Regional Pliocene Exhumation of the
891   Lesser Himalaya in the Indus Drainage, *Solid Earth*, doi:10.5194/se-2018-132.
892   Clift, P. D., P. Zhou, D. F. Stockli, and J. Blusztajn (2019b), Regional Pliocene Exhumation of
893   the Lesser Himalaya in the Indus Drainage, *Solid Earth*, *10*, 647–661, doi:10.5194/se-10-
894   647-2019.
895   Colleps, C. L., R. N. McKenzie, D. F. Stockli, N. C. Hughes, B. P. Singh, A. A. G. Webb, et al.
896   (2018), Zircon (U-Th)/He thermochronometric constraints on Himalayan thrust belt
897   exhumation, bedrock weathering, and Cenozoic seawater chemistry, *Geochem. Geophys.*
898   *Geosyst.*, *19*, 257– 271, doi:10.1002/2017GC007191.
899   Colleps, C. L., D. F. Stockli, N. R. McKenzie, A. G. Webb, and B. K. Horton (2019), Neogene
900   kinematic evolution and exhumation of the NW India Himalaya: Zircon geo-
901   /thermochronometric insights from the fold-thrust belt and foreland basin, *Tectonics*, *38*,
902   2059–2086, 10.1029/2018TC005304.

903 Courtillot, V., Y. Gallet, R. Rocchia, G. Féraud, E. Robin, C. Hofmann, et al. (2000), Cosmic
904   markers, 40Ar/39Ar dating and paleomagnetism of the KT sections in the Anjar Area of
905   the Deccan large igneous province, *Earth Planet. Sci. Letts.*, *182*, 137-156.
906 Crawford, M. B., and M. P. Searle (1992), Field relationships and geochemistry of pre-
907   collisional (India-Asia) granitoid magmatism in the central Karakoram, northern Pakistan,
908   *Tectonophysics*, *206*(1-2), 171-192.
909 Dailey, S. K., P. D. Clift, D. K. Kulhanek, J. Blusztajn, C. M. Routledge, G. Calvès, et al.
910   (2019), Large-scale Mass Wasting on the Miocene Continental Margin of Western India,
911   *Geol. Soc. Am. Bull.*, doi:/10.1130/B35158.1.
912 DeCelles, P. G., G. E. Gehrels, Y. Najman, A. J. Martin, A. Carter, and E. Garzanti (2004),
913   Detrital geochronology and geochemistry of Cretaceous-Early Miocene strata of Nepal:
914   implications for timing and diachroneity of initial Himalayan orogenesis, *Earth Planet. Sci.*
915   *Letts.*, *227*(3-4), 313-330.
916 DeCelles, P. G., G. E. Gehrels, J. Quade, B. LaReau, and M. Spurlin (2000), Tectonic
917   implications of U-Pb zircon ages of the Himalayan orogenic belt in Nepal, *Science*,
918   *288*(5465), 497-499, doi:10.1126/science.288.5465.497.
919 Deniel, C., P. Vidal, A. Fernandez, P. Fort, and J.-J. Peucat (1987), Isotopic study of the Manaslu
920   granite (Himalaya, Nepal): inferences on the age and source of Himalayan leucogranites,
921   *Contribs. Min. Petrol.*, *96*(1), 78-92.
922 Deptuck, M. E., D. J. Piper, B. Savoye, and A. Gervais (2008), Dimensions and architecture of
923   late Pleistocene submarine lobes off the northern margin of East Corsica, *Sedimentology*,
924   *55*(4), 869-898.
925 Dettman, D. L., M. J. Kohn, J. Quade, F. J. Ryerson, T. P. Ojha, and S. Hamidullah (2001),
926   Seasonal stable isotope evidence for a strong Asian monsoon throughout the past 10.7 m.y,
927   *Geology*, *29*(1), 31-34.
928 Dunlap, W. J., and R. Wysoczanski (2002), Thermal evidence for Early Cretaceous
929   metamorphism in the Shyok suture zone and age of the Khardung volcanic rocks, Ladakh,
930   India, *J. Asian Earth Sci.*, *20*(5), 481-490.
931 Dunlea, A. G., R. W. Murray, J. Sauvage, A. J. Spivack, R. N. Harris, and S. D'Hondt (2015),
932   Dust, volcanic ash, and the evolution of the South Pacific Gyre through the Cenozoic,
933   *Paleocean.*, *30*(8), 1078-1099, doi:10.1002/2015PA002829.
934 Fedo, C. M., H. W. Nesbitt, and G. M. Young (1995), Unraveling the effects of potassium
935   metasomatism in sedimentary rocks and paleosols, with implications for paleoweathering
936   conditions and provenance, *Geology*, *23*, 921–924.
937 Fleitmann, D., S. J. Burns, M. Mudelsee, U. Neff, J. Kramers, A. Mangini, et al. (2003),
938   Holocene forcing of the Indian monsoon recorded in a stalagmite from southern Oman,
939   *Science*, *300*(5626), 1737-1739.
940 Folk, R. L. (1974), *Petrology of Sedimentary Rocks*, 182 pp., Hemphill Press, Austin, Texas.
941 Fraser, J. E., M. P. Searle, R. R. Parrish, and S. R. Noble (2001), Chronology of deformation,
942   metamorphism, and magmatism in the southern Karakoram Mountains, *Geol. Soc. Am.*
943   *Bull.*, *113*(11), 1443-1455.
944 Gaedicke, C., H.-U. Schlueter, H.-A. Roeser, A. Prexl, B. Schreckenberger, H. Meyer, et al.
945   (2002), Origin of the northern Indus Fan and Murray Ridge, northern Arabian Sea;
946   interpretation from seismic and magnetic imaging, *Tectonophysics*, *355*, 127-143.
947 Garzanti, E., S. Andò, and G. Vezzoli (2009), Grain-size dependence of sediment composition
948   and environmental bias in provenance studies, *Earth Planet. Sci. Letts.*, *277*(3-4), 422-432.

949 Garzanti, E., A. Baud, and G. Mascle (1987), Sedimentary record of the northward flight of India
950   and its collision with Eurasia (Ladakh Himalaya, India), *Geodin. Acta*, *1*(4/5), 297–312.
951 Garzanti, E., W. Liang, S. Andò, P. D. Clift, A. Resentini, P. Vermeesch, et al. (2020),
952   Provenance of Thal Desert sand: Focused erosion in the western Himalayan syntaxis and
953   foreland-basin deposition driven by latest Quaternary climate change, *Earth Sci. Rev.*, *207*,
954   103220, doi:10.1016/j.earscirev.2020.103220.
955 Garzanti, E., G. Vezzoli, S. Ando, C. France-Lanord, S. K. Singh, and G. Foster (2004), Sand
956   petrology and focused erosion in collision orogens: the Brahmaputra case, *Earth Planet.*
957   *Sci. Letts.*, *220*(1-2), 157-174.
958 Garzanti, E., G. Vezzoli, S. Ando, P. Paparella, and P. D. Clift (2005), Petrology of Indus River
959   sands; a key to interpret erosion history of the western Himalayan syntaxis, *Earth Planet.*
960   *Sci. Letts.*, *229*(3-4), 287-302, doi: 10.1016/j.epsl.2004.11.008.
961 Gehrels, G. (2012), Detrital Zircon U-Pb Geochronology: Current Methods and New
962   Opportunities, in *Tectonics of Sedimentary Basins*, edited by C. Busby and A. Azor, pp.
963   47-62, Wiley, doi:10.1002/9781444347166.ch2.
964 Gehrels, G. E., P. Kapp, P. DeCelles, A. Pullen, R. Blakely, A. Weislgel, et al. (2011), Detrital
965   zircon geochronology of pre-Tertiary strata in the Tibetan-Himalayan orogen, *Tectonics*,
966   *30*(TC5016), doi:10.1029/2011TC002868.
967 Gehrels, G. E., V. Valencia, and J. Ruiz (2008), Enhanced precision, accuracy, efficiency, and
968   spatial resolution of U-Pb ages by laser ablation–multicollector–inductively coupled
969   plasma–mass spectrometry, *Geochem. Geophys. Geosyst.*, *9*(Q03017),
970   doi:10.1029/2007GC001805.
971 Guidry, M. W., and F. T. Mackenzie (2000), Apatite weathering and the Phanerozoic phosphorus
972   cycle, *Geology*, *28*(7), 631-634.
973 Gupta, A. K., D. M. Anderson, and J. T. Overpeck (2003), Abrupt changes in the Asian
974   southwest monsoon during the Holocene and their links to the North Atlantic Ocean,
975   *Nature*, *421*, 354–356.
976 Hart, N. R., D. F. Stockli, and N. W. Hayman (2016), Provenance evolution during progressive
977   rifting and hyperextension using bedrock and detrital zircon U-Pb geochronology, Mauléon
978   Basin, western Pyrenees, *Geosphere*, *12*(4), 1166-1186, doi:10.1130/GES01273.1.
979 Herron, M. M. (1988), Geochemical classification of terrigenous sands and shales from core or
980   log data, *J. Sed. Petrol.*, *58*, 820–829.
981 Hildebrand, P. R., S. R. Noble, M. P. Searle, D. J. Waters, and R. R. Parrish (2001), Old origin
982   for an active mountain range; geology and geochronology of the eastern Hindu Kush,
983   Pakistan, *Geol. Soc. Am. Bull.*, *113*(5), 625-639.
984 Hodges, K. (2003), Geochronology and thermochronology in orogenic systems, in *The Crust*,
985   edited by R. Rudnick, pp. 263-292, Elsevier-Science, Amsterdam.
986 Hodges, K. V. (2000), Tectonics of the Himalaya and southern Tibet from two perspectives,
987   *Geol. Soc. Am. Bull.*, *112*(3), 324-350.
988 Honegger, K., V. Dietrich, W. Frank, A. Gansser, M. Thoni, and V. F. Trommsdorf (1982),
989   Magmatism and metamorphism in the Ladakh Himalayas (The Indus-Tsangpo suture
990   zone), *Earth Planet. Sci. Letts.*, *60*, 178-194.
991 Howell, A. L., S. J. Bentley, K. Xu, R. E. Ferrell, Z. Muhammad, and E. Septama (2014), Fine
992   sediment mineralogy as a tracer of latest Quaternary sediment delivery to a dynamic
993   continental margin: Pandora Trough, Gulf of Papua, Papua New Guinea, *Mar. Geol.*, *357*,
994   108-122, doi:10.1016/j.margeo.2014.08.003.

995 Hu, X., E. Garzanti, J. Wang, W. Huang, W. An, and A. Webb (2016), The timing of India-Asia
996   collision onset – Facts, theories, controversies, *Earth Sci. Rev.*, *160*, 264-299,
997   doi:10.1016/j.earscirev.2016.07.014.
998 Huyghe, P., A. Galy, J.-L. Mugnier, and C. France-Lanord (2001), Propagation of the thrust
999   system and erosion in the Lesser Himalaya: Geochemical and sedimentological evidence,
1000   *Geology*, *29*(11), 1007–1010.
1001 Inger, S., and N. Harris (1993), Geochemical constraints on leucogranite magmatism in the
1002   Langtang Valley, Nepal Himalaya, *J. Petrol.*, *34*(2), 345-368.
1003 Jackson, S. E., N. J. Pearson, W. L. Griffin, and E. A. Belousova (2004), The application of laser
1004   ablation-inductively coupled plasma-mass spectrometry (LA-ICP-MS) to in situ U–Pb
1005   zircon geochronology, *Chem. Geol.*, *211*, 47–69.
1006 Jaeger, J.-J., V. Courtillot, and P. Tapponnier (1989), Paleontological view of the ages of the
1007   Deccan Traps, the Cretaceous/Tertiary boundary, and the India-Asia collision, *Geology*,
1008   *17*(4), 316-319, doi:10.1130/0091-7613(1989)017<0316:Pvotao>2.3.Co;2.
1009 Jonell, T. N., A. Carter, P. Böning, K. Pahnke, and P. D. Clift (2017), Climatic and glacial
1010   impact on erosion patterns and sediment provenance in the Himalayan rain shadow,
1011   Zanskar River, NW India, *Geol. Soc. Am. Bull.*, *129*(7-8), 820-836, doi:10.1130/B31573.
1012 Jonell, T. N., Y. Li, J. Blusztajn, L. Giosan, and P. D. Clift (2018), Signal or noise? Isolating
1013   grain size effects on Nd and Sr isotope variability in Indus delta sediment provenance,
1014   *Chem. Geol.*, *485*, 56–73, doi:10.1016/j.chemgeo.2018.03.036.
1015 Khan, M. A., R. J. Stern, R. F. Gribble, and B. F. Windley (1997), Geochemical and isotopic
1016   constraints on subduction polarity, magma sources, and palaeogeography of the Kohistan
1017   intra-oceanic arc, northern Pakistan Himalaya, *J. Geol. Soc.*, *154*, 935–946.
1018 Khim, B.-K., K. Horikawa, Y. Asahara, J.-E. Kim, and M. Ikehara (2019), Detrital Sr-Nd
1019   isotopes, sediment provenances, and depositional processes in the Laxmi Basin of the
1020   Arabian Sea during the last 800 kyrs, *Geol. Mag.*, 1-13, doi:10.1017/S0016756818000596.
1021 Klootwijk, C. T., J. S. Gee, J. W. Peirce, G. M. Smith, and P. L. McFadden (1992), An early
1022   India-Asia contact: Paleomagnetic constraints from Ninetyeast Ridge, ODP Leg 121,
1023   *Geology*, *20*(5), 395-398, DOI: 10.1130/0091-7613(1992)020.
1024 Kolla, V., and F. Coumes (1987), Morphology, internal structure, seismic stratigraphy, and
1025   sedimentation of Indus Fan, *AAPG Bull.*, *71*, 650–677.
1026 Krol, M. A., P. K. Zeitler, and P. Copeland (1996), Episodic unroofing of the Kohistan Batholith,
1027   Pakistan: Implications from K-feldspar thermochronology, *J. Geophys. Res.-Solid Earth*,
1028   *101*(B12), 28149-28164.
1029 Kurian, S., B. N. Nath, N. C. Kumar, and K. K. C. Nair (2013), Geochemical and Isotopic
1030   Signatures of Surficial Sediments from the Western Continental Shelf of India: Inferring
1031   Provenance, Weathering, and the Nature of Organic Matter Geochemical and Isotopic
1032   Signatures of Sediments From The Indian West Coast, *J. Sed. Res.*, *83*(6), 427-442,
1033   doi:10.2110/jsr.2013.36.
1034 Lavé, J., and J. P. Avouac (2000), Active folding of fluvial terraces across the Siwaliks Hills
1035   (Himalayas of central Nepal), *J. Geophys. Res.*, *105*, 5735–5770, doi:
1036   10.1029/1999JB900292.
1037 Lawrence, R. L., R. Cox, R. W. Mapes, and D. S. Coleman (2011), Hydrodynamic fractionation
1038   of zircon age populations, *GSA Bulletin*, *123*(1-2), 295-305, doi:10.1130/B30151.1.
1039 Le Fort, P., F. Debon, and J. Sonet (1983), Petrography, geochemistry and geochronology of
1040   some samples from the Karakoram Batholith (N. Pakistan), in *Granites of the Himalayas,*

1041   *Karakoram and Hindu Kush*, edited by F. A. Shams, pp. 377–387, Punjab University,
1042   Lahore, Pakistan.
1043 Li, Y., P. D. Clift, P. Böning, J. Blusztajn, R. W. Murray, T. Ireland, et al. (2018), Continuous
1044   Signal Propagation in the Indus Submarine Canyon since the Last Deglacial, *Mar. Geol.*,
1045   *406*, 159–176, doi:10.1016/j.margeo.2018.09.011.
1046 Li, Y., P. D. Clift, and P. O'Sullivan (2019), Millennial and Centennial Variations in Zircon U-
1047   Pb and Apatite Fission Track Ages in the Quaternary Indus Submarine Canyon, *Basin Res.*,
1048   *31*, 155–170, doi:10.1111/bre.12313.
1049 Malusà, M. G., A. Resentini, and E. Garzanti (2016), Hydraulic sorting and mineral fertility bias
1050   in detrital geochronology, *Gondwana Res.*, *31*, 1-19, doi:10.1016/j.gr.2015.09.002.
1051 Marsh, A. D., W. G. Parker, D. F. Stockli, and J. W. Martz (2019), Regional correlation of the
1052   Sonsela Member (Upper Triassic Chinle Formation) and detrital U-Pb zircon data from the
1053   Sonsela Sandstone bed near the Sonsela Buttes, northeastern Arizona, USA, support the
1054   presence of a distributive fluvial system, *Geosphere*, *15*(4), 1128-1139, doi:10.1130
1055   /GES02004.1.
1056 Marsh, J. H., and D. F. Stockli (2015), Zircon U–Pb and trace element zoning characteristics in
1057   an anatectic granulite domain: Insights from LASS-ICP-MS depth profiling, *Lithos*, *239*,
1058   170-185, doi:10.1016/j.lithos.2015.10.017.
1059 Molnar, P. (2001), Climate change, flooding in arid environments, and erosion rates, *Geology*,
1060   *29*(12), 1071-1074.
1061 Mukhopadhyay, G., S. Mukhopadhyay, M. Roychowdhury, and P. Parui (2010), Stratigraphic
1062   correlation between different Gondwana basins of India, *J. Geol. Soc. India*, *76*(3), 251-
1063   266.
1064 Myrow, P. M., N. C. Hughes, L. A. Derry, R. N. McKenzie, G. Jiang, A. A. G. Webb, et al.
1065   (2015), Neogene marine isotopic evolution and the erosion of Lesser Himalayan strata:
1066   Implications for Cenozoic tectonic history, *Earth Planet. Sci. Letts.*, *417*, 142-150,
1067   doi:10.1016/j.epsl.2015.02.016.
1068 Najman, Y. (2006), The detrital record of orogenesis: A review of approaches and techniques
1069   used in the Himalayan sedimentary basins, *Earth Sci. Rev.*, *74*(1-2), 1-72.
1070 Najman, Y., E. Appel, M. Boudagher-Fadel, P. Bown, A. Carter, E. Garzanti, et al. (2010),
1071   Timing of India-Asia collision: Geological, biostratigraphic, and palaeomagnetic
1072   constraints, *J. Geophys. Res.*, *115*(B12416), doi:10.1029/2010JB007673.
1073 Najman, Y., M. Bickle, E. Garzanti, M. Pringle, D. Barfod, N. Brozovic, et al. (2009),
1074   Reconstructing the exhumation history of the Lesser Himalaya, NW India, from a
1075   multitechnique provenance study of the foreland basin Siwalik Group, *Tectonics*,
1076   *28*(TC5018), doi:10.1029/2009TC002506.
1077 Najman, Y., D. Jenks, L. Godin, M. Boudagher-Fadel, I. Millar, E. Garzanti, et al. (2017), The
1078   Tethyan Himalayan detrital record shows that India–Asia terminal collision occurred by 54
1079   Ma in the Western Himalaya, *Earth Planet. Sci. Letts.*, *459*, 301-310,
1080   doi:10.1016/j.epsl.2016.11.036.
1081 Nesbitt, H. W., G. Markovics, and R. C. Price (1980), Chemical processes affecting alkalis and
1082   alkaline earths during continental weathering, *Geochim. Cosmochim. Acta*, *44*, 1659–1666.
1083 Pandey, D. K., P. D. Clift, D. K. Kulhanek, S. Andò, J. A. P. Bendle, S. Bratenkov, et al.
1084   (2016a), Site U1456, in *Arabian Sea Monsoon. Proceedings of the International Ocean
1085   Discovery Program*, edited by D. K. Pandey, P. D. Clift and D. K. Kulhanek, International
1086   Ocean Discovery Program, College Station, TX, doi:10.14379/iodp.proc.355.103.2016.

1087   Pandey, D. K., P. D. Clift, D. K. Kulhanek, S. Andò, J. A. P. Bendle, S. Bratenkov, et al.
1088   (2016b), Site U1457, in *Arabian Sea Monsoon. Proceedings of the International Ocean*
1089   *Discovery Program*, edited by D. K. Pandey, P. D. Clift and D. K. Kulhanek, International
1090   Ocean Discovery Program, College Station, TX, doi:10.14379/iodp.proc.355.104.2016.
1091   Pandey, D. K., P. D. Clift, D. K. Kulhanek, and Expedition 355 Scientists (2016c), Arabian Sea
1092   Monsoon, *Proc. Int. Ocean Disc. Prog.*, *355*, doi:10.14379/iodp.proc.355.2016.
1093   Pandey, D. K., P. D. Clift, D. K. Kulhanek, and Expedition 355 Scientists (2016d), Arabian Sea
1094   Monsoon: Expedition Summary, *Proc. Int. Ocean Disc. Prog.*, *355*, 1-32,
1095   doi:10.14379/iodp.proc.355.101.2016.
1096   Pandey, O. P., P. K. Agrawal, and J. G. Negi (1995), Lithospheric structure beneath Laxmi
1097   Ridge and late Cretaceous geodynamic events, *Geo-Mar. Lett.*, *15*, 85-91.
1098   Parrish, R. R., and K. V. Hodges (1996), Isotopic constraints on the age and provenance of the
1099   Lesser and Greater Himalayan sequences, Nepalese Himalaya, *Geol. Soc. Am. Bull.*,
1100   *108*(7), 904-911.
1101   Parrish, R. R., and R. Tirrul (1989), U-Pb age of the Baltoro Granite, Northwest Himalaya, and
1102   implications for monazite U-Pb systematics, *Geology*, *17*, 1076–1079.
1103   Paton, C., J. Hellstrom, B. Paul, J. Woodhead, and J. Hergt (2011), Iolite: Freeware for the
1104   visualisation and processing of mass spectrometric data, *J. Analyt. Atom. Spect.*, *26*(12),
1105   2508–2518.
1106   Petrus, J. A., and B. S. Kamber (2012), VizualAge: A novel approach to laser ablation ICP-MS
1107   U-Pb geochronology data reduction, *Geostand. Geoanalyt. Res.*, *36*(3), 247–270.
1108   Quade, J., T. E. Cerling, and J. R. Bowman (1989), Development of Asian monsoon revealed by
1109   marked ecological shift during the latest Miocene in northern Pakistan, *Nature*, *342*(6246),
1110   163-166.
1111   Ravikant, V., F. Y. Wu, and W. Q. Ji (2009), Zircon U-Pb and Hf isotopic constraints on
1112   petrogenesis of the Cretaceous-Tertiary granites in eastern Karakoram and Ladakh, India,
1113   *Lithos*, *110*, 153-166.
1114   Roddaz, M., A. Said, S. p. Guillot, P. O. Antoine, J. M. Montel, F. Martin, et al. (2011),
1115   Provenance of Cenozoic sedimentary rocks from the Sulaiman fold and thrust belt,
1116   Pakistan: implications for the palaeogeography of the Indus drainage system, *J. Geol. Soc.*,
1117   *168*, 499-516 doi: 10.1144/0016-76492010-100.
1118   Rolland, Y., C. Picard, A. Pecher, H. Lapierre, D. Bosch, and F. Keller (2002), The Cretaceous
1119   Ladakh arc of NW himalaya—slab melting and melt–mantle interaction during fast
1120   northward drift of Indian Plate, *Chem. Geol.*, *182*, 139–178.
1121   Routledge, C. M., D. K. Kulhanek, L. Tauxe, G. Scardia, A. D. Singh, S. Steinke, et al. (2019),
1122   Revised geological timescale for IODP Sites U1456 and U1457, *Geol. Mag.*,
1123   doi:10.1017/S0016756819000104.
1124   Schärer, U., P. Copeland, T. M. Harrison, and M. P. Searle (1990), Age, cooling history, and
1125   origin of post-collisional leucogranites in the Karakoram Batholith; a multi-system isotope
1126   study, *J. Geol.*, *98*(2), 233-251.
1127   Schärer, U., R.-H. Xu, and C. J. Allègre (1984), U-Pb geochronology of Gangdese
1128   (Transhimalaya) plutonism in the Lhasa-Xigaze region, Tibet, *Earth Planet. Sci. Letts.*,
1129   *69*(2), 311-320.
1130   Searle, M. P. (1996), Cooling history, erosion, exhumation and kinematics of the Himalaya-
1131   Karakoram-Tibet orogenic belt, in *The Tectonic Evolution of Asia*, edited by A. Yin and T.
1132   M. Harrison, pp. 110-137, Cambridge University Press, Cambridge.

1133 Searle, M. P., and R. J. Phillips (2007), Relationships between right-lateral shear along the
1134   Karakoram Fault and metamorphism, magmatism, exhumation and uplift; evidence from
1135   the K2-Gasherbrum-Pangong ranges, north Pakistan and Ladakh, *J. Geol. Soc.*, *164*(2),
1136   439-450.
1137 Searle, M. P., A. J. Rex, R. Tirrul, D. C. Rex, A. Barnicoat, and B. F. Windley (1989),
1138   Metamorphic, magmatic and tectonic evolution of the Central Karakoram in the Biafo-
1139   Baltoro-Hushe regions of north Pakistan, *Geol. Soc. America Spec. Pap.*, *232*, 47-73.
1140 Shanmugam, G., and R. Moiola (1991), Types of submarine fan lobes: models and implications
1141   (1), *AAPG Bull.*, *75*(1), 156-179.
1142 Shuaib, S. M. (1982), Geology and hydrocarbon potential of offshore Indus Basin, Pakistan,
1143   *AAPG Bull.*, *66*, 940–946.
1144 Singh, S., R. Kumar, M. E. Barley, and A. K. Jain (2007), SHRIMP U–Pb ages and depth of
1145   emplacement of Ladakh batholith, eastern Ladakh, India, *J. Asian Earth Sci.*, *30*(3), 490–
1146   503.
1147 Singh, S., B. Parkash, A. K. Awasthi, and S. Kumar (2011), Late Miocene record of
1148   palaeovegetation from Siwalik palaeosols of the Ramnagar sub-basin, India, *Current Sci.*,
1149   *100*(2), 213-222.
1150 Singh, S. K., and C. France-Lanord (2002), Tracing the distribution of erosion in the
1151   Brahmaputra watershed from isotopic compositions of stream sediments, *Earth Planet. Sci.*
1152   *Letts.*, *202*(3-4), 645-662.
1153 Spencer, C. J., C. L. Kirkland, and R. J. M. Taylor (2016), Strategies towards statistically robust
1154   interpretations of in situ U–Pb zircon geochronology, *Geoscience Frontiers*, *7*(4), 581-589,
1155   doi:10.1016/j.gsf.2015.11.006.
1156 Stephenson, B. J., M. P. Searle, D. J. Waters, and D. C. Rex (2001), Structure of the Main
1157   Central Thrust zone and extrusion of the High Himalayan deep crustal wedge, Kishtwar-
1158   Zanskar Himalaya, *J. Geol. Soc.*, *158*(4), 637-652.
1159 Stewart, R. J., B. Hallet, P. K. Zeitler, M. A. Malloy, C. M. Allen, and D. Trippett (2008),
1160   Brahmaputra sediment flux dominated by highly localized rapid erosion from the
1161   easternmost Himalaya, *Geology*, *36*(9), 711–714, doi: 10.1130/G24890A.1.
1162 Sundell, K., and J. E. Saylor (2017), Unmixing detrital geochronology age distributions,
1163   *Geochem. Geophys. Geosyst.*, *18*, 2872–2886.
1164 Taylor, S. R., and S. M. McLennan (1995), The geochemical evolution of the continental crust,
1165   *Rev. Geophys.*, *33*, 241–265.
1166 Thiede, R. C., B. Bookhagen, J. R. Arrowsmith, E. R. Sobel, and M. R. Strecker (2004), Climatic
1167   control on rapid exhumation along the Southern Himalayan Front, *Earth Planet. Sci. Letts.*,
1168   *222*(3-4), 791-806.
1169 Thiede, R. C., T. A. Ehlers, B. Bookhagen, and M. R. Strecker (2009), Erosional variability
1170   along the northwest Himalaya, *J. Geophys. Res.*, *114*(F01015),
1171   doi:10.1029/2008JF001010.
1172 Vermeesch, P. (2004), How many grains are needed for a provenance study?, *Earth Planet. Sci.*
1173   *Letts.*, *224*, 351–441.
1174 Vermeesch, P., A. Resentini, and E. Garzanti (2016), An R package for statistical provenance
1175   analysis, *Sed. Geol.*, *336*, 14-25, doi:10.1016/j.sedgeo.2016.01.009.
1176 Vögeli, N., Y. Najman, P. van der Beek, P. Huyghe, P. M. Wynn, G. Govin, et al. (2017), Lateral
1177   variations in vegetation in the Himalaya since the Miocene and implications for climate
1178   evolution, *Earth Planet. Sci. Letts.*, *471*, 1–9, doi:10.1016/j.epsl.2017.04.037.

Wallis, D., A. Carter, R. J. Phillips, A. J. Parsons, and M. P. Searle (2016), Spatial variation in exhumation rates across Ladakh and the Karakoram: New apatite fission track data from the Eastern Karakoram, NW India, *Tectonics*, *35*, 704–721, doi:10.1002/2015TC003943.

Wallis, D., R. J. Phillips, and G. E. Lloyd (2014), Evolution of the Eastern Karakoram Metamorphic Complex, Ladakh, NW India, and its relationship to magmatism and regional tectonics, *Tectonophysics*, *626*, 41–52, doi:10.1016/j.tecto.2014.03.023.

Webb, A. A. G. (2013), Preliminary palinspastic reconstruction of Cenozoic deformation across the Himachal Himalaya (northwestern India), *Geosphere*, *9*, 572-587.

Weinberg, R. F., and W. J. Dunlap (2000), Growth and Deformation of the Ladakh Batholith, Northwest Himalayas: Implications for Timing of Continental Collision and Origin of Calc-Alkaline Batholiths, *J. Geol.*, *108*, 303–320, DOI: 10.1086/314405.

Whipple, K. X. (2009), The influence of climate on the tectonic evolution of mountain belts *Nature Geosci.*, *2*, 1-8, doi: 10.1038/ngeo413.

White, A. F., and S. L. Brantley (1995), *Chemical weathering rates of silicate minerals*, 581 pp., Mineralogical Society of America.

Whittington, A., G. Foster, N. Harris, D. Vance, and M. Ayres (1999), Lithostratigraphic correlations in the western Himalaya - An isotopic approach, *Geology*, *27*(7), 585-588.

Wilson, S. A. (1997), Data compilation for USGS reference material BHVO-2, Hawaiian Basalt, *U.S. Geol. Surv. Open-File Rept*.

Wobus, C. W., K. V. Hodges, and K. X. Whipple (2003), Has focused denudation sustained active thrusting at the Himalayan topographic front?, *Geology*, *31*(10), 861-864.

Yang, S., F. Zhang, and Z. Wang (2012), Grain size distribution and age population of detrital zircons from the Changjiang (Yangtze) River system, China, *Chem. Geol.*, *296-297*, 26-38.

Yin, A., C. S. Dubey, T. K. Kelty, A. A. G. Webb, T. M. Harrison, C. Y. Chou, et al. (2010), Geologic correlation of the Himalayan orogen and Indian craton: Part 2. Structural geology, geochronology, and tectonic evolution of the Eastern Himalaya, *GSA Bulletin*, *122*(3-4), 360-395, 10.1130/B26461.1.

Zeilinger, G., J. P. Burg, U. Schaltegger, and D. Seward (2001), New U/Pb and fission track ages and their implication for the tectonic history of the lower Kohistan Arc Complex, northern Pakistan, *J. Asian Earth Sci.*, *19*(3S), 79-81.

Zeitler, P. K., and C. P. Chamberlain (1991), Petrogenetic and Tectonic Significance of Young Leukogranites from the Northwestern Himalaya, Pakistan, *Tectonics*, *10*(4), 729-741.

Zeitler, P. K., C. P. Chamberlain, and H. A. Smith (1993), Synchronous Anatexis, Metamorphism, and Rapid Denudation at Nanga-Parbat (Pakistan Himalaya), *Geology*, *21*(4), 347-350.

Zeitler, P. K., J. F. Sutter, I. S. Williams, R. E. Zartman, and R. A. K. Tahirkheli (1989), Geochronology and temperature history of the Nanga Parbat-Haramosh Massif, Pakistan, in *Tectonics of the western Himalayas*, edited by L. L. Malinconico and R. J. Lillie, pp. 1–22, Geological Society of America, Boulder, CO.

Zhou, P., A. Carter, Y. Li, and P. D. Clift (2019), Slowing Rates of Regional Exhumation in the Western Himalaya: Fission Track Evidence from the Indus Fan, *Geol. Mag.*, doi:10.1017/S001675681900092X.

Zhuang, G., Y. Najman, S. Guillot, M. Roddaz, P.-O. Antoine, G. Métaise, et al. (2015), Constraints on the collision and the pre-collision tectonic configuration between India and Asia from detrital geochronology, thermochronology, and geochemistry studies in the

1224   lower Indus basin, Pakistan, *Earth Planet. Sci. Letts.*, *432*, 363–373,
1225   doi:10.1016/j.epsl.2015.10.026.
1226 Zhuang, G., Y. Najman, Y. Tian, A. Carter, L. Gemignani, J. Wijbrans, et al. (2018), Insights
1227   into the evolution of the Hindu Kush-Kohistan-Karakoram from modern river sand detrital
1228   geo- and thermochronological studies, *J. Geol. Soc.*, doi:10.1144/jgs2018-007.
1229

1230

1232 **Figure 1.** A) Shaded bathymetric and topographic map of the Arabian Sea and surrounding area
1233 showing the location of the drilling sites considered by this study. Map also shows the major
1234 tributary systems of the Indus River, as well as smaller peninsular India rivers and their source
1235 mountains. B) Inset map shows detail of the Laxmi Basin and location of the drill sites
1236 considered in this study. Numbered red circles indicate existing scientific boreholes from Deep
1237 Sea Drilling Project (DSDP) and Ocean Drilling Program (ODP). KK = Karakoram; NP = Nanga
1238 Parbat. C) Geological map of the western Himalaya showing the major tectonic units that are
1239 eroded by the Indus River and its tributaries. Map is modified after Garzanti *et al.* [2005]. Rivers
1240 as shown in thick black lines. ISZ = Indus Suture Zone, MCT = Main Central Thrust, MBT =
1241 Main Boundary Thrust and MFT = Main Frontal Thrust. Thick black line shows the boundary of
1242 the Indus drainage, while thinner lines demark the limits of the major Himalayan tributaries.
1243 Figure is modified from Clift *et al.* [2019b].

1244

1245 **Figure 2.** Simplified lithologic logs of the two drill sites considered in this study. Black arrows
1246 show the location of the samples analyzed. Modified from Pandey *et al.* [2016c]. Pale shaded
1247 intervals show inferred lithologies based on small amounts of recovered core. Because induration
1248 is progressive and there is no sharp division, we make no attempt to distinguish between
1249 sediments and indurated rocks. Numerical ages are from Pandey *et al.* [2016a] for Site U1456
1250 and from Pandey *et al.* [2016b] for Site U1457, with updates from Routledge *et al.* [2019].

1251

1252 **Figure 3.** Grainsize range of all samples analyzed for U-Pb zircon dating from the Laxmi Basin
1253 shown on the scheme of Folk [1974]. Samples are marked to show those published by Clift *et al.*
1254 [2019b], rather than presented new here (Table 2). Note the dominance of silty sand and sandy
1255 silt in the analyzed samples.

1256

1257 **Figure 4.** Detailed grain size spectra showing the range of sizes of the different samples
1258 considered within this study. Most of the sediment is fine sand to coarse silt in size and typically
1259 shows a coarse-skewed. A) Samples younger than 7 Ma, b) samples older than 7 Ma. Samples
1260 are marked to show those published by Clift *et al.* [2019b](gray text labels and white ringed
1261 symbol), rather than presented new here (Table 2) (black text labels and black ringed symbol).

1262

1263 **Figure 5.** (A) Geochemical signature of the analyzed samples illustrated by a CN-A-K ternary
1264 diagram [Fedo *et al.*, 1995]. CN denotes the mole weight of Na_2O and CaO* (CaO* represent the
1265 CaO associated with silicate, excluding all the carbonate). A and K indicate the content of Al_2O_3
1266 and K_2O respectively. Samples closer to A are rich in kaolinite, chlorite and/or gibbsite
1267 (representing by kao, chl and gib). CIA values are also calculated and shown on the left side,

1268 with its values are correlated with the CN-A-K. Samples from the delta have the lowest values of
1269 CIA and indicates high contents of CaO and Na_2O and plagioclase. Abbreviations: sm (smectite),
1270 pl (plagioclase), ksp (K-feldspar), il (illite), m (muscovite). B) Geochemical classification of
1271 sediments from this study as well as those from the Indus delta [*Clift et al.*, 2010], Indus Canyon
1272 [Li *et al.*, 2018] and western Indian shelf [Kurian *et al.*, 2013] following the scheme of Herron
1273 [1988].

1274

1275 **Figure 6.** Cross plot of Zr concentration against median sample grain size. No strong correlation
1276 is observed.

1277

1278 **Figure 7.** Kernal density estimate (KDE) diagram showing the range of the zircon U-Pb ages for
1279 individual sand grains back to 3000 Ma. Colored strips show the range of populations with
1280 diagnostic links to critical source terrains in the headwaters of the Indus. Data from the Siwaliks,
1281 as well as the Tethyan, Greater and Lesser Himalaya are compiled from DeCelles *et al.* [2004].
1282 Karakoram data is from is from Le Fort *et al.* [1983], Parrish and Tirrul [1989], Schärer *et al.*
1283 [1990], Fraser *et al.* [2001] and Ravikant *et al.* [2009]. Nanga Parbat data is from Zeitler and
1284 Chamberlain [1991] and Zeitler *et al.* [1993]. Transhimalayan data is from Honegger *et al.*
1285 [1982], Schärer *et al.* [1984], Krol *et al.* [1996], Weinberg and Dunlap [2000], Zeilinger *et al.*
1286 [2001], Dunlap and Wysoczanski [2002], Singh *et al.* [2007], and Ravikant *et al.* [2009].
1287 Samples are marked to show those published by Clift *et al.* [2019b], and those presented new
1288 here.

1289

1290 **Figure 8.** Kernal density estimate (KDE) diagram showing the range of the zircon U-Pb ages for
1291 individual sand grains back to 200 Ma. Colored strips show the range of populations with
1292 diagnostic links to critical source terrains in the headwaters. See Figure 6 caption for data
1293 sources.

1294

1295 **Figure 9.** Upper continental crust normalized compositions of the sediments whose zircons are
1296 the focus of the study. Bulk settlement compositions are normalized according to the average of
1297 the continental crust from Taylor and McLennan [1995].

1298

1299 **Figure 10.** Plots of relative abundance of provenance sensitive zircon age populations in
1300 individual samples compared with sample median grain size. The coarsest samples show
1301 preference for the oldest U-Pb ages and a relative lack of the younger populations.

1302

Figure 11. Multidimensional scalar (MDS) diagrams made from zircon U-Pb age data showing (A) how the different sediment samples from IODP Expedition 355 compare with one another and post-glacial sediments from the Indus delta (TH-10-8 and KB-40-4) and (B) with the major source terranes in the Indus catchment, as well as the modern rivers of the Indus catchment, i.e., the main or trunk stream of the Indus, upstream of Attock, and its major eastern tributaries. Solid lines join sediments to their most similar neighbor, while dashed lines join the next most similar. Sources of bedrock age data come from the literature, as described in Figure 6. River data is from Alizai *et al.* [2011]. Note that sediments older than 5 Ma plot towards the right in Figure 10B, in the direction of Karakoram bedrock sources, whereas there is a progressive migration towards the left, towards Himalayan sources after that time. Diagram was constructed using the statistical package of Vermeesch *et al.* [2016].

Figure 12. Pie diagrams showing the predicted source compositions of the zircon populations in sands from the Laxmi Basin as unmixed using the software of Sundell and Saylor [2017]. Note the significant reduction in flux from the Karakoram starting ~5.72 and again at 3.02 Ma. Samples are marked to show those published by Clift *et al.* [2019b], and those presented new here.

Figure 13. Comparison of climate, erosion and exhumation proxies in the Himalaya. (a) Smoothed Nd isotope history for the Indus River with grey background showing effective uncertainties from Clift *et al.* [2018]. (b) Breakdown of the sources of detrital zircons based on the unmixing procedure of Sundell and Saylor [2017]. (c) Carbon isotope character of pedogenic carbonate in Pakistan as an indicator of dominant vegetation in the Potwar Plateau of Pakistan [Quade *et al.*, 1989], and NW India [*Singh et al.*, 2011]. (d) Relative exhumation rates of the Greater Himalaya tracked by bedrock Ar-Ar dating [*Clift et al.*, 2008b] and zircon fission track from foreland basin sediment [Chirouze *et al.*, 2015]. (e) Rates of sediment supply to the Arabian Sea calculated from regional seismic [*Clift*, 2006].

Table Captions

Table 1. Major elements major elements geochemical analysis of the samples considered in this study.

Table 2. Analytical results from the laser particle size analyzer for all bulk samples considered in this study.

1338

1339   **Table 3.** Analytical data for the zircon U-Pb dating of grains presented in this work.

1340

1341   **Table 4.** Results of the mixing modelling performed by the DZMix software of Sundell and
1342   Saylor [2017] on the detrital samples from the Laxmi Basin.